THE ROLE OF OSTEOPONTIN IN POSTNATAL VASCULAR GROWTH: FUNCTIONAL EFFECTS IN ISCHEMIC LIMB COLLATERAL VESSEL FORMATION AND LONG BONE FRACTURE HEALING

A Dissertation
Presented to
The Academic Faculty

by

Craig L. Duvall

In Partial Fulfillment
of the Requirements for the Degree
Doctor of Philosophy in the
Wallace H. Coulter Department of Biomedical Engineering

Georgia Institute of Technology
May 2007

THE ROLE OF OSTEOPONTIN IN POSTNATAL VASCULAR GROWTH: FUNCTIONAL EFFECTS IN ISCHEMIC LIMB COLLATERAL VESSEL FORMATION AND LONG BONE FRACTURE HEALING

Approved by:

Dr. Robert Guldberg, Advisor
School of Mechanical Engineering
Georgia Institute of Technology

Dr. W. Robert Taylor, Advisor
School of Medicine
Emory University

Dr. Oskar Skrinjar
Department of Biomedical Engineering
Georgia Institute of Technology

Dr. Larry McIntire
Department of Biomedical Engineering
Georgia Institute of Technology

Dr. David Harrison
School of Medicine
Emory University

Dr. Ravi Bellamkonda
Department of Biomedical Engineering
Georgia Institute of Technology

Date Approved: December 21, 2006

For my family, especially my grandfather
Henry Clay Winn (1926-2006), an example of a true hero.

ACKNOWLEDGEMENTS

When I left Kentucky to start graduate school, I was excited to start something new but mostly considered it a necessary evil and a means to the ends that I wished to pursue later in life. I knew that, in the process of getting a top-notch education, I would probably enjoy my mid-20's and make the transition from a "college-kid" to an "adult" in a fun city, Atlanta. At the time, the overwhelming feeling was that I needed to get this over with as quickly and painlessly as possible and get on to the real world. However, as time passed, this feeling began to fade and Atlanta became my comfort zone. By the time that the end of the journey was in sight, what I thought was going to be a "thank goodness and good riddance" moment has turned out to be a feeling of mixed emotions and of strong attachment to the people and the place that have filled my life for the past 5 1/2 years. Whether the transition to adulthood that I mentioned above ever actually happened is tremendously debatable. Regardless, the one thing I did learn was that working toward a Ph.D., like any experience in life, is something to savor and not a constant race to the end. In this section of my thesis, I will attempt to acknowledge those who have enhanced my grad school experience and have helped to make Atlanta a great place to live.

First and foremost, I owe a tremendous amount of gratitude to my thesis coadvisors, W. Robert Taylor and Robert E. Guldberg (aka "Bob T & G" or "the Bobs"). It has always been difficult to explain why I have been coadvised by a mechanical engineer at Georgia Tech and a cardiologist at Emory. I have also often said that it is pretty to easy to see why being coadvised as a graduate student doesn't typically work

out, especially when the professors' primary interests do not have significant overlap. However, the Bobs provided the perfect mix of intellectual support, selflessness, freedom to find my own way and satisfy my own curiosities, and an environment that has allowed me to grow as an independent thinker. As advisors, they have always remained supportive, yet demanded that I get the best from myself, and for that, I am appreciative. Moreover, they have tried to ensure that I have every opportunity to move on and gain my own successes, independent of their own. Additionally, both Bobs have always served as friends and been truly compassionate about my well-being and life outside of research, which has been equally integral to my motivation and peace of mind during grad school. Overall, this unique setup between the Bobs has allowed me to gain an incredibly meaningful, diverse, and rich experience.

I also am thankful for the advisement of my thesis committee members. Dr. Skrinjar has been a tremendous resource for imaging and image processing related work. Dr. Bellamkonda has remained an inquisitive member of the group that has provided expertise in vascular contrasts, ensured that I understood the big picture of my work, and been a valuable mentor in my pursuits and interests for postdoctoral work. Dr. Harrison has provided a valuable clinical perspective in addition to many valuable insights into my understanding of vascular biology. Dr. McIntire has supplied additional expertise on vascular biology from a cellular perspective and has been integral to progression of this project.

I am also grateful to the staff and administrators within the Emory Division of Cardiology, IBB, and BME, which have made my life much easier during grad school. In particular, I would like to thank Dr. Nerem for granting me the opportunity to work in

his lab when I first came to Georgia Tech. On a larger scale, he has created a cutting edge scientific community within IBB that is equipped with all of the necessary pieces to ensure development and success of the researchers there. On a personal level, he has always taken the time to provide meaningful advice and valuable contacts within the scientific community. In addition, I am grateful to Don Giddens, Larry McIntire, Ajit Yoganathan, and Steve DeWeerth for their impeccable leadership and dedication to building and evolving a BME department that is second to none. Lastly, I would like to thank Tracey Couse for sharing her remarkable histology knowledge and skills during her tenure at IBB.

I am also sincerely indebted to my colleagues within IBB wing 2D, the Emory Division of Cardiology, and other students of BME program. Many of these coworkers and fellow students have also served double duty as my closest friends. Wing 2D was my first real grad school residence as I began work on the micro-CT imaging studies. I must acknowledge that the combined Guldberg, Garcia, Levenston, and Boyan labgroups share a great deal of camaraderie and also possess incredible scientific capacity, which combine to form an extremely positive academic work environment. I especially want to think Andres Garcia and his lab, which was actually my first home in wing 2D during my first research rotation. Andres has remained a close friend and provided advice and opinions in his typical unabashed style on topics from research, to potential postdocs, to the current state of my *alma mater's* sports teams. I also want to say thanks to my close affiliates in the Levenston labs, particularly Chris Wilson, Ashley Palmer, and Eric Vanderploeg, with whom it has been intellectually resourceful and a joy to work over the years, not to mention the many good times that we have shared outside the lab.

From the Guldberg lab, I first want to thank Blaise Porter for "grandfathering" me into a fun working environment, even though he once almost killed me mountain biking in Vail. Thanks for taking the focus off of my own exploits through your propensity for mashed potato thievery and other such adventures. I also have to throw a shout out to the original master of ceremonies, Galen Robertston (aka G-Rob), whose hosting of the grind on Bourbon Street is a memory that will never fade. I next want to thank Chris Gemmiti for being my partner in crime in many Guldberg trips/festivities and also for his ABC connections, golf outings, and untouchable super bowl extravaganzas. I want to thank Dr. Alex Peister, an excellent newer member of the lab, for her cheerful demeanor and offering to help proofread this thesis. I also know that the lab is in good shape with the remaining new and experienced students of the lab: Rhima Coleman, Megan Oest, Yash Kolambkar, Ken Dupont, Mela Johnson, Joel Boerckel, Chris Dosier, and Eric Deutsch. Next, I must mention Srin Nagaraja and Angela Lin, fellow members of the Guldberg lab, along with Catherine Reyes, whom comprise my co-conspirators in the official activities of "the corner". Srin, we've had some great times, especially on conference trips and thrashing the competition in IM basketball over the years. Angela, you've been a great asset to me in the lab in terms helping with micro-CT, mechanical testing, and critiques of my writing. However, your contributions far exceed lab-related help, and we've shared many memories, none of which can be overshadowed by your trip up to Kentucky for Derby'06. Cathy, you're an amazingly gifted person with a fantastic outlook and persona, and your husband is ok too. Speaking of Dr. Gersbach, Charlie, we became good friends from the start of grad school, and if it weren't for a little coaching from you, I probably would've drowned during my first triathlon.

From the Taylor lab, there are also many people to whom I owe many thanks. First off, thanks to Fadi Alameddine for being my first mentor in using animal models and in angiogenesis research. Exposure to you and all of the many cardiology fellows that have passed through the lab has provided a diversity of perspectives during grad school. Just as the other fellows that have come before you, the most recent duo, Parker Grow and Juan Velasquez, have been a joy to work with and provided great intellect and positive contributions to the dynamic within the lab. I also am grateful for assistance on this project from the instructors, postdocs, and other members of the lab including Patrick Cowan, Diane Sutcliffe, Giji Joseph, Daiana Weiss, Elethia Woolfolk, and Natalia Landazuri. I owe a special thanks Patrick for teaching me about the "soft touch", Diane for taking care of my last minute ordering needs, Giji for assistance with histology, and Daiana for an immeasurable amount of help in maintenance of the animal colonies and in other technical aspects of the project.

Lastly, I owe a special thanks to my fellow Taylor lab grad students. Between the shared lunches and many hours in the lab, we have, to say the least, kept each other on our toes with our constant ribbing of one another. To Matt Whalin, the human encyclopedia, I owe many thanks for sharing his significant knowledge and contributing to the molecular and cell biology related aspects of this project. As Matt and I finish up in the lab, I am assured that the grad student contingent remains a formidable group that includes the following cast of characters: Katie Maiellaro, Scott "Scrob" Robinson, "Young Nicolas" Nick Willett, and Ebony Washington. Katie, as Scott and Patrick have always said, you're pretty cool for a dude with long hair. In all seriousness, you're one of the most sincere, upbeat, and fun people I've been around, and you have always cheered

me up whenever I've had a bad day. Nick, your laid back, Colorado cool has been a great fit to our group, so it's on your shoulders to keep the good karma going long term.

I owe many good times during grad school to Torrence Welch, Neal Weinrich, and Scott Robinson, residents of the Heights at Cheshire Bridge (and the revelers of the many fine establishments in this area). Scrob, between co-hosting "celebrations of life", Harvey's heroics at Okemo, late night lessons in gang symbols, tailgating with big shot CEO's, mountain biking, triathlons, dominating all takers under the alias of team tanktop, attending Poison and many other concerts, and futile attempts at dismissing the common appraisal of us as the division of cardiology meatheads, the good times have kept rolling. Chunk/Maple I am sorry that many of the aforementioned activities have likely contributed to your negligent care, but just think of it as fate catching up to you for the annoying car rides.

To King Big Head's household, I would like to express much gratitude for making halloween one of my favorite holidays. Special recognition goes to John Wilson for crafting a giant paper mache head with Matt's face on it, which could've been the most entertaining costume in history. I must also mention that the frequent cookouts and weekend mountain biking trips enjoyed with you guys kept me sane after long workweeks. I owe tremendous gratitude to Matt (Big Head) Rhyner for planning and faithfully participating in all of these events. Alongside this group, I must also say thanks to Sean (PSJI) Sullivan, with whom I forged a bond the first time I met on grad student recruiting weekend when I realized (after Sean talked for 45 consecutive minutes without taking a breath) that I had finally found someone that might be able to supplant my own knowledge of college basketball. You and Matt were the go to guys when looking for

company on the many road trips to Nashville and the Kentucky Derby, with the "collars up" derby being an experience for the ages. The entertainment value of the many consecutive ABC, Golden Buddha, NBA, PT Fridays goes without saying.

I must also thank my roommates from grad school, starting with the Pennsylvanians, Jeff Gross and Blaine Zern. Jeff, we've shared some great times since we became friends on day one of grad school. You're a stand-up guy with an incredibly bright future. I still say you owe me for your marriage to Taryn for dragging you to the mixer that night at Twain's. BZ, exploits as the channel 4 news team, hand prints on the hallway walls, feats of strength from the balcony, and many IM sports highlight the memories from our year in apartment 1513. I must finally thank Bryan Marshall for sharing his home and giving me a place to stay for the last few months of grad school. Although you're a Hoosier, I admire, not only your quirky dance moves, but also your intellect, kindness, and energy.

Next, I must thank those closest to me. First, I would like to thank my better half, Gina Addington. You have been a constant source of love and support, and I'm sure that the sustenance you provided was the only reason that I was able to endure the emotional and intellectual challenges that I had to overcome during the last few months of grad school. I also appreciate your patience, openness, and support as I try to figure what's going to be next in life. You and your parents have provided a much-needed outlet from school and become a home away from home for me.

Finally, I must thank my family. First, I want to thanks my grandparents, Henry and Wada Winn, for the exemplary lives they've led, their constant love and support, and always greeting me with a hug that made me glad to be home. I want to thank Jennifer

and Brad Shelby for making a great sister / brother-in-law combo that I infinitely enjoy spending time with during our visits to see each other. I especially want to commend Brad for his love and unwavering support of my sister, and I want to thank Jenni for being a role model, setting the bar high, and paving a path that has made my own pursuits clearer and easier to obtain. I'm very proud to call you "sis". Lastly, I want to thank my parents. It's impossible to describe the respect and admiration that I have for you and the lives that you've built for yourselves. I want to say thanks for your constant love and support and helping me to obtain all of my dreams. You've given me the utmost freedom to make my own decisions in life, and your impeccable work ethic and exemplary model for understanding the simple things in life have motivated me to always do my best yet hopefully keep a keen perspective on what is really important. I can't imagine having a more solid foundation on which to build by own life.

TABLE OF CONTENTS

LIST OF TABLES

Page

LIST OF FIGURES

Page

LIST OF SYMBOLS AND ABBREVIATIONS

2-D	two-dimensional
3-D	three-dimensional
AFM	atomic force microscopy
AMI	acute myocardial infarction
ANOVA	analysis of variance
BM	bone marrow
BMPs	bone morphogenic proteins
BMT	bone marrow transplant
BSP	bone sialoprotein
CAM	chick chorioallantoic membrane
CURVES	curve evolution for vessel segmentation
ECM	extracellular matrix
EPCs	endothelial progenitor cells
FGF	fibroblast growth factor
FGFR	fibroblast growth factor receptor
FIRST	FGF initiating revascularization trial
FN	fibronectin
Fx	fracture
HA	hydroxyapatite
HSC	hematopoietic stem cell
LDPI	laser Doppler perfusion imaging

LOX	lysyl oxidase
LV	left ventricle
MCP-1	monocyte chemotactic protein 1
micro-CT	microcomputed tomography
MIP	maximum intensity projection
MRA	magnetic resonance angiography
MRA	magnetic resonance angiography
MRA	magnetic resonance angiography
MRA	magnetic resonance angiography
OPN	osteopontin
PAD	peripheral arterial occlusive disease
PSR	picrosirius red
RAVE	regional angiogenesis with vascular endothelial growth factor
RGD	arginine-glycine-aspartate
RT-PCR	reverse transcription polymerase chain reaction
SEM	scanning electron microscopy
SVVYGLR	serine-valine-valine-tyrosine-glycine-leucine-arginine
TRAFFIC	therapeutic angiogenesis with recombinant fibroblast growth factor-2 for intermittent claudication
VEGF	vascular endothelial growth factor
VEGFR	vascular endothelial growth factor receptor
VIVA	vascular endothelial growth factor in ischemia for vascular angiogenesis
VOI	volume of interest
WT	wild type

SUMMARY

Postnatal vascular growth is a complex process involving multiple cells types whose functionality is orchestrated by a variety of soluble extracellular growth factors, mechanical stimuli, and matrix derived cues. The central goal for this dissertation project was to elucidate the role of osteopontin, a non-collagenous extracellular matrix protein, in postnatal vascular growth.

At the onset, we concluded that the current methods for measurement of vascularity in small animal models were lacking. To address this shortcoming, we pursued micro-CT imaging for analysis of three-dimensional blood vessel architecture. We were able to demonstrate that micro-CT imaging provides an objective, quantitative, and three-dimensional methodology for evaluation of vascular networks that has broad applicability to preclinical studies.

Next, we sought to apply the developed imaging techniques along with other complementary methodologies to explore the role of osteopontin in postnatal vascular growth. Osteopontin was previously known to elicit survival, migration, and other relevant activities in multiple cell types involved in postnatal vascular growth. Therefore, we sought to determine the *in vivo* significance of osteopontin in this process. To do so, we compared wild type and Osteopontin$^{-/-}$ mice for (1) their ability to form collateral vessels and functionally recover following acute induction of hind limb ischemia and (2) their capacity for neovascularization, mineralization, remodeling, and the restoration of mechanical properties during fracture healing. Data suggested that OPN is a critical regulator of collateral vessel formation and that this effect is driven by its role in mediating monocyte/macrophage migration and functionality. Secondly, we found that

the presence of osteopontin was essential for normal early callus formation, neovascularization, late stage callus remodeling, and restoration of biomechanical strength. Abnormal collagen organization was observed within the remodeling fractures of Osteopontin$^{-/-}$ mice, and we hypothesize that a unifying link between the vascular and bone defects may be related to deficient matrix organization and remodeling.

In conclusion, the imaging techniques developed in this thesis provide a novel methodology for quantitative analysis of vascular structures in small animal models. Secondly, this project has yielded an improved understanding of the basic pathophysiological mechanisms that control postnatal blood vessel growth and bone fracture healing.

CHAPTER 1

SPECIFIC AIMS

Introduction

Better understanding the mechanisms of postnatal vascular growth has clinical relevance in a myriad of applications including treatment of cardiovascular disease, cancer therapy, enhancing wound healing, and growth of engineered tissues. For example, therapeutic stimulation of blood vessel growth could alleviate pathological conditions such as tissue ischemia caused by peripheral or coronary artery disease. Peripheral limb arterial occlusion, common in diabetic patients, causes formation of chronic skin ulcers and often requires limb amputation. Myocardial ischemia is the leading cause of morbidity and mortality in the world (1), and it has traditionally been treated by coronary artery bypass surgery, a highly invasive procedure that often leaves ischemic areas in the cardiac tissue that are not amenable to revascularization. In addition, accelerating wound repair and the success of many applications in the growing field of tissue engineering depend on an adequate blood supply in order to maximize cellular viability and functional tissue regeneration.

Our long-term goal is to further elucidate the biological processes of angiogenesis and collateral development and gain knowledge that can help to develop improved clinical strategies that will optimize vascular function in ischemic, injured, and engineered tissues. To this end, we have investigated improved methods for quantifying vascular growth and utilized these methods to explore the potential role of osteopontin (OPN) in ischemic limb collateral development and in angiogenesis and healing of bone fractures. OPN, a non-collagenous extracellular matrix protein, has recently been

suggested to play a role in the regulation of angiogenesis (2,3). Based on these studies, the central hypothesis for this study was that OPN plays a physiologically relevant role in control of non-pathological, postnatal vascular growth *in vivo*. The overall objective of this project was to utilize microcomputed tomography (micro-CT) imaging and a combination of *in vivo* and *in vitro* studies to develop new methods for quantification of blood vessel network morphology and to gain new insights into the role of OPN in blood vessel formation. Our collaborative team, which possesses expertise in cardiovascular biology, vascular imaging, bone healing, tissue engineering, and biomechanics, has approached this objective through the following specific aims.

Aim I

Validate micro-CT imaging as a method for quantifying vascular network morphology.

Our *working hypothesis* was that micro-CT imaging in combination with perfused contrast agents can provide a highly objective and quantitative method for analysis of three-dimensional (3-D) blood vessel architecture in small animal models. To accomplish this aim, we utilized the previously characterized mouse hind limb ischemia model to provide a well-controlled environment for analyzing collateral vessel formation. We also completed sensitivity analyses on the effects of image voxel size and binarization threshold on micro-CT analyses. Standard histology assessments were used to validate this method.

Aim II

Characterize the role of OPN in collateral development during hind limb ischemia.

Our *working hypothesis* was that OPN deficient mice would show a reduced capacity for collateral vessel formation compared to wild type controls. We employed the hind limb ischemia model to evaluate the potential for neovessel formation in $OPN^{-/-}$ and wild type mice. Quantitative, anatomical evaluations of collateral vessels were completed using the novel micro-CT techniques developed in Specific Aim I. Laser Doppler perfusion imaging was used as a functional assessment of restoration of distal limb perfusion, and an exercise endurance test was utilized as a physiological examination of ischemic limb functional recovery. Aortic ring and macrophage migration assays were employed to gain mechanistic insight into our findings.

Aim III

Define the effects of OPN on neovascularization, mineralization, and biomechanical properties of long bones during fracture healing.

Our *working hypothesis* was that $OPN^{-/-}$ mice would display reduced angiogenesis and altered healing in long bone fractures relative to wild type controls. To test this hypothesis, a well-established femoral fracture healing model (4) was utilized to study the time course of fracture healing in wild type and $OPN^{-/-}$ mice. Micro-CT, quantitative reverse transcription polymerase chain reaction (RT-PCR), and histology were used to evaluate vessel growth, matrix formation, and bone remodeling at the fracture site. In addition, mechanical testing of fractured femurs was performed to test whether OPN

deficiency compromised the restoration of mechanical strength during the healing process.

Innovation and Significance

This work is innovative because it utilized 3-D micro-CT imaging for evaluating blood vessel growth within ischemic tissue and at sites of injury. In doing so, our group has developed a technique that is more quantitative and reproducible than the commonly used two-dimensional (2-D) histological analyses, laser Doppler perfusion imaging, or micro-angiography. In addition, the available OPN knockout mouse colony provided a unique setting that allowed us to precisely determine the previously unknown role of OPN in the biological processes of collateral vessel formation and fracture healing.

Successful angiogenic therapy requires temporal control, specificity to a targeted tissue, and avoidance of undesirable side effects associated with hypervascularity such as tumorigenesis and proliferative retinopathy. Therefore, this work is significant because an improved understanding of the underlying biological mechanisms and the role of factors involved in vascular growth will aid in the development of safe and clinically effective treatment options. This project has acquired a new understanding of postnatal vascular growth that could potentially be incorporated into development of new clinical treatments, and it has also provided a new platform methodology that can be applied for the screening of other pro- and anti-angiogenic factors in future studies. In summary, this thesis project has yielded the following outcomes. First, the imaging techniques developed are expected to become a standard for quantitative, volumetric analysis of neovascular responses in small animal models. Secondly, application of these techniques, combined with the use of the available osteopontin deficient mouse colony,

has yielded an improved understanding of the basic pathophysiological mechanisms that control postnatal blood vessel growth and bone fracture healing.

CHAPTER 2

BACKGROUND AND LITERATURE REVIEW

Postnatal Vascular Growth

Vascular Anatomy and Accepted Modes of Postnatal Vascular Growth

The basic constituents of normal blood vessels are endothelial cells, smooth muscle cells, fibroblasts and pericytes, basement membrane, and extracellular matrix (see Figure 2.1). Postnatal blood vessel development is a complicated, incompletely understood process involving a complex cascade that includes a wide range of cell types, growth factors, extracellular matrix (ECM) proteins, cell surface receptors, and intracellular signaling pathways. This process is relevant to pathological neovascularization in the setting of tumorigenesis, proliferative retinopathy, and rheumatoid arthritis, but it is also vital to formation of new vessels for restoration of normal blood perfusion to ischemic tissues.

The three different mechanisms that have been hypothesized to contribute to formation of new vascular structures are arteriogenesis, angiogenesis, and vasculogenesis (see Figure 2.2). Arteriogenesis occurs when preexisting arterioles dilate and remodel through endothelial and smooth muscle cell expansion to meet increased physiologic demands (5,6). It is hypothesized that this process, which is mediated at least in part by monocytes and macrophages, is triggered by the increased shear stress that occurs in small, interarterial anastomoses following occlusion of a parent artery (7). Angiogenesis involves sprouting or intussusception of new capillaries from pre-existing vessels and is triggered by tissue ischemia. Intussusceptive angiogenesis involves column formation

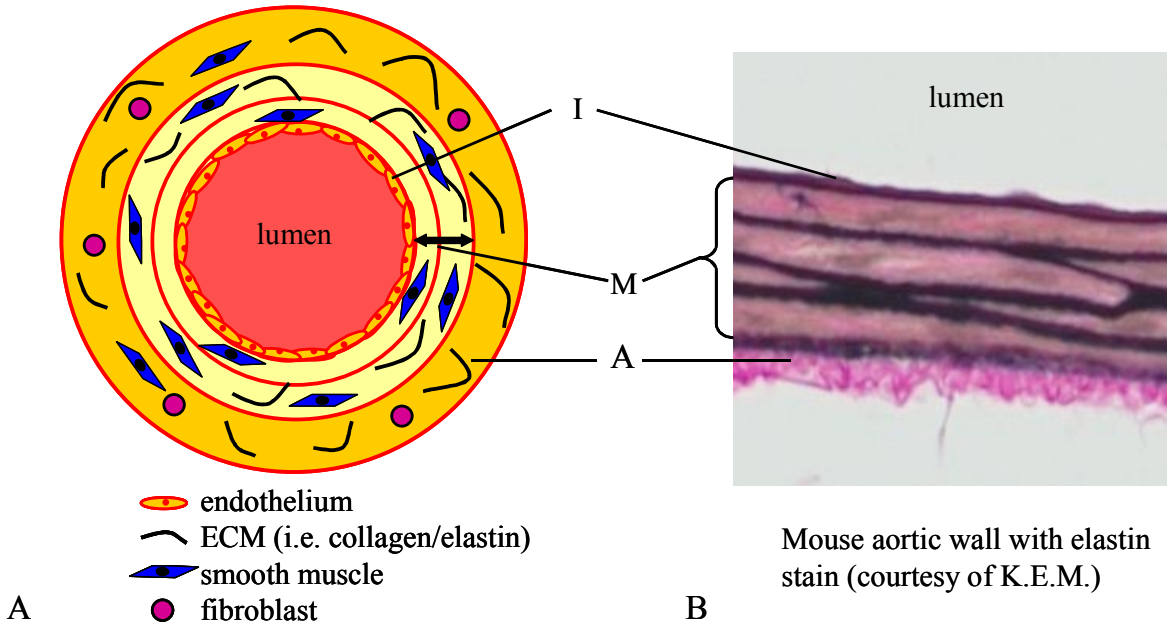

Figure 2.1. Arterial Anatomy. (A) Schematic and (B) histological image of a normal arterial wall cross-section. I = Intima: endothelial cells on basement membrane. A = Adventitia: fibroblasts, collagens, elastin, etc. M = Media: smooth muscle cells, collagens, elastin, vitronectin, laminin

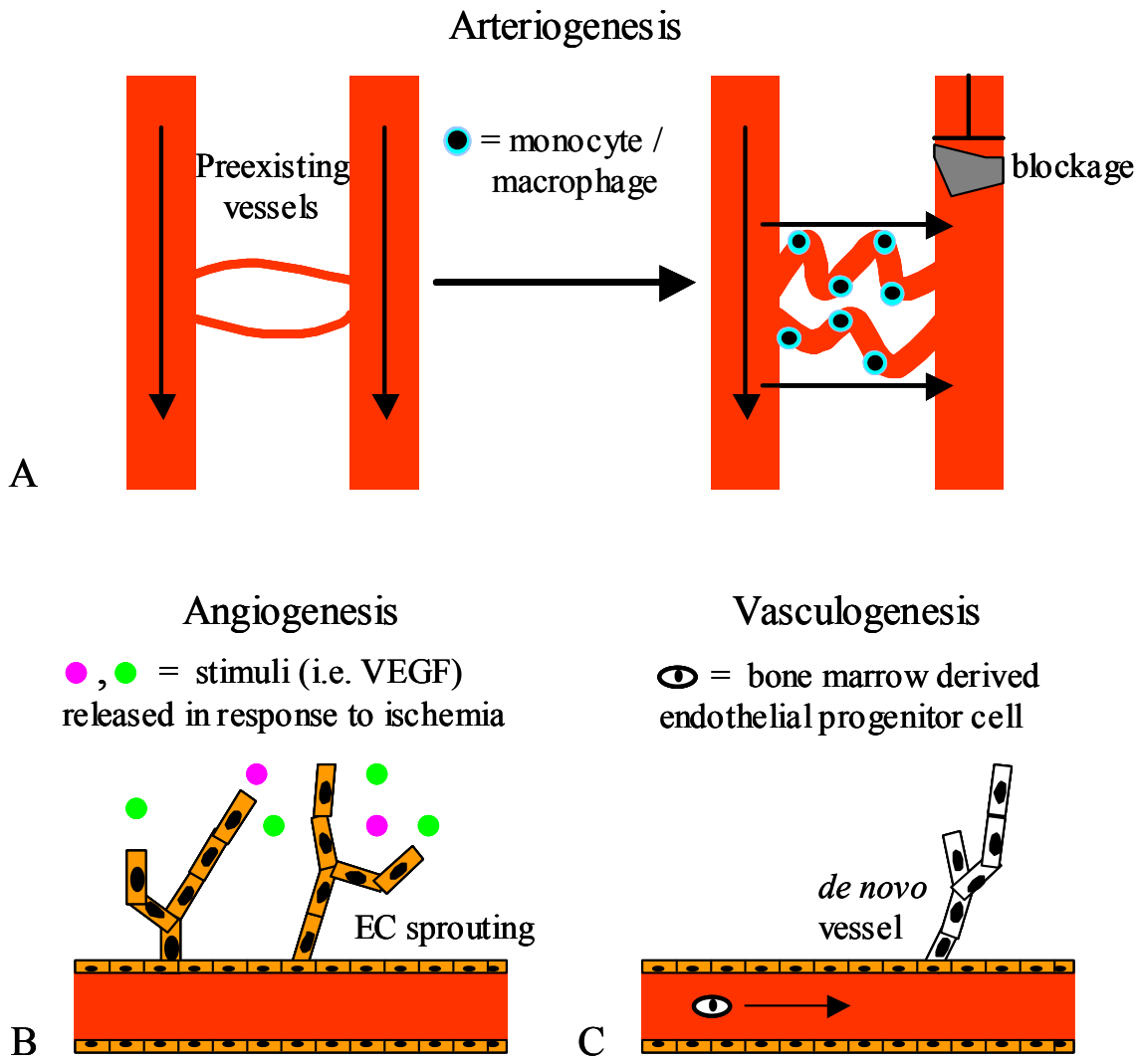

Figure 2.2. Three modes of postnatal vascular growth that are thought to occur *in vivo*. (A) Arteriogenesis involves recruitment of pre-existing vessels to remodel and increase their blood flow capacity. (B) Angiogenesis entails sprouting of new capillaries from existing vasculature. (C) In vasculogenesis, or *de novo* vessel formation, bone marrow derived cells home to the sites of ischemia and participate in neovascularization.

within the lumen of a preexisting vessel, partitioning the remodeling vessel into two new capillaries. Sprouting angiogenesis involves basement membrane degradation, endothelial cell migration toward angiogenic factors, endothelial cell proliferation, lumen formation, and vessel stabilization by basement membrane production and association with periendothelial cells (8). Finally, there is evidence that vasculogenesis or *de novo* blood vessel formation by bone-marrow derived endothelial progenitor cells may play a role in postnatal vessel growth, although this remains controversial (9,10). Arteriogenic recruitment of preexisting collaterals is widely believed to be the best means for reestablishing normoxia following arterial occlusion since it occurs relatively quickly and leads to formation of larger arteries that have higher blood flow capacity compared to nascent capillary structures (5).

Control of Vascular Growth

VEGF and FGF

The majority of researchers studying treatments for ischemic disease have focused on the clinical potential of administering vascular endothelial growth factor (VEGF) and fibroblast growth factor (FGF) to enhance blood flow via new vessel formation. This idea, termed therapeutic angiogenesis, has been applied for both myocardial ischemia and peripheral arterial disease. Numerous efforts have been directed at testing the efficacy and safety of delivering these growth factors as recombinant proteins or via gene therapy for stimulation of angiogenesis and arteriogenesis in ischemic tissues.

VEGF was first discovered over 20 years ago, when it was originally termed vascular permeability factor due to its inherent ability to promote vascular leakage (11-13). It is up regulated in response to ischemia (14) and serves as a well-known mediator

of both physiological and pathological angiogenesis through promotion of proliferation, survival, and migration in endothelial cells. There is a 5-member family of VEGF proteins that includes VEGF-A, VEGF-B, VEGF-C, VEGF-D, and placental growth factor. These factors act through three tyrosine kinase receptors (VEGFR-1, -2, -3) to activate downstream signaling pathways. VEGF-A (commonly referred to as VEGF) has been the most researched as a potential therapeutic agent. The importance of VEGF-A in vascular development is clearly illustrated by the fact that knocking out VEGF-A or either of its receptors (VEGFR-1 and VEGFR-2) results in embryonic lethality (15-17). Other growth factors, such as FGF, complement the angiogenic activity of VEGF, and there is likely considerable cross-talk between these factors (18).

The FGF family consists of as many as 25 members which are named in consecutive order (FGF-1, -2, etc) (19). The different FGF family members contain a highly preserved core amino acid sequence that leads to structural homogeneity between family members (20,21). There is thought to be significant redundancy in the functionality of the FGF family members, as evidenced by the relatively mild phenotype that results in FGF-1, FGF-2, and even FGF-1 / FGF-2 double knockouts (22-24). FGFs act on numerous cell types and are involved in a variety of biological effects including but not limited to development, cell proliferation and migration, wound healing, and tumorigenesis. The effects are believed to be transmitted through FGF activation of signal transduction pathways via its family of 4 tyrosine kinase receptors (FGFR1-4) as reviewed by Powers and colleagues (25). FGF-1 (acidic FGF) and FGF-2 (basic FGF) are the two best characterized family members and have been studied extensively for

their roles in angiogenesis. Up to this point, clinical trials have focused on therapeutic potential of FGF-2 for stimulation of angiogenesis.

Preclinical data from animal studies using both VEGF and FGF have shown tremendous promise in a variety of animal models (26-30). However, many of the initial human clinical trials did not corroborate these results and have shown almost no improvement in clinical outcome. The VIVA, RAVE, FIRST, and TRAFFIC trials are examples of the most prominent double-blind, placebo controlled trials to date. The VIVA (Vascular endothelial growth factor in Ischemia for Vascular Angiogenesis) trial was a double-blind, placebo-controlled study that found that delivery of recombinant VEGF produced mild improvement in angina but did not significantly affect other endpoints analyzed (31). The RAVE (Regional Angiogenesis with Vascular Endothelial growth factor) trial, which tested adenoviral VEGF gene transfer for the treatment of peripheral artery disease, found no increase in exercise performance or quality of life as a result of treatment (32). FIRST (FGF Initiating RevaScularization Trial) involved delivery of recombinant FGF-2 for treatment of coronary artery disease, which produced a trend towards decreased angina at 90 days but no improvement in exercise tolerance or myocardial perfusion (33). Lastly, the TRAFFIC (Therapeutic Angiogenesis with Recombinant Fibroblast Growth Factor-2 for Intermittent Claudication) trial found peripheral arterial disease to be modestly alleviated through delivery of recombinant FGF, which was found to increase peak walking time (34).

Unfortunately, as mentioned, there have been a limited number of double blind, placebo controlled clinical trials to test therapeutic agents, and these studies have found only mildly promising results. However, these trials have shown enough clinical

potential to warrant further investigation, and one could postulate that therapeutic angiogenesis may be a viable clinical option with the optimal growth factor, appropriate dosage, most effective delivery method (recombinant protein versus viral vector or naked DNA gene therapy), and location of delivery (intracoronary, intravenous, intramuscular, etc). In addition, temporal considerations must be made, particularly in the case of acute myocardial infarction (AMI), in order to determine the ideal delivery protocol (time post-AMI and single versus multiple treatments). More research is clearly needed in multiple areas in order to find the optimal clinical protocol for delivery of pro-angiogenic treatments. Also, it is imperative that scientists are able to define the roles of all factors involved in this process, and clinicians must carefully consider the roles of ECM mediators in addition to the potential synergistic effects from using combined growth factor therapies. Hence, it is possible that, ultimately, the optimal treatment will contain a "cocktail" of therapeutic agents, which could potentially include not only growth factors, but also other "extracellular modulators" and progenitor or stem cells that may aid in vascular regeneration.

The Role of ECM

The cellular components of the postnatal vascularization process are coordinated by direct cell-cell communication, paracrine and autocrine growth factor stimulation, and lastly, cues provided by the extracellular environment. Type I collagen, laminin, fibronectin, vitronectin, and osteopontin are among the many ECM proteins thought to play a role in blood vessel formation and remodeling. ECM components provide the structural scaffolding that maintains the organization of vascular cells into blood vessels and also initiate signals that stimulate specific cellular responses. ECM generated signals

are primarily mediated through the integrin receptors and elicit events such as cellular survival, proliferation, and migration. The integrins are heterodimeric transmembrane receptors that consist of the combination of one α and one β subunit. There are 18 α and 8 β subunits known to exist, and through different combinations of these subunits, about 24 unique integrins are generated. As reviewed by Serini *et al*., currently, nine of these integrins have been characterized for their implications in blood vessel formation (35). In general, docking of these integrins to the ECM activates signaling pathways through integrin-associated kinases and other signaling molecules located on the intracellular side of the cell membrane. These signaling pathways then propagate to the nucleus to alter gene expression and trigger a subsequent cellular response.

ECM proteins are able to induce specific cellular responses based upon the integrin(s) that they bind. For example, collagen and fibronectin are thought to act through $\alpha_1\beta_1$, $\alpha_2\beta_1$, $\alpha_5\beta_1$, and $\alpha_v\beta_3$ to activate endothelial cells and promote proliferation and tube formation, while laminin rich matrices promote endothelial stabilization and maturation through $\alpha_6\beta_1$ and $\alpha_3\beta_1$ (36). In this sense, it is thought that the multiplicity of proteins in the ECM is able to function cooperatively to orchestrate the appropriate cell signals. However, based on the large degree of functional overlap, it is impossible to assign clearly defined roles to each ECM and integrin constituent. For instance, $\alpha_v\beta_3$, one of the most extensively studied angiogenesis-related integrins, binds specifically to the arginine-glycine-aspartate (RGD) motif, a peptide sequence common to a number of ECM proteins including collagen, fibronectin, vitronectin, and osteopontin. Through these overlapping pathways, it is possible for the same integrin to convey different signals depending upon its mode of activation and the surrounding biological milieu.

The integrin(s) that control the ECM signaling pathways also depend upon the cell's activation by other factors. For example, studies have shown that the $\alpha_v\beta_3$ signaling dominates during FGF induced angiogenesis, while $\alpha_v\beta_5$ dictates VEGF induced angiogenesis (37). Other modes of cross talk are also thought to exist between the ECM and other angiogenic factors. For instance, VEGF induces endothelial expression of $\alpha_1\beta_1$ and $\alpha_2\beta_1$, sensitizing these cells to ECM effects (38). Furthermore, the ECM is thought to immobilize growth factors to the matrix in order to make them readily available to cellular receptors and to provide directional cues to the intracellular migratory machinery. One example of this paradigm is illustrated by a study that showed that VEGF binds directly to fibronectin in a way that enables them to serve as signaling cofactors in the angiogenesis process (39). It is obvious that ECM-integrin signaling represents an intricate system that plays a significant role in postnatal vascularization. While much knowledge has been garnered on the regulation of neovascularization at this level, there is clearly a lot left to learn about the complexities of this system, including its interrelationship with other growth factors and cellular activities that control vascular growth.

The Role of Monoctyes / Macrophages

Although macrophages are not thought to be a substantial constituent of normal, healthy vasculature, it is well-known that they localize to the vascular wall at sites of angiogenesis and arteriogenesis where they play an important role in modulation of these processes (6). Wolfgang Schaper has been a leader in this field and has extensively studied the role of these cells in models of ischemia since his initial observations of monocyte homing to the inner vascular surfaces of forming collateral vessels in a model

of coronary artery stenosis in dogs (40). It was only shortly after this publication that activated macrophages were reported to also play a role in angiogenesis (41). Subsequent studies have shown a direct functional link between circulating monocyte concentration and arteriogenic collateral vessel formation (42,43).

Monocyte Chemotactic Protein 1 (MCP-1) is thought to be the primary stimulus for induction of monocyte infiltration and is known to play a role in mediating inflammatory related neovascularization (44). Treatment with VEGF and FGF-2 has been found to induce MCP-1 expression in endothelial cells indicating crosstalk between MCP-1 and other angiogenic growth factors (45,46). To further support this hypothesis, delivery of MCP-1 has been shown to accelerate collateralization and recovery in hind limb ischemia models in a wide range of rabbit, pig, and mouse studies (47-53). Conversely, animals deficient in MCP-1 or CCR2-chemokine receptor, an MCP-1 receptor, have been shown to display reduced monocyte / macrophage infiltration and collateral formation (54,55). These studies indicate that, once they home to the vascular wall, monocytes produce growth factors and proteases that induce vascular endothelial and smooth muscle cell proliferation and stimulate remodeling of the vascular wall in order to satisfy increased blood flow demands. Taken together, these reports have convincingly shown that monocytes play an important role in mediating collateral vessel formation and that stimulating monocyte homing and survival at sites of arteriogenesis enhances collateral blood vessel formation.

Endothelial Progenitor Cells

Nearly 10 years ago, Asahara and colleagues first isolated circulating endothelial progenitor cells (EPCs) from peripheral blood and showed that these cells were capable

of homing to sites of ischemia and incorporating into angiogenic vasculature (56). Shortly thereafter, using bone marrow transplantation techniques, Asahara *et al*. and Shi *et al*. reported that these circulating EPCs were mobilized from bone marrow and were capable of endogenously incorporating into angiogenic vasculature in skin wounds, sites of peripheral and myocardial ischemia, and developing tumors, in addition to lining the flow surfaces of implanted vascular grafts (9,57). These discoveries spurred a rapid expansion in EPC research, which has created a plethora of generally positive, yet controversial data due to the lack of standardized cell isolation protocols and functional assays in this nascent field.

Since the inception of EPC research, numerous animal studies have been performed in multiple species to measure the regenerative and reparative potential of EPCs. These studies have generally shown accelerated recovery following EPC delivery in animal models of myocardial and peripheral ischemia (reviewed in (58)). Many of these authors have reported direct incorporation (albeit to varied degrees) of transplanted progenitor cells into the vascular endothelium *in vivo* using angiogenesis models of hind limb, myocardial, and cerebral ischemia and tumorigenesis (59-65). However, this notion has been increasingly challenged. Some recent studies have claimed that few or no EPCs actually incorporate into the endothelium, leading to the idea that the angiogenic effects of these progenitors may be primarily due to paracrine stimulation of tissue resident cells (66-71).

Human studies have further indicated that EPCs play a role in general endothelial maintenance and possess the potential to stimulate therapeutic angiogenesis and accelerate recovery following myocardial infarction. It has been reported that EPC

counts serve as a potential marker of endothelial function and are inversely proportional to cardiovascular risk (72-74). Likewise, diabetes, smoking and hypercholesterolaemia have been shown to decrease EPC counts, while statin therapy and regular exercise have been found to increase EPC number (73,75-80). In terms of therapeutic angiogenesis, the TOPCARE-AMI (Transplantation of Progenitor Cells And Regeneration Enhancement in Acute Myocardial Infarction) study investigated effects of both circulating EPC and bone marrow derived progenitor infusion following AMI. In this relatively small trial, safety and favorable effects on left ventricle (LV) remodeling were found following infusion of both progenitor cell types (81). In a similar AMI trial, autologous bone marrow was found to lead to improved LV function relative to controls (82).

One major shortcoming in the field of EPC research has been the inconsistent definition of the EPC itself. Several animal studies have utilized unpurified bone marrow, which likely contains EPCs in addition to other progenitor cells. Others have used magnetic bead or fluorescence activated cell sorting to obtain enriched cell populations based on co-uptake of acetylated ldl / lectin or expression of surface markers such as VEGFR2, CD31, CD45, CD105, CD133, Sca1, vWF, and VE-cadherin, with the most commonly used technique being isolation based on VEGFR2, CD31, and/or CD133 expression. It remains unclear whether different cell selection methodologies yield different cell populations or the same cell population at different stages of maturity, and it has not been clearly determined which if any of these populations might possess the greatest therapeutic potential. Unfortunately, this lack of a consistent EPC definition and isolation protocol makes it difficult to draw conclusions based on direct comparisons between studies. Clearly, many questions and controversy over EPC biology remain to

be resolved. However, these cells undoubtedly possess great therapeutic potential, and preliminary success in animal and human trials demands further investigation and design of larger clinical trials.

Inhibition of Neovascularization

While the discussion up to this point has primarily focused on factors that stimulate neovascularization, excessive angiogenesis is believed to exacerbate certain pathological conditions including tumorigenesis, rheumatoid arthritis, and intraocular neovascular syndromes. In this context, research has concentrated on inhibition of neovascularization. It has been 35 years since Folkman originally proposed the idea that inhibition of angiogenesis could serve as a means for stopping tumor growth (83). Then, in 1993 it was shown that VEGF neutralizing antibodies significantly attenuate tumor angiogenesis and growth *in vivo*, but it wasn't until over ten years later that FDA approval was granted for the first anti-angiogenic agent for cancer therapy, bevacizumab (Avastin; Genentech) (84,85). While bevacizumab is a neutralizing VEGF monoclonal antibody, many other approaches including but not limited to inhibiting VEGF receptor activation and administering soluble VEGF receptor or "VEGF traps" have been found to be effective means for anti-cancer therapy and are currently undergoing clinical tests (reviewed in (86,87)). Meanwhile, analogous approaches for inhibition of neovascularization have also shown merit for treatment of macular degeneration and are being used clinically (88-90). In addition to antagonism of VEGF signaling, other methods of angiosuppression are being tested clinically including exogenous delivery of naturally occurring angiogenesis inhibitors, inhibitors of proteases that facilitate ECM

degradation and vascular sprouting, and inhibitors of endothelial integrin (i.e. $\alpha_v\beta_3$) binding and activation (91-93).

Experimental Models and Endpoints for Studying Angiogenesis

With the recent expansion in research related to control of postnatal vascular growth, the requirement for quantitative, physiologically relevant models for preclinical studies has become increasingly apparent. Although *in vitro* studies can serve as a useful initial screening tool for potential stimulants or inhibitors of endothelial cell function and growth, their relevance is often compromised by the fact that they lack the inherent complexity and milieu of cell types and factors present *in vivo*. On the other hand, *in vivo* animal models obviously present the most appropriate systems for testing angiogenic substances, yet they often lack reproducibility due to technical difficulty and variability between animals, physiologically relevant stimuli, and endpoints amenable to quantitative analysis. The subsequent discussion on *in vitro* and *in vivo* techniques covers some of the common and most relevant angiogenesis models but is by no means meant to be all-inclusive.

Cell proliferation, migration, and tube formation in response to specific angiogenic modulators comprise the majority of *in vitro* studies. Cell proliferation studies typically measure replicating cells through incorporation of a fluorescent or radiolabeled thymidine analogue or quantification of total cell number using colorimetric / fluorescent readings based on dye-DNA complexes. Migration and chemotaxis assays typically employ cell culture inserts that can be placed into multi-well tissue culture plates. The cells are seeded into these inserts, which contain a membrane with a pore size ranging from approximately 3-10 microns. Then, the chemotactic agent is placed into the

media in the bottom of the well in order to stimulate cell migration from the top of the membrane into the lower chamber containing the chemotactic substance. Lastly, at a chosen endpoint, the remaining cells can be removed from the top of the membrane, and the cells that have migrated to the lower side are stained and counted using microscopy. The monolayer scratch assay provides a separate and somewhat crude, but effective migration assay. This technique involves creation of a "wound" in the endothelial monolayer using a pipette tip and then monitoring migration (and proliferation if the endpoint is long enough) of the cells into the scratch. Lastly, endothelial cells can be cultured in 3-D in matrigel to assess tube-forming capabilities of endothelial cells under specific stimuli. Each of these *in vitro* methodologies possesses merit in certain applications, particularly as an initial platform for screening the effects of potentially pro- or anti-angiogenic substances. These assays are well controlled, repeatable, and generally quantitative, yet their relevance can be limited by the absence of many of the important modulators present *in vivo*. One problem is that, due to repeating tissue culture passaging, cells are selected for a more proliferative phenotype than what is present *in vivo*. Also, cells are often isolated from a species (i.e. bovine) and from an anatomical location (ie. vein or large arteries such as aorta) that don't necessarily make them good models of the human microvascular endothelium that would typically participate in an angiogenic response.

As an intermediate to *in vitro* and *in vivo* studies, researchers commonly use *ex vivo* organ culture assays. The most common of these is the aortic ring vascular sprouting assay. This assay involves embedding aortic rings into either collagen gels or fibrin clot and has been utilized in explants from both mice and rats. Rat explants have

been found to sprout endothelial tubes in serum free conditions, while mouse specimens require homologous serum in order to consistently form angiogenic extensions from the aortae (94-96). This assay provides a more complete environment including non-endothelial cell types, lacks artifacts introduced from extended tissue culture passaging, yet offers a good deal of the experimental control afforded by *in vitro* studies. However, as mentioned for *in vitro* studies, use of the aorta is not an ideal choice for modeling the microvascular endothelium.

Following initial screening tests based on *in vitro* and / or *ex vivo* studies, animal experimentation is a necessity prior to testing potential angiogenic modulators in human trials. The chick chorioallantoic membrane (CAM) is one of the oldest, simplest, and most popular *in vivo* angiogenesis assays (97,98). It is generally considered an *in vivo* assay because it is a test carried out on a whole animal (embryo). In this assay, an angiogenic substrate is placed directly onto the CAM and then tested for its ability to either inhibit or increase vascular development in this area of the embryo. This assay is relatively easy, inexpensive, and high throughput, but doesn't provide maximum utility due to its use of chick cells, lack of quantification, and difficulty in discriminating between effects of the tested agent and the rapid vascular changes that are naturally occurring during embryonic development.

The next group of commonly employed *in vivo* angiogenesis models involves subcutaneous placement of angiogenic substrates. These types of models involve implantation of a sponge or matrigel plug under the dorsal skin to induce neovascular ingrowth (99-102). This model also allows for delivery of angiogenic modulators, which can be done using osmotic mini-pumps. This procedure is simple and easy to replicate,

but it does not use a site where angiogenesis typically occurs *in vivo* and is confounded by the non-specific inflammatory response the results from implantation of the material.

Corneal angiogenesis assays are another popular mechanism for *in vivo* screening of angiogenesis related compounds. The cornea is naturally avascular and therefore provides a good test bed for neovascularization studies, and this model has been used in multiple species including rabbits and mice (103-106). In this method, a small pocket is made in the cornea, and slow release formulations of angiogenic factors or tumor cells/tissue can be introduced into this pocket in order to induce vascular growth toward this stimulus. For testing anti-angiogenic therapies, the therapeutic agent is generally administered systemically and tested for its ability to inhibit angiogenesis towards the pro-angiogenic corneal implant. Neovascularization can be tracked longitudinally *in vivo* using a stereoscope or with histology at predetermined endpoints. The main advantage of this assay is that all measurable vasculature is neoangiogenic in nature and does not have to be discriminated from preexisting vessels. However, this assay is technically demanding, and the fact that angiogenesis does not normally occur in avascular regions *in vivo* diminishes the assay's relevance.

The last set of models to be discussed involves ischemia and arterial blockage induced vascular growth. These animal studies have been performed in a variety of species, particularly rats, rabbits, and mice, and typically test the effects of agents for therapeutic stimulation of neovascularization for alleviation of peripheral or coronary artery disease (107-110). These models involve ligation of a proximal conduit artery (ie. femoral artery), which provides a reproducible, physiologically relevant stimulus for a vascular response. This insult stimulates a combination of ischemia-induced

angiogenesis in addition to arteriogenesis triggered by changes in arterial flow patterns within the preexisting vasculature. This complex stimulus is likely the most relevant model of human ischemic diseases, but offers the added problem of discriminating neoangiogenic and arteriogenic vessels from each other and from the preexisting vasculature. In addition, this model is time intensive and relatively expensive due to the number of animals necessary to detect differences due to inherent animal-to-animal variability and lack of sensitive methods for endpoint quantification. This model is also particularly useful for studies of transgenic or knockout animals since it can be readily applied to mice (107). When considering methods for inducing tissue ischemia versus the previously discussed models, one must consider the different levels of complexity and potential merit of each model depending upon the setting being studied (pro- versus anti-angiogenic therapy) and the available resources.

As mentioned, in addition to inherent animal-to-animal variability and user variability due to technical difficulty in implementation of animal models, *in vivo* studies are further complicated by lack of objective, quantitative methods for endpoint analysis. It is generally understood that collateral vessel formation can help to functionally compensate for obstructive vascular lesions in patients with atherosclerosis and that animal models of vessel blockage are vital to preclinical research that tests the efficacy and safety of therapeutic agents delivered to stimulate reperfusion of ischemic tissues. While the utility of the hind limb ischemia model is particularly well established in this arena, the available methodologies for quantification of collateral vessel development in this setting are not ideal.

Investigators have utilized a variety of techniques to evaluate vascular structures in this animal model. Histology is commonly employed to analyze capillary or arteriole density, but it is relatively subjective, not truly quantitative, two-dimensional (2-D), and not necessarily representative of vascularity throughout the entire sample. Laser Doppler perfusion imaging (LDPI) has been used to analyze blood flow in hind limbs because it offers quantitative data and a good measure of tissue perfusion (5,107,111-113). However, this technique does not provide anatomical information and is limited by the fact that only the most superficial, cutaneous blood flow is measured. Another popular technique, X-ray microangiography, provides high-resolution, 2-D angiograms of the hind limb vascular anatomy but lacks the ability to employ a quantitative, volumetric analysis (113-115). Injection of colored or fluorescent microspheres presents a method for longitudinal study of reconstitution of perfusion to ischemic tissues using quantitative spectrophotometry or flow cytometry analyses (116-120). However, the required arterial catheterization or injection of microspheres into the left ventricle or atrium presents a considerable challenge in mice because of their small size. Other imaging modalities such as magnetic resonance angiography and positron emission tomography serve as viable methods for analyzing vascularity, but the resolution of these methods is typically not sufficient for studies involving small animals. Micro-CT has emerged as a promising technology that can overcome several of the challenges associated with evaluation of vascular networks. Recently, vascular imaging procedures have been developed for small animal models based on the use of perfused contrast agents and X-ray micro-CT (121-129). The goal of these studies has been to visualize 3-D vascular networks in

organs (i.e. heart and kidneys) or tumors, and more recently, we have extended these techniques into analysis of neovascularization and collateral vessel development (130).

Micro-CT Imaging

Hounsfield originally introduced computed tomography in the early 1970's, an invention that eventually earned him a Nobel prize (131,132). In the late 1980's, Feldkamp *et al*. pioneered the field of three-dimensional computed tomography on the micron scale (micro-CT) for analysis of bone micro-architecture (133). Since then, the field of micro-CT has advanced tremendously, and commercially available micro-CT systems have become a major component of many research laboratories. These systems combine a microfocus X-ray source, a detector, and a cone-beam reconstruction algorithm to nondestructively recreate a 3-D object (see Figure 2.3 A). Using this setup, the specimen is rotated on a fixed stage while an X-ray source is passed through it. However, newer generation scanners exist that allow for *in vivo* scanning of anesthetized animals. In these systems, the animal remains stationary and the x-ray source and detector rotate around the specimen. The detector then records the intensity of the attenuated X-ray beam that has passed through the specimen. This projection value recorded by the detector is a function of the thickness and linear attenuation coefficient of the material through which the X-ray beam has passed. This relationship can be described by Lambert's law of absorption where I is the recorded beam intensity after passing through the specimen, I_o is the unattenuated beam density, μ is the linear attenuation coefficient of the material within the sample, and x is the thickness of the material.

Equation 2.1. $$I = I_o e^{-\mu x}$$

Based on the intensity of the X-ray projections recorded as the specimen (or source) is advanced through multiple rotational positions, serial, two-dimensional attenuation maps (tomograms or slices) are reconstructed from the raw data using a cone beam filtered backprojection algorithm (see Figure 2.3 B) (134). During the reconstruction of image projections, a grayscale value that represents the capacity of the material within that space to attenuate x-rays is assigned to each voxel. These grayscale values within the 2-D slices represent the linear attenuation coefficient of the material within the voxel space, which is a function of the X-ray source and the atomic composition of the material sample. Then an image threshold is defined, which represents the cutoff grayscale (attenuation) value that partitions the image voxels into either the background or the segmented object. During the thresholding process, if the grayscale value for the voxel is higher than the assigned threshold, it remains in the 3-D image as part of the segmented object. After application of the global attenuation threshold value, the binarized tomograms are used to render a 3-D image of the segmented object. Morphometric analysis based on model independent, direct distance transform methods can be subsequently applied to the 3-D images to quantify parameters of morphology, anisotropy, and connectivity (135-137).

As mentioned, due to the inherent radiodensity of hard tissue, initial micro-CT related work was done in the bone field. However, more recent applications in micro-CT imaging have evolved into analysis of biomaterials, soft tissues, and skeletal development (138,139). However, due to the comparatively low radiodensity of soft tissues and vasculature, application of a radiopaque contrast agent is necessary. For these applications and countless others not mentioned here, micro-CT presents many

advantages over other, traditional methods of specimen imaging and analysis. Since the imaging process is nondestructive, the internal features of the same sample may be examined multiple times, and samples remain available after scanning for additional biological or mechanical testing. Specifically, micro-CT is often advantageous over other methods because it provides high resolution, quantitative, 3-D, and completely objective data analysis. Relative to micro-CT, histology and microscopy, the traditional standards in tissue specimen analysis, require destructive tissue processing, lack the ability to employ a quantitative 3D analysis, and require increased sample preparation and analysis time.

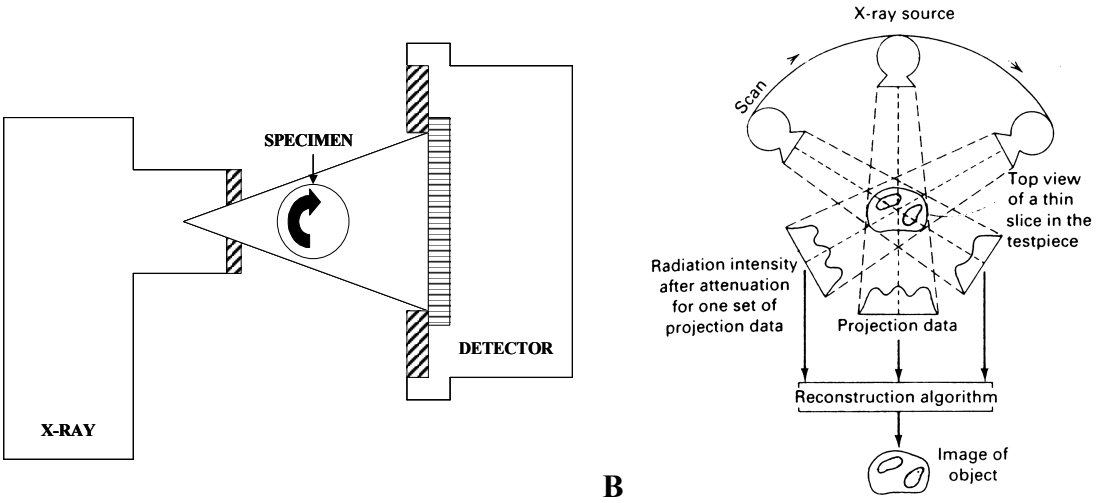

Figure 2.3. Micro-CT Components and Image Reconstruction. (A) Schematic view of the basic components of micro-CT imaging systems. An X-ray source is passed through a rotating specimen, and the transmitted signal is detected on the other side. (B) Schematic of the computed tomography process and illustration of the method for reconstruction of micro-CT images from X-ray projections (borrowed from (140)).

Bone Fracture Healing

Unlike soft tissue injuries, which generally result in scar tissue formation, bone healing involves regeneration of the native tissue in a unique process where the original tissue properties are largely restored. The capacity for true tissue regeneration in adults is thought to be due to the fact that fracture repair to a large degree recapitulates the process of embryonic skeletal formation (141). The majority of bone fracture healing cases involve both intramembranous (direct bone formation) and endochondral ossification (bone formation through a cartilage intermediate). Rarely does primary bone healing occur through an intramembranous ossification route, and this is thought to occur only when contact is restored and rigidly fixated between fractured bone ends (142). Conversely, the endochondral route of bone repair is thought to dominate in less stabilized fractures, and it is this process that closely resembles fetal endochondral ossification (141,143).

The majority of bone healing occurs through indirect fracture healing, which involves a combination of intramembranous and endochondral ossification. This involves a highly coordinated cascade of biological events that includes, in temporal order, hematoma formation, inflammation, soft cartilaginous callus formation, neovascularization, osteoblastic callus mineralization, and osteoclastic remodeling of the woven bone hard callus into lamellar bone (144). The morphological changes that occur during fracture healing are highlighted in the histology images shown in Fig 2.4. This cascade of events is orchestrated by a variety of cell types, starting with bone marrow, periosteal, and tissue resident cells which subsequently chemoattract or differentiate into inflammatory cells, endothelial cells, fibroblasts, chondrocytes, osteoclasts, osteoblasts,

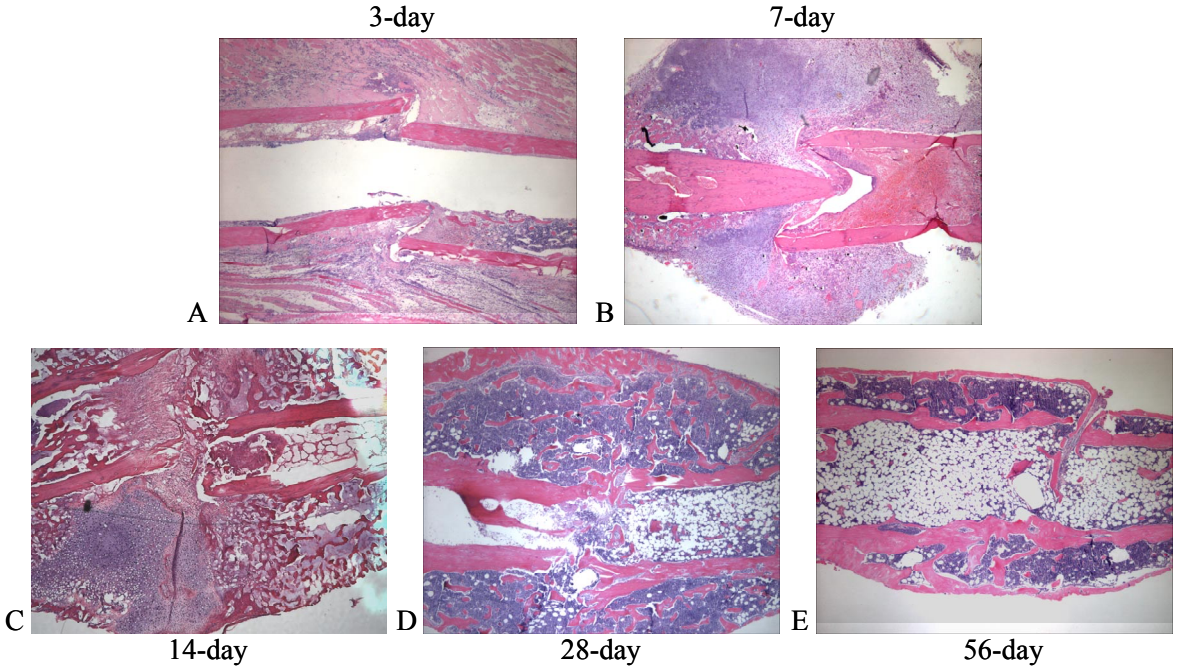

Figure 2.4. Histological time course of fracture healing. H&E staining of 5 micron paraffin embedded histological sections is shown to illustrate the time course of fracture healing in a mouse femoral fracture model. Note that surrounding soft tissues were left intact on the 3-day histological specimen, but the fracture callus was dissected away from the surrounding musculature at other time points. (A) At 3 days post fracture, inflammatory cells have migrated to the fracture site and produced cytokines that induce MSC migration, proliferation, and formation of an initial layer of fibrous connective tissue for stabilization of the fracture site. (B) By 7 days post fracture, endochondral ossification has ensued, as indicated by the proliferation and differentiation of MSCs into a cartilaginous soft tissue callus at the fracture site. Note that a modest amount of intramembranous bone formation can be seen at the periosteal region of the cortex immediately adjacent to the fracture site. Also, neovascularization, while not evident in these images, has begun to occur at the ends of the fracture callus. (C) Later, by 14 days post fracture, chondrocyte hypertrophy is evident within the remaining soft fracture callus, and cartilage adjacent to the fracture has begun to mineralize and undergo resorption. At this point a substantial amount of vascular invasion has occurred, which is thought to be directly coupled to onset of mineralization and chondrocyte removal from the soft callus. (D) By 28 days, the mineralized cartilage has been replaced by remodeling woven bone, and a bony bridge has formed across the fracture gap. (E) At 56 days, the woven bone of the fracture callus has remodeled inward, and the remaining tissue is continuing to approach the structure of the native lamellar bone.

and osteocytes. During this complex sequence of biological activity, functionality of these cell types is regulated by a variety of cytokines, growth factors, and matricellular proteins that induce differentiation, chemotaxis, and haptotaxis of the cell types responsible for mediating these events.

Recent studies have helped to elucidate the roles of many of these signaling molecules in bone healing. In initial stages of healing, pro-inflammatory cytokines such as interleukin-1 and tumor necrosis factor-alpha have been found to be highly expressed by inflammatory cells and are thought to play an important role in initiating the repair process by stimulating chemotaxis and proliferation of other cell types at the fracture site (145,146). Other studies have detailed the importance of soluble growth and differentiation factors during fracture healing. For example, the family of bone morphogenic proteins (BMPs), a subset of the transforming growth factor-beta superfamily, has been thoroughly characterized for induction of osteogenesis at fracture sites and is utilized clinically to promote bone regeneration (147). The BMPs, which bind extracellular receptors and activate intracellular signaling cascades, are thought to be the key regulators of bone formation and have also been characterized for their ability to couple the biological processes of angiogenesis and bone formation (148-150). This coupling is particularly important considering that vascular invasion of the fracture callus is thought to be a necessity for normal bone repair, specifically for triggering conversion of the cartilage callus into the mineralized, hard callus. For example, Street *et al* have shown that VEGF, a known promoter of angiogenesis, stimulates neovascularization and promotes fracture healing, while treatment with angiogenesis inhibitors that specifically target vascular cells blocks fracture healing and produces atrophic nonunions (151,152).

Furthermore, it has been shown that fracture repair is impaired in MMP9 deficient mice as a result of reduced angiogenic capacity in these mice (153). Lastly, ECM proteins play an important role in regulation of bone healing. As reviewed by Alford *et al*., extracellular matrix (ECM) proteins, while not always vital for normal embryonic bone development, play an important role in mediating cellular function and serve as important modulators of bone regeneration (154). Non-collagenous ECM proteins interact with other matrix proteins, cellular receptors such as integrins, and soluble growth factors and proteases. In this way, they play a role in modulation of matrix organization and remodeling, cellular function, and hence, the fracture healing process. Further understanding of the intricate interplay between this diverse set of cell types, endogenous factors, and matrix proteins is a necessity for the development of improved therapeutic strategies for promoting bone repair.

Osteopontin

OPN Structure and Function

OPN, generally an ECM protein, is synthesized as a 34-kDa protein and is especially prominent in the matrix of mineralized tissues (see Figure 2.5 for an illustration of some of the features of OPN). It undergoes a large degree of post-translational modification and, depending upon tissue type, is secreted with varied degrees of phosphorylation and glycosylation. It also binds to hydroxyapatite, contains a thrombin cleavage site, and, due to its acidic nature and negative charge, binds to calcium. In addition, OPN possesses multiple cell recognition motifs and functions in a variety of biological processes including but not limited to inflammatory response, immunity, angiogenesis, wound repair, tumor formation and metastasis, cell adhesion,

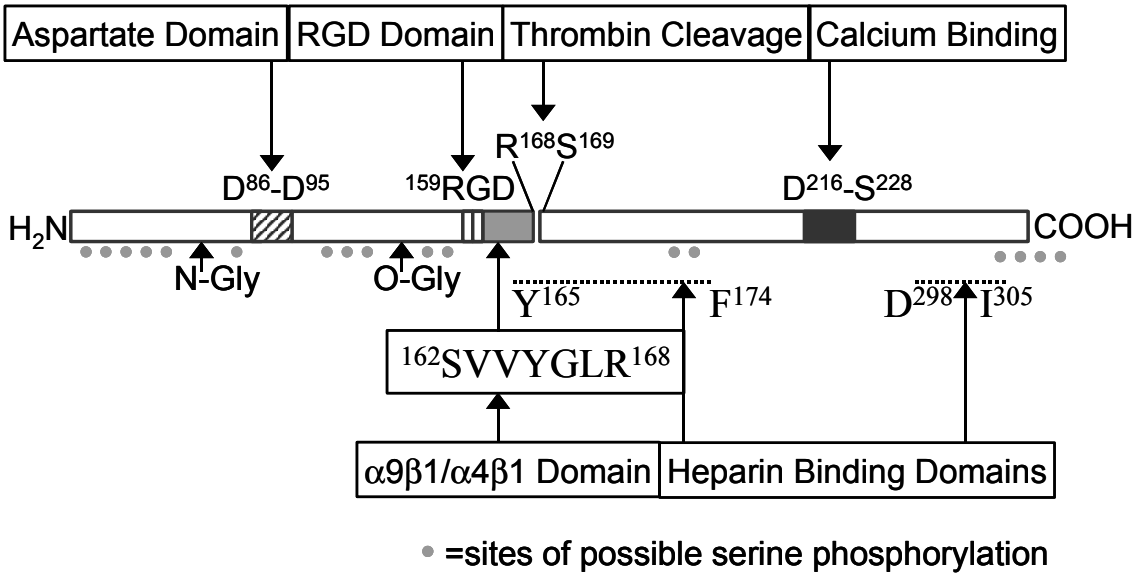

Figure 2.5. Schematic of human OPN. The structure shown here highlights the binding domains of OPN that are thought to confer its biological activity. O-glycosylation and phosphorylation sites are meant to be representative and can vary depending upon tissue localization, etc. Schematic redrawn and adapted from (155).

cell migration, and bone mineralization and remodeling. Through its multiple cellular binding sites, OPN is able to interact with multiple cell surface receptors and activate intracellular activity that elicits downstream cellular functions. While OPN is generally considered to fall into the general group of "noncollagenous ECM proteins", it has more recently become known by some as a matricellular protein (156). This categorization has been created for nonfibrillar ECM proteins that mediate cellular functions by providing a functional link between cell surface receptors, ECM molecules that are primarily structural in form, and more biologically active cytokines, growth factors, and proteases. By these means, it is likely that OPN is capable of eliciting a diversity of specified biological responses based on local content of the structural matrix, availability of

bioactive molecules, interactions with different cell types or surface receptors, and its own state of cleavage, phosphorylation, and glycosylation.

OPN Cellular Interactions

The integrin family and CD44 (hyaluronic acid receptor) are the two classes of cell surface receptors known to interact with OPN. As mentioned previously, integrin-mediated signals provide a vital link between the cells and their environment and represent an important point of control in the neovascularization process. OPN interaction with heterodimeric integrin receptors is not only able to mediate cellular adhesion to the matrix, but also activate intracellular second messengers, which propagate signals to the nucleus and alter gene expression. The integrin receptors known to interact with OPN include $\alpha_v\beta_1$, $\alpha_v\beta_3$, $\alpha_v\beta_5$, $\alpha_4\beta_1$, $\alpha_5\beta_1$, $\alpha_8\beta_1$, and $\alpha_9\beta_1$. The majority of these interactions occur through the RGD site, a common three amino acid recognition sequence found in OPN and other ECM proteins, except for $\alpha_4\beta_1$ and $\alpha_9\beta_1$, which interact with a more novel serine-valine-valine-tyrosine-glycine-leucine-arginine (SVVYGLR) binding sequence (155,157-161). The interaction of OPN with many of these integrins is regulated by thrombin cleavage, which is thought to increase accessibility of cell receptors to their binding domains and greatly enhance the cellular effects of OPN in many cases (162). Different integrins respond differently to the full length versus cleavage fragments, indicating that this represents a key point of regulation of OPN function. For example, while $\alpha_5\beta_1$ reacts with the RGD sequence and $\alpha_9\beta_1$ with SVVYGLR, both of these integrins are believed to only interact with OPN cleavage fragments and not the full length protein (159,161). In addition, while the SVVYGLR fragment, which is located between the RGD and thrombin cleavage sites, can only be

bound by $\alpha_9\beta_1$ following cleavage, $\alpha_4\beta_1$ is able to interact with OPN before and after cleavage (158,161). Integrin-OPN interactions can also be cell specific. For example, $\alpha_v\beta_3$ adhesion of B lymphocytes to the RGD site of OPN is greatly enhanced following thrombin cleavage, but $\alpha_v\beta_3$ platelet adhesion to OPN's RGD motif is no different in full length versus cleaved OPN (163). It is this cell specific control of binding to a multiplicity of integrin receptors that likely affords OPN the ability to convey a diversity of signals to multiple cell types.

The other commonly studied OPN receptor, CD44, is a cell surface glycoprotein involved in cell-to-cell interactions, in addition to cell adhesion and migration. Its principal ligand is considered to be hyaluronic acid, but it also binds to other ECM proteins such as OPN, fibronectin, collagen, and laminin. Alternative splicing into functionally distinct isoforms are thought to confer the multifunctionality of CD44 (164). Weber *et. al* initially reported the CD44-OPN receptor-ligand interaction and postulated that this relationship may be important for induction of cellular chemotaxis during metastatic tumor cell invasion (165). Later, it was found that different splice variants of CD44 can interact with multiple domains on both the amino- and carboxy-terminal portions of OPN independent of the RGD motif in order to stimulate cell motility and chemotaxis (166). More recently, Zohar and colleagues determined that the interaction of CD44 and other molecules with an intracellular, unsecreted form of OPN (iOPN) is an integral component in cell migration of multiple cell types including embryonic fibroblasts, activated macrophages, and metastatic cells (167).

As mentioned, OPN acts through these receptors primarily to control cell adhesion, migration, and chemotaxis. Studying the role of these interactions in

tumorigenesis, inflammation, and wound repair have all been well-represented areas of research. In the cancer field, OPN is thought to be related to both tumorigenesis and metastasis, and it was long ago found to be a secreted by transformed cells in culture (168). As reviewed by Rittling and authors, numerous studies have reported that increased OPN expression in tumors and in the blood correlate with advanced tumorigenesis and metastasis, but its mechanistic role in cancer remains unclear (169). OPN has also been described for its role in immune and inflammatory responses. It is expressed in response to inflammatory cytokines, serves as a chemoattractant to macrophages, and plays a role in immune response to viral and bacterial infection (155). The effects of OPN on macrophage function are likely a contributing factor to the larger role that OPN plays in tissue remodeling and wound repair. In fact, upon the initial development of the OPN knockout mouse, the primary phenotype of these animals was reported by Liaw *et al*. to be diminished macrophage activity and matrix reorganization following skin injury (170). It is noteworthy that some very recent studies have indicated that OPN plays a role in regulation of the stem cell niche and progenitor mobilization from the bone marrow, but the physiological relevance of this finding remains to be seen (171,172). While OPN has implications in these and other normal and pathological processes, the properties of OPN relevant to postnatal vascular growth and bone fracture healing are of primary interest to this thesis.

Vascular Functions of OPN

While many researchers initially studied OPN for its role in bone, it is also important for normal arterial physiology (173) and is produced by all of the primary cell types involved in blood vessel growth and remodeling: monocytes/macrophages,

endothelial cells, and smooth muscle cells (174). Previously reported *in vitro* studies have demonstrated that vascular cell interactions with OPN mediated through cell surface integrins regulate a wide variety of cellular functions that are potentially important to angiogenesis and arteriogenesis. For example, OPN signaling through the $\alpha_v\beta_3$ integrin has been found to mediate endothelial cell survival in a process that involves the NF-κB signaling pathway (175). Also, the angiogenic growth factor VEGF has been shown to trigger an increase in $\alpha_v\beta_3$ expression, OPN expression, and thrombin cleavage of OPN, which provides a cooperative mechanism that triggers a tremendous enhancement of endothelial cell migration (176). In addition, OPN expression is induced by stimulation with FGF, and this cross-talk may provide a mechanism for recruitment of monocytes and amplification of FGF-induced angiogenesis (177). Also, OPN mediates several processes relevant to arteriogenic collateral vessel formation including adhesion and migration of both macrophages and smooth muscle cells. (178-180).

Several studies have also suggested an *in vivo* role for OPN in neovascularization. For example, OPN has been associated with the angiogenesis-related processes of tumor growth and metastasis in lung, breast, bone, and other tissues, indicating an active role of this protein in blood vessel growth (181-185). Another recent study showed that OPN mRNA is locally upregulated at the site of ischemia induced retinal neovascularization in mice (3). Also, in a study on the role of OPN in mediating osteoclast function, OPN deficient mice were found to display decreased resorption of ectopic bone implants, an effect the authors hypothesized to be secondary to reduced angiogenesis in these animals (2). These studies and others implicate OPN in angiogenesis outside the context of

tumorigenesis, but no studies to date have fully elucidated the *in vivo* role of this factor in regulating postnatal blood vessel growth.

OPN in Bone

OPN, a multifunctional protein, is one of the major non-collagenous proteins in bone extracellular matrix, and it has been most extensively studied for its role in control of mineralization and remodeling in bone tissue. In normal murine bone, OPN is expressed by osteoblasts, osteocytes, and hypertrophic chondrocytes (186). OPN deficient mice have no obvious bone phenotype, and OPN was originally reported to play no major role in normal bone development (170,187). However, *in vitro* studies have indicated that OPN binds tightly to hydroxyapatite, which leads to an inhibition of mineral crystal formation and growth (188,189). Correspondingly, subsequent studies using Fourier transform infrared imaging found that OPN deficient mice possessed increased mineral content and crystallinity (190). While OPN deficiency was originally found to result in grossly normal bones, initial reports found that osteoclast formation from OPN deficient cells was abnormal *in vitro* (187). More recent studies have found that OPN-CD44 interaction is of great importance in bone tissue due to its role as an key mediator of osteoclast recruitment and function (187,191,192). The *in vivo* importance of this interaction during bone remodeling has been further demonstrated by the fact that OPN deficient mice undergo significantly less bone resorption compared to wild type mice in response to reduction in mechanical loading, ovariectomy, stimulation by parathyroid hormone, or administration of a high phosphate diet (193-196).

In terms of bone fracture healing, *in situ* hybridization studies have noted OPN expression in the fracture callus by osteoprogenitors in woven bone, hypertrophic

chondrocytes in the transitional are between cartilage and bone, and in the osteocytes, osteoblasts, and osteoclasts of the hard callus (144,197,198). In addition, OPN and CD44 have been shown to be colocalized during late stage remodeling of the hard fracture callus, which indicates that the interaction of these molecules may also play a role in bone remodeling during fracture healing (197). Based on these observational data gained from studying the temporal and spatial expression of OPN, scientists have speculated that OPN plays an important role in triggering mineralization during fracture healing (199). However, based on studies in tumorigenic and cardiovascular tissues, whether OPN initiates or inhibits ectopic calcification remains unclear (200,201). In addition, although OPN is considered a primary marker of osteoblast differentiation, a recent report suggests that OPN is a negative regulator of proliferation and differentiation of osteoblasts and found that overexpression of OPN inhibited mineral deposition (202). Furthermore, OPN is thought to be vital for osteoclast function and bone remodeling (191,192). Considering this diversity of sometimes conflicting data, the overall effect of OPN on fracture healing remains to be understood. Therefore, this thesis project has sought to more clearly elucidate the role of OPN in fracture healing *in vivo*.

CHAPTER 3

QUANTITATIVE MICROCOMPUTED TOMOGRAPHY ANALYSIS OF COLLATERAL VESSEL DEVELOPMENT FOLLOWING ISCHEMIC INJURY

Introduction

Collateral vessel formation can functionally compensate for obstructive vascular lesions in patients with atherosclerosis. Animal models of peripheral limb ischemia play a vital role in preclinical research efforts that test the efficacy of administering angiogenic factors and other therapeutic agents to stimulate formation of collaterals to compensate for blocked arteries. One such model, the mouse hind limb ischemia model, has been used extensively in efforts to define the mechanisms involved in postnatal blood vessel formation (107). While the utility of this model is well established, the available methodologies for quantification of collateral vessel development in this setting are not ideal.

In the context of hind limb ischemia, three different mechanisms may contribute to reconstitution of limb perfusion. Angiogenesis involves sprouting or intussusception of new capillaries from pre-existing vessels and is triggered by tissue ischemia. Arteriogenesis occurs when preexisting arterioles dilate and remodel through endothelial and smooth muscle cell expansion to meet increased physiologic demands (5,6). It is generally accepted that this process, which is mediated at least in part by monocytes and macrophages, is triggered by the increased shear stress that occurs in small, interarterial anastomoses following occlusion of a parent artery (7). Finally, there is evidence that

vasculogenesis or *de novo* blood vessel formation by bone-marrow derived endothelial progenitor cells may play a role in post-natal vessel growth, although this remains controversial (9). Collateral vessel growth, primarily via an arteriogenic pathway, is widely believed to be the most efficient means for reconstituting perfusion following arterial occlusion (5).

Investigators have utilized a variety of techniques to evaluate vascular structures in animal models. Histology is commonly employed to analyze capillary or arteriole density, but it is relatively subjective, not truly quantitative, 2-D, and not necessarily representative of vascularity throughout the entire sample. Laser Doppler perfusion imaging has been used to analyze functional blood flow in hind limbs because it offers semi-quantitative data and a measure of functionality (5,107,111-113). However, this technique does not provide anatomical information and is limited by the fact that only the most superficial, cutaneous blood flow is measured. Another popular technique, x-ray microangiography, provides high-resolution, 2-D angiograms of the hind limb vascular anatomy but lacks the ability to employ a quantitative, volumetric analysis (113-115). Injection of colored or fluorescent microspheres presents a method for longitudinal study of reconstitution of perfusion to ischemic tissues using quantitative spectrophotometry or flow cytometry analyses (116-120). However, the required arterial catheterization or injection of microspheres into the left ventricle or atrium presents a considerable challenge in mice because of their small size. Other imaging modalities such as magnetic resonance angiography and positron emission tomography serve as viable methods for analyzing vascular function, but the resolution of these methods is typically not sufficient for studies involving small animals.

Micro-CT has emerged as a promising technology that can overcome several of the challenges associated with evaluation of vascular networks. Recently, vascular imaging procedures have been developed for small animal models based on the use of perfused contrast agents and x-ray micro-CT (121-129). The goal of these studies has been to visualize 3-D vascular networks in organs (i.e. heart and kidneys) or tumors. The objective of the current study was to use micro-CT vascular imaging methods to examine the time course of collateral formation induced by femoral artery excision in the mouse hind limb ischemia model. In addition to vessel volume, measures of vascular network morphology and anisotropy were quantified and the effects of varying the imaging parameters voxel size and binarization threshold were analyzed. The developed micro-CT-based techniques represent an innovative and quantitative approach for investigating 3-D vascular responses associated with a broad range of conditions, including vascular injury, tumorigenesis, coronary artery disease, aneurysm formation, skeletal development, and fracture healing. In these settings, micro-CT imaging in combination with an appropriate contrast agent has the potential to overcome the shortcomings of other vascular imaging techniques because it can provide high resolution, volumetric, objective, and highly quantitative analyses.

Methods

Animals

Male C57BL/6 mice were purchased from the Jackson Laboratory (Bar Harbor, ME). All mice were between 10 and 11 weeks of age. The animals were fed a standard chow diet ad libitum and had free access to water. All protocols were approved by the

Institutional Animal Care and Use Committee of Emory University and done in accordance with the NIH guidelines for the care and use of experimental animals.

Hind Limb Ischemia Model

To study collateral formation, we utilized the well characterized mouse hind limb ischemia model (107). Animals were anesthetized by intraperitoneal injection of xylazine (10 mg/kg) and ketamine (80 mg/kg). All hair was removed from the surgical site and the area was thoroughly cleansed with sterile water. A unilateral incision was then made over the right medial thigh of the mouse. The superficial femoral artery and vein were ligated proximal to the caudally branching deep femoral artery, and then a second ligation was performed just proximal to the branching of the tibial arteries. The length of the artery and vein was excised between the two ligation points, and the skin was closed with interrupted silk sutures. After awakening, animals were returned to their cages and allowed to ambulate freely. The mice were euthanized post-operatively for microcomputed tomography imaging at 0 (n=7), 3 (n=6), and 14 (n=5) days or histological analysis at 14 days (n=3).

Imaging Specimen Preparation

Tissues were prepared in concordance with previously described methods (121). Following euthanization, the thoracic cavity was opened and the inferior vena cava was severed. The vasculature was flushed with 0.9% normal saline containing heparin sodium (100 units/mL) at a pressure of approximately 100 mm Hg via a needle inserted into the left ventricle. Specimens were then pressure fixed with 10% neutral buffered formalin. Formalin was flushed from the vessels using heparinized saline, and the vasculature was injected with either a 15% barium sulfate, 2% gelatin suspension or a

radiopaque silicone rubber compound containing lead chromate (Microfil MV-122, Flow Tech Inc., Carver, MA).

In preliminary studies using barium-gelatin mixtures as the contrast agent, 15% barium sulfate and 2% gelatin were suspended into saline. To prepare the contrast agent for perfusion, the gelatin was added a small amount at a time as the saline was heated on a stir plate. The barium was subsequently added to the solution and the suspension was stirred until any clumps had dispersed. The warmed solution was then perfused into the animal, which was subsequently placed on ice for one hour to promote gelling of the suspension within the vasculature. Samples were then stored at 4 °C in 10% neutral buffered formalin until imaging.

For studies using the silicone rubber injection agent, the manufacturer's protocol was followed with the exception that no diluent was used in order to maximize the lead chromate content. Samples were stored at 4°C overnight for contrast agent polymerization. Mouse hind limbs were dissected from the specimens and soaked for 4 days in 10% neutral buffered formalin to ensure complete tissue fixation. Tissues were subsequently treated for 48 hours in a formic acid based solution, Cal Ex II (Fisher Scientific, Pittsburgh, PA), to decalcify the bone and facilitate image thresholding of the hind limb vasculature from the surrounding tissues. Samples were rinsed thoroughly, soaked for 1 hour in water, and then stored at 4 °C in 10% neutral buffered formalin until microcomputed tomography imaging.

Micro-CT Imaging

Hind limb vasculature was imaged using a high-resolution (8-36 μm isotropic voxel size) desktop micro-CT imaging system (μCT 40, Scanco Medical, Bassersdorf,

Switzerland). The scanner was set to a voltage of 55 kVp and a current of 145 μA. Resolution was set to medium, which created a 1024 x 1024 pixel image matrix. Serial tomograms were reconstructed from raw data using a cone beam filtered backprojection algorithm adapted from Feldkamp et al (134). Noise was removed using a low pass Gaussian filter (sigma=1.2, support=2). The tomograms were globally thresholded based on x-ray attenuation and used to render binarized 3-D images of the hind limb vascular network segmented (i.e. partitioned) from the surrounding tissues. Histomorphometric analysis based on direct distance transform methods was subsequently applied to the 3-D images to quantify parameters of vascular network morphology and anisotropy (135,136).

Micro-CT Parametric Analysis

One representative control (left) hind limb was chosen at random to test the effects of resolution and threshold on the histomorphometric analysis of vessel volume, connectivity, number, thickness, separation, and degree of anisotropy. This specimen was scanned at voxel sizes of 16, 20, 30, and 36 μm. The 36 μm voxel scan was used to test the effects of threshold on histomorphometric parameters. A threshold of 80 was initially chosen based on visual interpretation of thresholded two-dimensional tomograms. The 36 μm voxel size scan was evaluated to determine the output of the histomorphometric analysis using thresholds of 60, 70, 80, 90, and 100. These threshold values directly correlate to the linear coefficient of attenuation of the material in the image space.

Analysis of Blood Vessel Morphology in Ischemic Hind Limbs

Surgery and control limbs were evaluated individually to quantify the 3-D histomorphometric values vessel volume, connectivity, number, thickness, thickness distribution, separation, and degree of anisotropy (Table 3.1). These parameters are standard for the analysis of trabecular bone microstructure but have not been determined previously for microvascular networks (136). In this study, these measures were taken in a volume of interest (VOI) defined as the upper hind limb, extending from the proximal femoral artery ligation point distally to the lower ligation point.

Table 3.1. Overview of Vessel Morphology Parameters

Parameter	Unit	Definition
Volume	mm^3	-Image voxel size multiplied by the number of voxels in segmented image
Connectivity	$1/mm^3$	-Maximal number of branches that can be broken within a blood vessel network before it is divided into two unconnected parts
Number	1/mm	-Inverse of the mean spacing between the mid-axes of the blood vessels
Thickness	mm	-Average of the local vessel thicknesses determined at each voxel within the segmented vessel network
Separation	mm	-Average of the distance between neighboring vessels determined at each voxel within the image background space
Degree of Anisotropy	1	-Determined based on the directional orientation of the vascular network (1 = isotropic; >1 = preferential orientation exists)

Vessel volume was computed based on the voxel size and the number of segmented voxels in the 3-D image following application of the binarization threshold. Connectivity was determined using the method of Odgaard and Gunderson (137), which is based on the Euler characteristic and is free from assumptions on the three-dimensional structure of the segmented object. Here, connectivity is defined as the maximal number of branches that can be broken within a structure before it is divided into two separate parts. Vessel number, thickness, thickness distribution, and separation were calculated

using a model-independent method for assessing thickness in 3-D images (135). This technique defines a local thickness at every point (voxel) in the VOI as the diameter of the largest sphere that both contains the point (not necessarily at its center) and is completely within the structure of interest (segmented object versus background space surrounding the object). The average of the local voxel thicknesses within the structure yields the vessel thickness parameter, and a similar calculation on the background voxels determines the vessel separation. To calculate vessel number, the segmented volume is skeletonized, leaving just the voxels at the mid axes of vessels in the structure. Vessel number is defined as the inverse of the mean spacing between the mid-axes of the structures in the segmented volume. Degree of anisotropy represents the degree to which the segmented vascular bed is oriented toward a specific direction. It is measured by determining the mean intercept length of blood vessels as a function of direction. Eigenanalysis is used to find the principal material directions, and, after this is determined, the ratio of the maximum and minimum eigenvalues yields the degree of anisotropy as described by Gunderson et al (203). A degree of anisotropy of 1.0 indicates that the network is perfectly isotropic, or does not contain a preferred orientation, and higher values of degree of anisotropy indicate that a structure contains a preferential material direction.

Using the semi-automated software that interfaces with the μCT 40 scanner, histograms were generated to display the distribution of the vessel sizes within the volume of interest. Volume weighted histograms were created that display the local thickness value for every point within the structure. In addition, a color-coded scale was mapped to the surface of the 3-D images to produce a visual representation of the vessel

size distribution. These images contain a color-coded map that correlates to vessel diameter.

Histological Analysis

Mice were euthanized, cleared using heparinized 0.9% normal saline, and perfusion fixed using 10% neutral buffered formalin. The adductor muscles were then excised from both the occluded and control limbs of each mouse. These tissues were processed and paraffin embedded for histological analysis. 5 μm thick sections were cut and immunostained with a mouse monoclonal smooth muscle α-actin antibody (Sigma Chemical, St. Louis, MO). In order to count arterioles using light microscopy, the primary antibody was detected using an avidin-biotin-alkaline phosphatase method from a commercially available kit (Vectastain ABC-AP, Vector Laboratories, Burlingame, CA). Sections were counterstained with hematoxylin, and the number of positively stained vessels was counted from two transverse tissue sections taken 150 microns apart at approximately 5 mm from the proximal insertion of the adductor. Arteriole densities were counted as the number of vessels per square millimeter and reported as ratio between the surgery and control limb for each specimen.

To qualitatively assess the ability of micro-CT to resolve vascular structures using different image resolutions, approximately 1 mm thick transverse cross sections of tissue were cut from the upper hind limb of contrast perfused specimens. These samples were then sequentially treated in 25%, 50%, 75%, 95%, and absolute ethanol for 24 hours each, followed by 24 hours in methyl salicylate (Sigma Chemical, St. Louis, MO) for tissue clearing. The cleared tissues were first transilluminated and photographed using a high-resolution digital camera. These same sections were then scanned using 8, 16, and

36 μm voxel sizes in order to qualitatively evaluate micro-CT in rendering the localized vascular structures.

Statistical Analysis

All data are presented as mean ± SEM. Statistical analyses were performed using the Minitab software. Tukey's method was used for post hoc analyses, and ANOVA was used to model the effect of time post surgery on all response variables. $P<0.05$ was interpreted as significant in all analyses.

Results

Evolution of Micro-CT Imaging and Hind Limb Ischemia Model Surgery Techniques

In preliminary studies, perfusion of barium sulfate and gelatin suspensions was used to enhance x-ray attenuation of the vasculature. Using this method, high resolution images of the hind limb vascular networks could only be generated at low thresholds that did not remove bone from the image. In order to eliminate the confounding effects bone imaging would have on the morphological analyses, we attempted to use higher thresholds to segment the vasculature only. However, this significantly diminished image quality (Figure 3.1). Conversely, closer inspection showed that, due to the high radiodensity of barium sulfate, the segmented object often appeared artifactually large when lower threshold values were used. Further investigation also demonstrated that the barium sulfate settled within the vessels after removing it from 4°C to place it within the micro-CT scanner, resulting in incomplete vascular filling and an inhomogeneous coefficient of attenuation within the vessels.

After gaining insight into some of the disadvantages of using barium sulfate in a gel suspension, we began to employ a silicone rubber contrast agent, which provides x-ray attenuation due to its lead chromate content. This compound polymerizes into a silicone rubber solid approximately 20 minutes after it is catalyzed by addition of a curing agent. Compared to preliminary studies using barium sulfate, the polymerized compound lowered the risk of displacing the contrast when manipulating the tissues to prepare for imaging. This compound also allowed us to maintain a more homogeneous mixture and hence x-ray attenuation within the vessels independent of the environment within the scanner during imaging.

Although the contrast agent formulation was chosen to maximize contrast of the perfused vasculature, image segmentation of vascular structures from bone remained a challenge. To circumvent this problem, specimens were placed in a decalcification solution for 48 hours. Following this treatment, a lower threshold could be used to segment the vasculature from the surrounding tissues, and superior quality images were produced (Figure 3.1 C and D). Improved imaging techniques also led to optimization of the surgery protocol. Figure 3.1 C illustrates that in pilot studies, the upper ligation point was too distal to prevent perfusion of major arteries branching from the femoral artery that supply the lower limb. Following this observation, shifting the ligation point proximally to preclude the branching of the deep femoral artery allowed us to create a more robust model of peripheral limb ischemia (Figure 3.1 D).

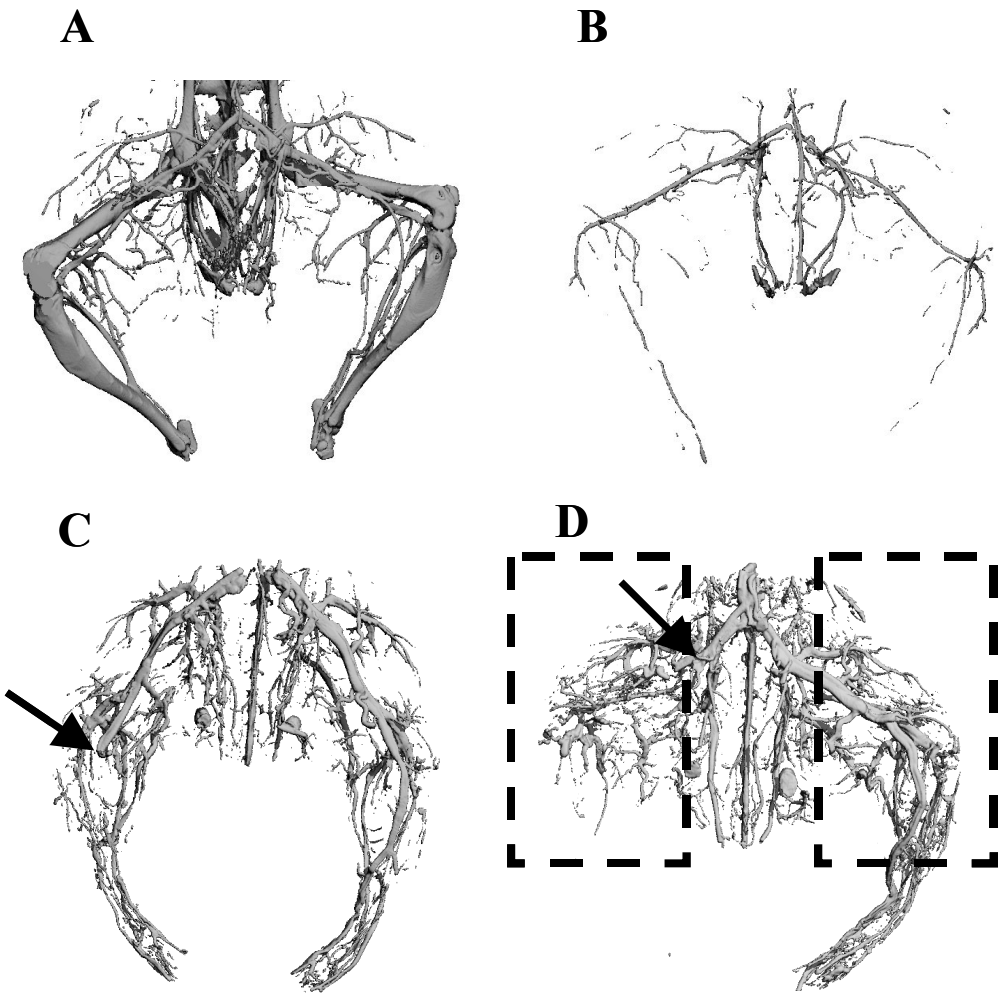

Figure 3.1. Micro-CT angiograms demonstrating the progression of our hind limb ischemia model specimen preparation and surgical techniques. (A) and (B) show images from preliminary studies using a 15% barium, 2% gelatin suspension as a contrast agent for vascular imaging. To remove the bone tissue from the image (B), use of a high threshold results in loss of small blood vessel definition that is evident at a lower threshold (A). Images in (C) and (D) were acquired following vascular perfusion using a silicon polymer and bone decalcification, which allows use of a lower threshold. These techniques circumvented previous problems associated with settling of barium particles within the suspension and thresholding out bone. Image (C), a day 0 post surgery control, showed that our original surgical procedures ligated the femoral artery too distally to preclude blood flow in arteries that can supply blood to the lower leg. Image (D), another day 0 post surgery control, demonstrates optimization of the surgical protocol by shifting the proximal ligation point. The dashed boxes represent the volume of interest considered in the control and surgery limbs for all morphological analyses.

Effects of Voxel Size and Binarization Threshold on Quantification of Vascular Network Morphological Parameters

Isotropic voxel size is a main determinant of the ability to resolve small objects on micro-CT scans and thus affects image quality. While smaller voxel sizes result in longer scan times and much larger data sets, it can be seen in Figure 3.2 A that they also afford the opportunity to resolve smaller caliber vessels that can't be visualized with larger voxel sizes. When evaluating the VOI defined in Figure 3.1 D for a representative control limb, it was evident that voxel resolution affects the different morphological parameters to varied degrees (Figure 3.2 B). Vascular volume decreased as voxel size increased due to the contribution of smaller vessels that could only be resolved when smaller voxel sizes were used. Vessel connectivity, the most drastically affected parameter, decreased markedly on larger voxel size scans that did not resolve the well-connected networks of small arterioles. In agreement with this conclusion, there was a discernable decrease in vessel number and an evident increase in both average vessel thickness and vessel separation at larger voxel sizes. Degree of anisotropy, one of the more mildly effected parameters, increased with larger voxel sizes, indicating that the smaller vessel networks resolved at smaller voxel sizes were more randomly oriented than the primary arteries.

Selection of an image threshold defines the cutoff grayscale (attenuation) value that partitions the image voxels into either the background or part of the segmented object. During reconstruction of image projections, a grayscale value that represents the capacity of the material within that space to attenuate x-rays is assigned to each voxel. If this coefficient is higher than the assigned threshold, the voxel remains in the 3-D image

as part of the segmented object. Selection of an optimal threshold value is made especially challenging by attempting to account for partial volume effects. At lower thresholds, smaller vessels that are apparent on the 2-D tomograms will remain as part of the segmented object, but larger vessels will appear artifactually large because the partially filled voxels surrounding them will remain in the image. Conversely, to gain the most accurate image of the larger vessels, a higher threshold must be used, and smaller vessels are often omitted from the 3-D rendering (Figure 3.3 A). Therefore, there is a tradeoff that exists, and when global thresholding is used, careful attention must be paid in choosing the best possible threshold.

The ability to define an appropriate threshold for binarizing computed tomography data sets is an important issue to resolve before completing a morphological analysis of the rendered 3-D image. Alteration of the threshold value had an observable effect on the morphometric parameters of the vascular tree, but this effect was not as substantial as that seen from varying voxel size (Figure 3.3 B). Vascular volume, connectivity, and vessel number all decreased with increasing threshold with, as before in the resolution test, connectivity being the most strongly affected parameter. Increasing the threshold also resulted in higher average thickness, separation, and degree of anisotropy of the vessel network. As with increasing voxel size, these trends result from removing smaller, partial voxel vessels from the segmented volume.

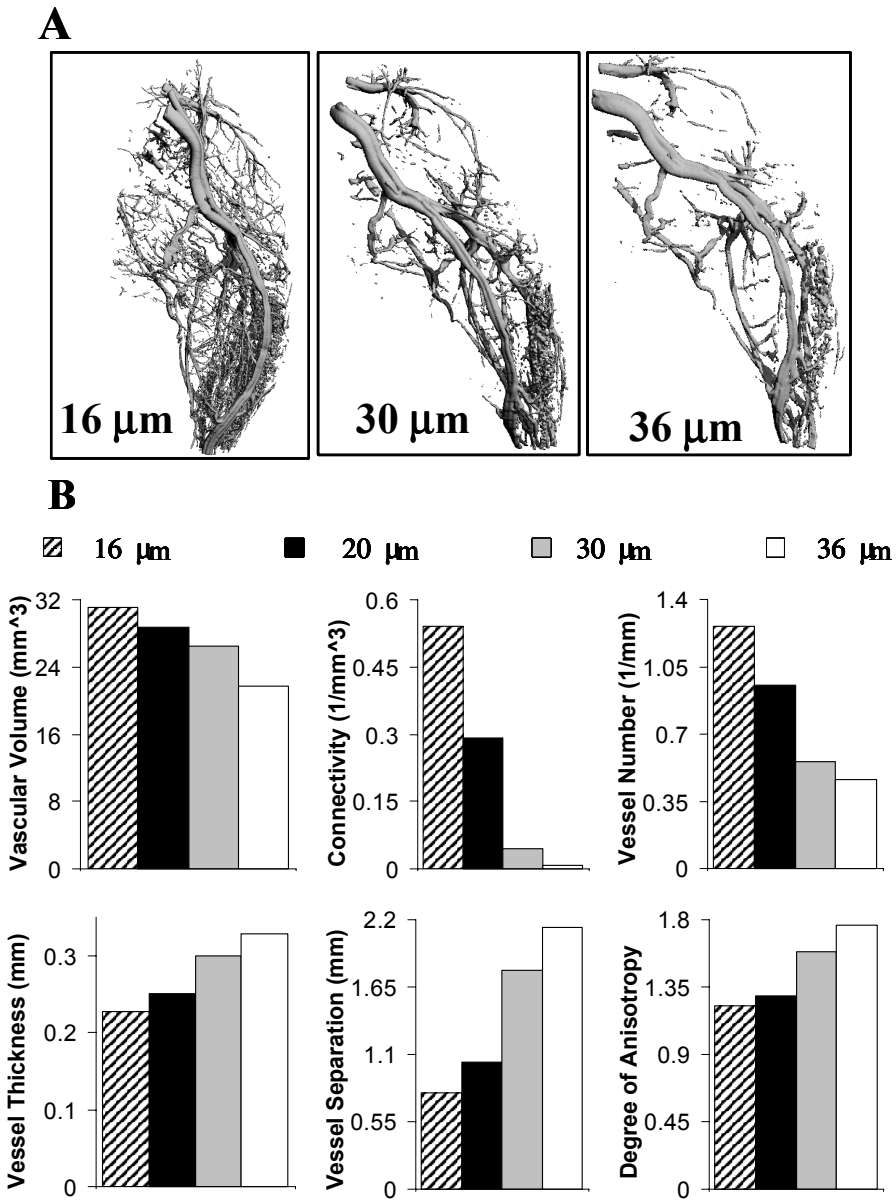

Figure 3.2. Voxel size sensitivity analysis. (A) Representative control limb micro-CT angiograms illustrating the effects of scanning the same sample at different resolutions. Image voxel size is listed in the lower left of each image. (B) Demonstration of the differences in the quantitative, morphometric parameters when 16, 20, 30, or 36 µm isotropic voxel sizes are used. All parameters are affected by altering voxel size. As voxel size is increased, vascular volume, connectivity, and vessel number decrease while average vessel thickness, average vessel separation, and degree of anisotropy increase. These trends result from the fact that the smallest vessels are not resolved at larger voxel sizes.

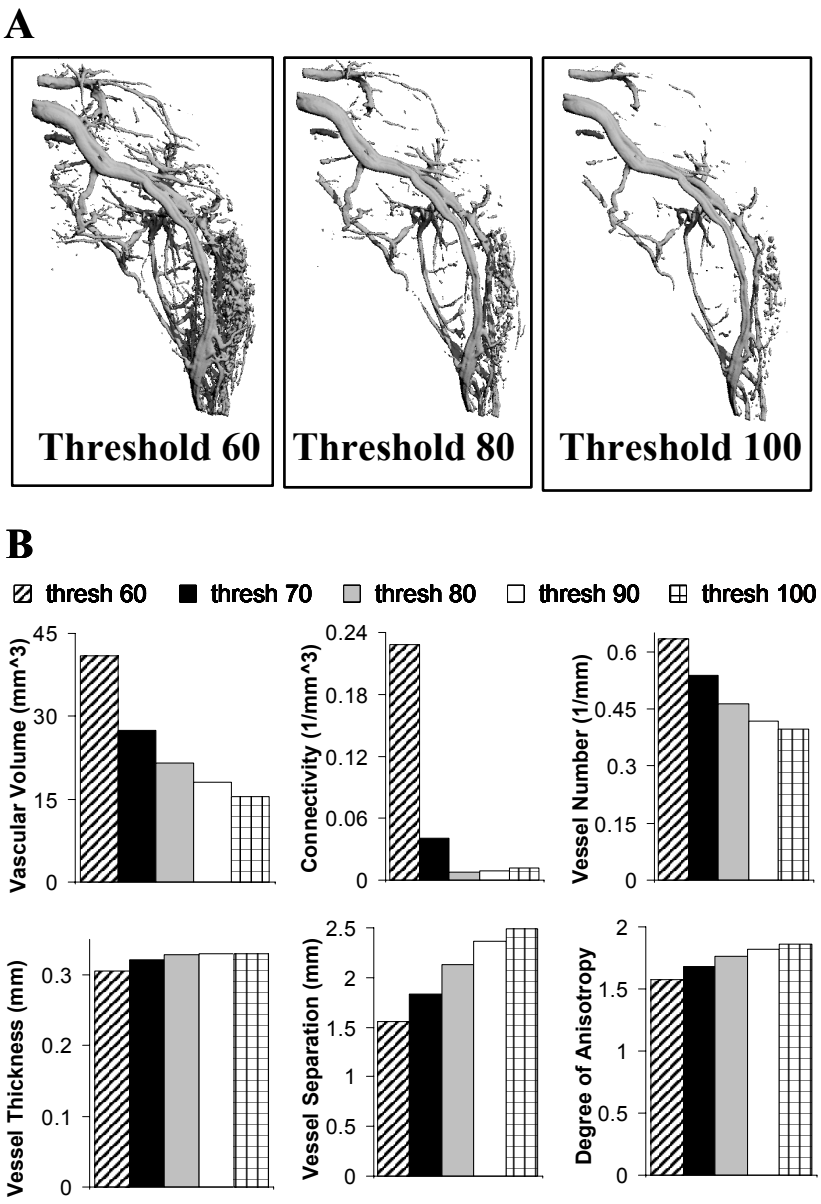

Figure 3.3. Threshold sensitivity analysis. (A) Representative control limb angiograms indicating the effects of using different binarization thresholds to produce rendered 3-D images from the same raw data set. (B) Demonstration of the changes in the morphological parameters based on using 60, 70, 80, 90, and 100 as the binarization threshold to evaluate the 36 μm resolution scan. All morphologic parameters are affected to some degree by varying the threshold, with connectivity showing the most drastic changes. As threshold is increased, partial volume voxels are removed from the image. This results in a decrease in vascular volume, connectivity, and vessel number with a concurrent increase in vessel thickness, separation, and degree of anisotropy.

Comparison of Control and Surgically Manipulated Hind Limb Blood Vessel Morphology

In order to obtain a more quantitative assessment of the forming collateral network, we evaluated the potential utility of several morphological parameters. As described in the methods section, vessel volume, connectivity, number, thickness, separation, and degree of anisotropy were determined for both the control and surgically manipulated limbs of all experimental animals (Figure 3.4). In acute preparations (day 0 post surgery), vascular volume was significantly reduced in experimental limbs compared to control limbs immediately following femoral artery excision. However, as early as 3 days post surgery, collateral vessels formed and the reconstituted vascular volume of the surgery legs was significantly higher than day 0 preparations. In fact, at both 3 and 14 days post surgery, the vascular volume was completely recovered and was not different from control limbs. Connectivity of the vascular network in the surgery limbs was significantly less than in controls at day 0, but it increased rapidly post surgery. While there was a trend toward increased connectivity at day 3, at 14 days, a more developed collateral system was formed, resulting in a connectivity value that was significantly higher than both 0-day surgery limbs and the contralateral control limbs. As the collateral network grew and a series of small, densely packed vessels augmented blood flow to the hind limb, the 3 and 14-day post surgery hind limbs had significantly increased vessel number compared to day 0 surgery limbs or control limbs. Average vessel thickness was decreased significantly following surgery and remained significantly lower at 3 and 14 days than in the intact control limbs, which contained the large, conduit femoral artery. There was a non-significant trend toward increased vessel separation in

acutely prepared samples, but as the collateral network developed, at 3 and 14 days post surgery, vessel separation became significantly less than in control or day 0 specimens. Lastly, surgery limb degree of anisotropy was significantly reduced compared to controls at all time points, indicating that the new collateral network was more isotropic than the original intact vessel network. These data indicate that vascular volume, vessel network connectivity, vessel number, and vessel separation may be particularly useful parameters for quantifying adaptive vascular changes following surgery in the hind limb ischemia model.

As an additional method of analysis, histograms were compiled to show the blood vessel size frequency distribution in the control and experimental limbs 0, 3, and 14 days post surgery (Figure 3.5). Control limbs represent the normal anatomical distribution of blood vessel sizes in non-manipulated limbs. Immediately post surgery (day 0), the ischemic limb had reduced perfusion to all vessel sizes. Relative to control limbs, 3-day and 14-day post surgery legs showed an increase in small, collateral-sized vessels and a decrease in the larger, conduit vessel diameters (14-day data not shown). In addition, a visual representation of the blood vessel size distribution was produced by mapping a color-coded scale to the object surface (Figure 3.6).

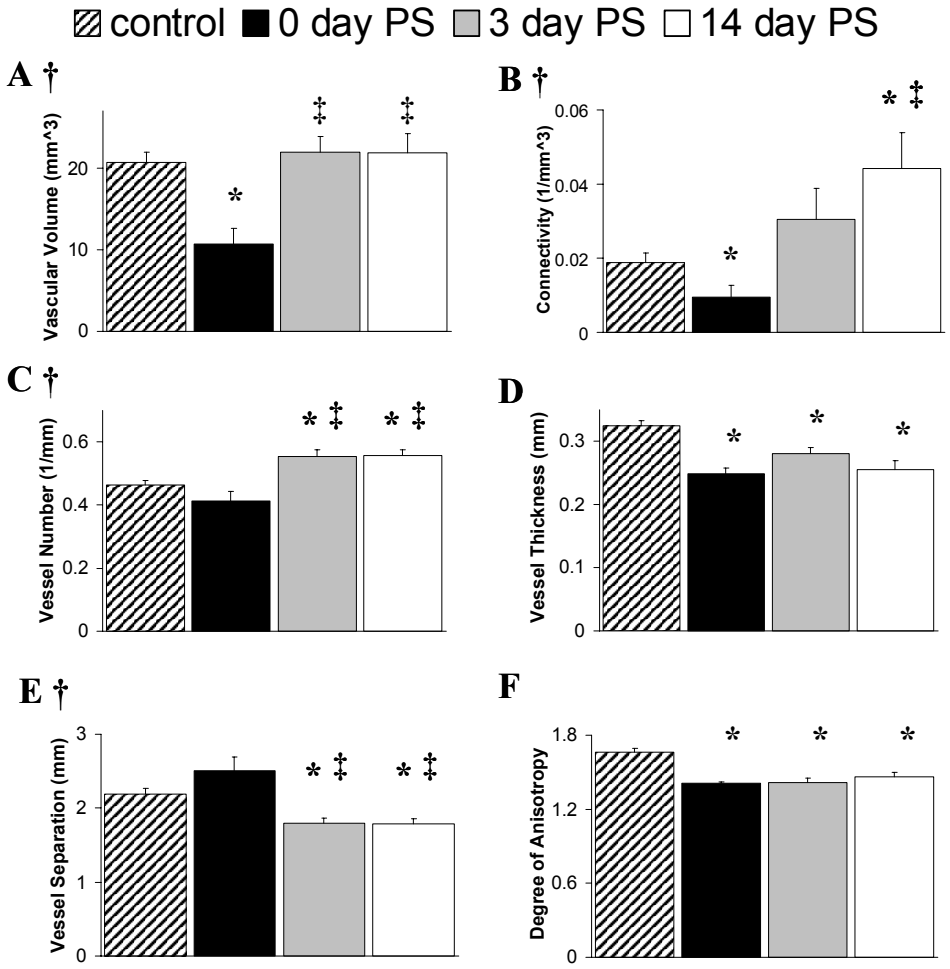

Figure 3.4. Demonstration of serial changes in quantitative assessment of vascular morphology after femoral artery ligation. Histomorphometric analysis of (A) vascular volume (B) connectivity (C) vessel number (D) vessel thickness (E) vessel separation and (F) vascular tree degree of anisotropy. Results (mean ± SEM) are given for control limbs (n=18) and surgery limbs 0 (n=7), 3 (n=6), and 14 days (n=5) post surgery (PS). ∗ = significant difference ($P<0.04$) compared with control limb at a given time point. ‡ = significant difference ($P<0.01$) between the indicated time point and 0-day post surgery specimens. † ($P<0.02$) denotes that the histomorphometric parameter changes significantly in surgically manipulated hind limbs as a function of time post surgery as determined by ANOVA.

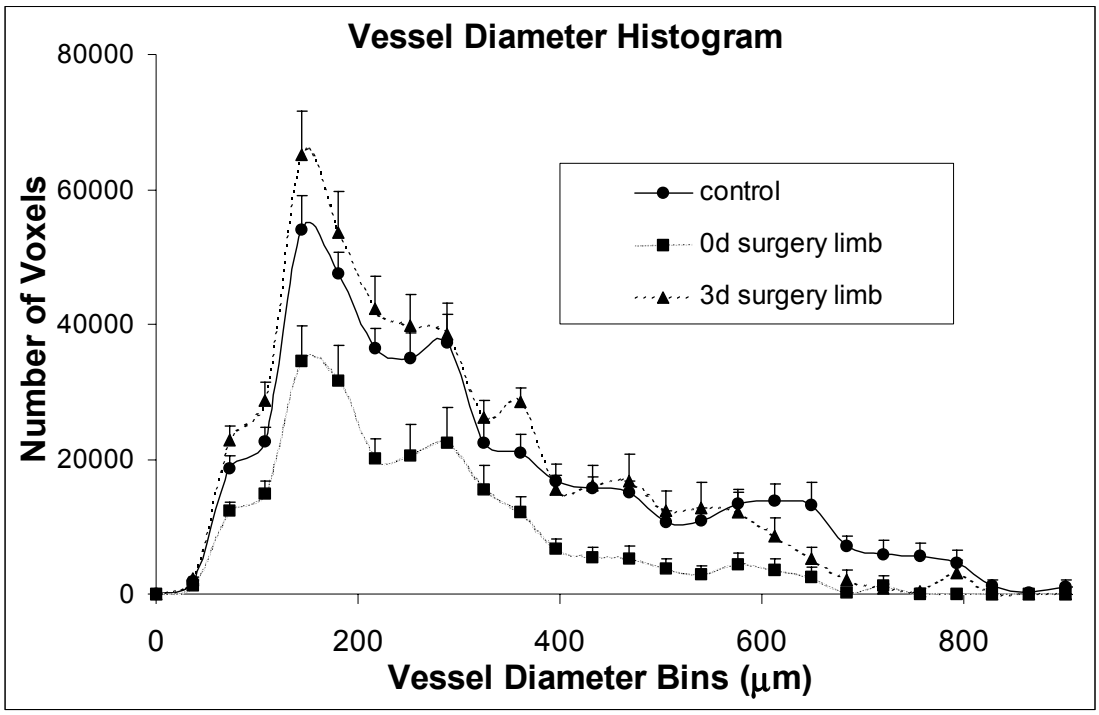

Figure 3.5. Vessel diameter histogram. This histogram shows mean blood vessel size distribution in control limbs (n=13) and experimental limbs 0 (n=7) or 3 days (n=6) post surgery. Control limbs represent the normal anatomical distribution of blood vessel sizes in non-manipulated limbs. 0 days post surgery, the ischemic limb has reduced perfusion to all vessel sizes. Relative to control limbs, 3-day post surgery legs showed an increase in small, collateral-sized vessels and a decrease in the larger, conduit vessel diameters. Since the trends were the same as those seen at 3 days, 14-day post surgery data were omitted for clarity.

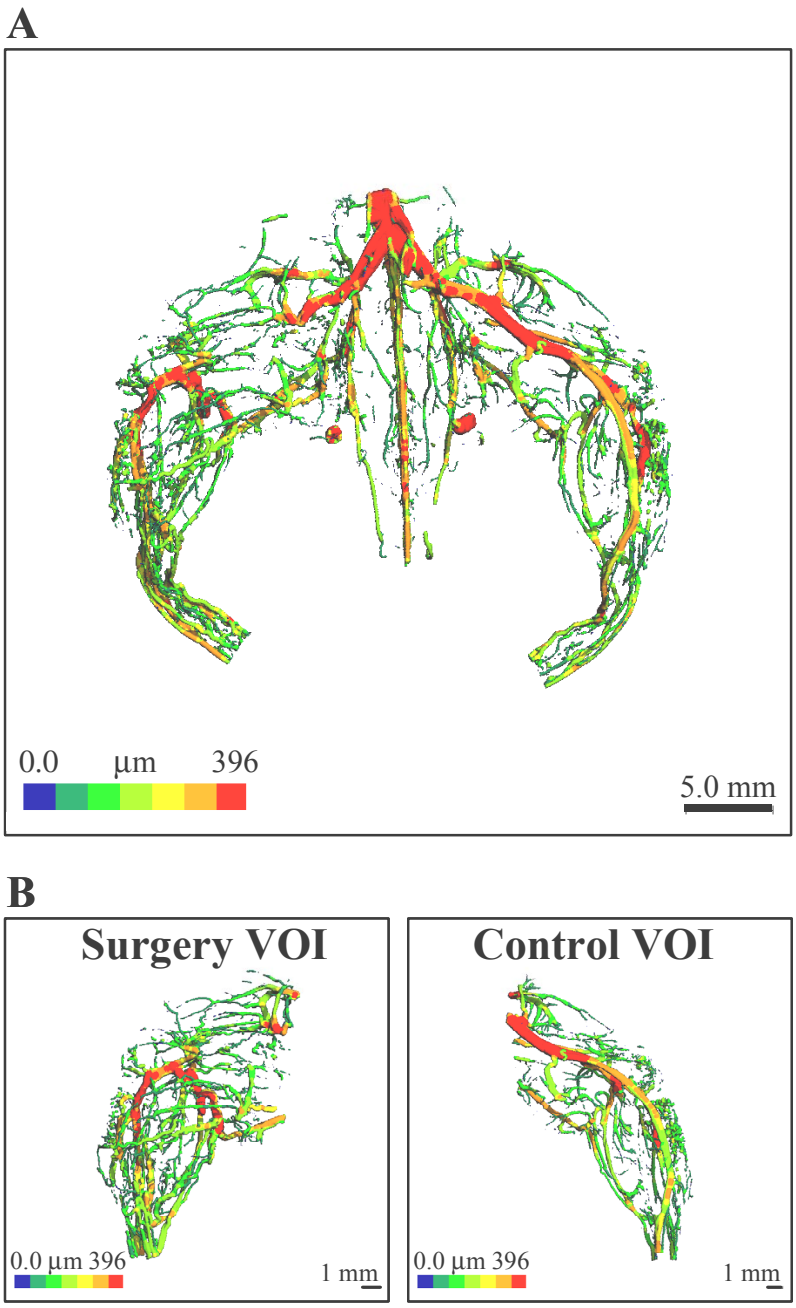

Figure 3.6. Representative 14-day post surgery micro-CT images with a color-coded vessel diameter scale mapped to the 3-D image surface. (A) Rendering of an entire hind limb. (B) shows the volume of interest analyzed in the surgically modified and control limbs. In these images, the color scale correlates to vessel size. Red is mapped to the surface of vessels with diameter greater than or equal to 396 µm, and the color scale is linear down to zero. Length scale bars are shown in the lower right of each image.

Comparison of Micro-CT and Histological Analysis

In order to confirm our micro-CT data using a previously used technique, we performed arteriole density analyses after smooth muscle α-actin staining. Since it is difficult to directly validate the micro-CT calculations, we compared the ratio of the surgery and control limb vessel number as determined by micro-CT with a similar ratio for the histologically determined arteriole density values. There was excellent agreement between these two methods at 14 days post surgery, at which point the ratio of vessel number in the surgical and control limbs was determined to be 1.26±0.07 using micro-CT and 1.28±0.28 using histology (Figure 3.7 A).

To further evaluate the accuracy of micro-CT in depicting localized vascular structures, a small, 1 mm section of tissue from a contrast filled hind limb was cleared and photographed yielding a vivid and precise representation of the vasculature. A qualitative comparison of this photograph and 8, 16, and 36 μm voxel size micro-CT images of the same specimen illustrates that micro-CT has the capability to accurately depict the smallest vessels when high resolution scans are used, but only larger arterioles and arteries can be effectively imaged using a 36 μm voxel size (Figure 3.7 B).

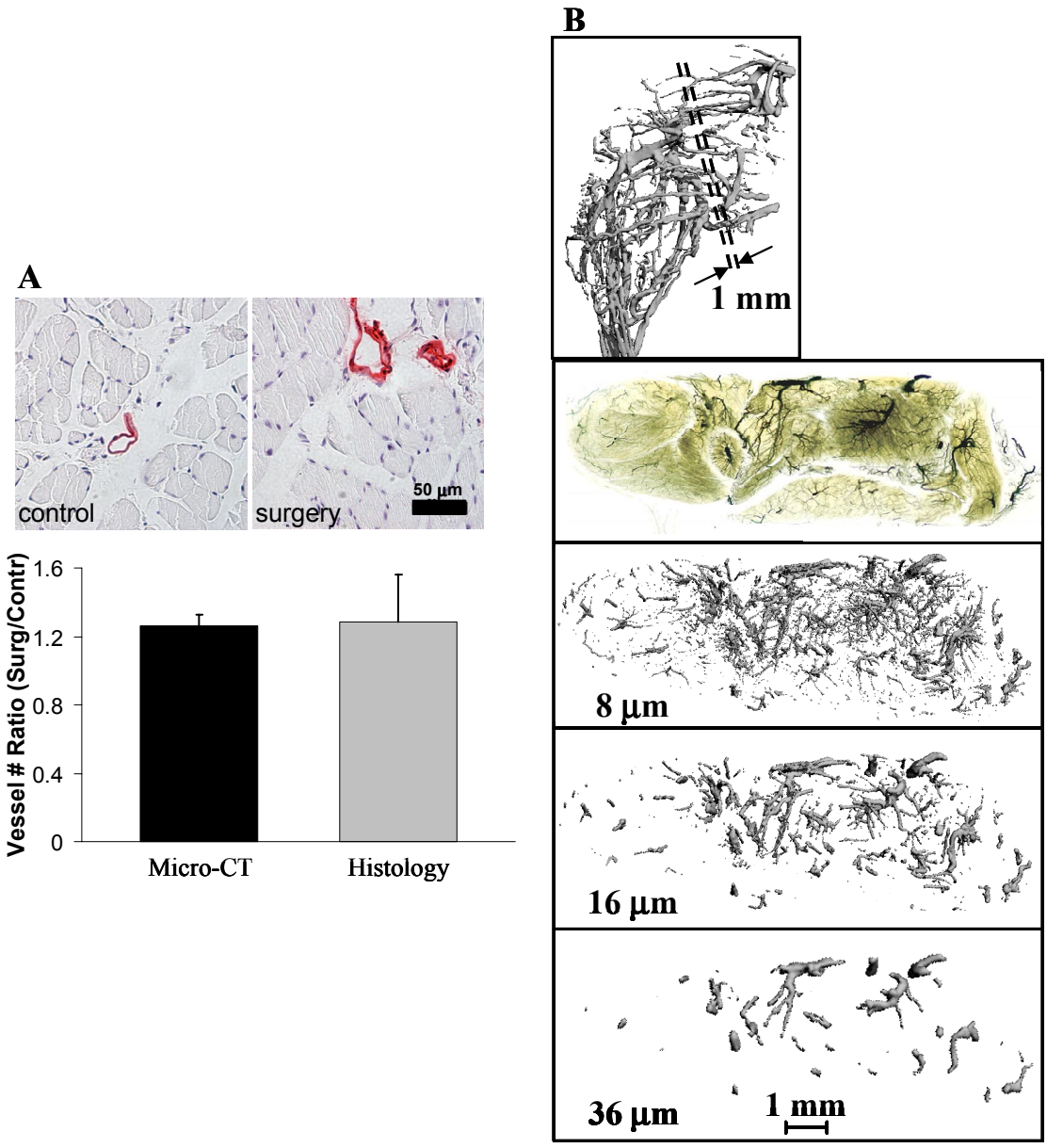

Figure 3.7. Histological Validation. (A) Example photomicrographs of muscle cross sections from 14-day post surgery control and experimental limb adductors identifying arterioles using a smooth muscle α-actin antibody and counterstained with hematoxylin. Quantification shows excellent agreement between the histological and micro-CT determinations of the surgery to control limb vessel number ratio. (B) Qualitative assessment of micro-CT vascular imaging using different voxel sizes. A representative 1 mm thick transverse tissue section was taken from a contrast-filled hind limb in the region shown. This tissue specimen was cleared using methyl salicylate and imaged with high resolution digital photography and micro-CT at voxel sizes of 8, 16, and 36 µm. These images illustrate that, as micro-CT voxel size is increased, small vessels are no longer clearly depicted while large arterioles and arteries are still accurately resolved.

Discussion

Small animal models have been utilized to study the mechanisms of angiogenesis and collateral vessel growth (99,100,107,204). Insights gained from these models have played a role in the design of therapeutic strategies for clinical trials aimed at recovering vascular function in patients with peripheral artery disease (34,205-212). Despite advances in analysis of these models, no current method offers an optimal analysis of blood vessel microarchitecture and function. The current study demonstrates that micro-CT imaging combined with the use of perfused contrast agents and bone decalcification provides a robust methodology for evaluation of vascular networks. Specifically, micro-CT is advantageous because it provides high resolution, quantitative, 3-D, and objective data analysis. This was evident in our validation study using immunohistochemistry, which found micro-CT to offer a highly accurate, less variable, and less time consuming alternative for quantitative measure of collateral development. Micro-CT techniques also offer flexibility to the user in defining the volume of interest be evaluated. A global analysis of the entire surgery and contralateral control hind limb vascular anatomy can be evaluated for comparative purposes, or if desired, the collateral vessels that form in the thigh can be digitally isolated for morphological evaluation as was done in this study. Alternatively, the functional reconstitution of the vascular network can be assayed by defining the VOI as the distal portion of the hind limb in order to quantify perfusion to the large conduit vessels in the lower portion of the leg. Thus, contrast-enhanced micro-CT imaging provides broad applicability to model systems that require a vigorous and highly quantitative evaluation of vascular structure or growth.

We examined vascular anatomy in the thigh of surgically manipulated and control hind limbs of wild type mice 0, 3, and 14 days following femoral artery ligation and excision. The blood vessel networks were evaluated within this VOI for vessel volume, connectivity, number, thickness, thickness distribution, separation, and degree of anisotropy. These lumped assessments of the vascular morphology led to the conclusion that removal of the large, conduit femoral artery stimulates reconstitution of vascular volume through a highly connected network of closely spaced, small vessels. Alternatively, histograms displaying a parameter's distribution within the specimen can be advantageous for alternative indices such as average vessel thickness. When the distribution of vessel diameters is evaluated, more information can be gathered and otherwise undetectable trends may become apparent. For example, at 0, 3, and 14 days post surgery, no significant difference in average vessel thickness was apparent, but clear differences were seen when the thickness distribution was calculated (Figure 3.5).

The rapid arteriogenic response detected represents a particularly interesting observation. Previous researchers have suggested that arteriogenesis is temporally dissociated from angiogenesis, and it has also been suggested that arterialization of preexisting vessels, rather than sprouting of new capillaries, is a more efficient means of establishing collateral flow following femoral artery ligation (5,7,213,214). Our data demonstrate that vascular volume of angiographically visible vessels was completely reconstituted compared to control as early as 3 days following surgery. Furthermore, there was no significant difference between 3 and 14-day post surgery specimens for any of the morphological parameters evaluated. Multiple researchers have reported different capacities for angiogenesis and collateral development in different background strains of

mice (5,215,216). The rapid response to occlusion observed here corroborates the work by Scholz et al indicating that, unlike other strains, resting hind limb perfusion in the inbred C57BL/6 mouse strain is significantly recovered as early as 3 days post surgery (5). Here, the authors found that the process of collateralization is so fast and efficient in these mice that ischemia is minimized and angiogenesis, therefore, does not occur.

The tradeoffs that exist when defining the binarization threshold and the scanning resolution are important methodological cautions that must be considered when using micro-CT imaging for analysis of vascular structures. When defining the binarization threshold, a value that is too high will delete small vessels from the image, but a threshold that is too low can make major vessels appear artifactually large. It is our recommendation that the user makes a visual determination of the optimal threshold by assessing several specimens and then keeps this value constant for all evaluations within a study. This value should be chosen based on the threshold that allows the capture of the intricate details with minimal overestimation of broader structures.

We believe that choosing the voxel size of the scan should be chosen based on the proposed application. Scanning with smaller voxel sizes provides more information by resolving smaller vessels that cannot be detected at larger voxel sizes. However, based on the type of information sought and sample throughput considerations, scanning at a larger voxel resolutions can be more effective for some applications. For example, when using the mouse hind limb ischemia model, we were interested in gaining a global perspective of collateral growth in the upper thigh as is commonly done in 2-D by investigators who utilize x-ray microangiography. We believe that a voxel size of 36 μm is the best choice for this application because it allows us to preferentially focus our

analysis on the larger, arteriole-sized vessels, which are the best indicators of ischemic limb recovery. However, as shown here through voxel size sensitivity analysis and assessment of different micro-CT voxel sizes for resolving local vascular anatomy in cleared tissue sections, higher resolution scans are necessary to image smaller vascular structures. For example, a voxel size of 8 μm or smaller may be required for studies whose aim is to measure angiogenesis or small blood vessel structure within a confined area (i.e. tumor growth or fracture healing models). When using smaller voxel sizes, the major disadvantage is the increased scan time, along with the increased computational time and complexity required for analyses of a much larger data set.

Another possible drawback of the techniques used in this study is that they do not allow for longitudinal analyses at different time points within the same animal. Since this is a post-mortem analysis, the number of animals required for completion of a time course study is increased compared to methods such as laser Doppler perfusion imaging, which offers the ability to acquire multiple scans on the same living animal at different time points post surgery. The recent commercial availability of high speed in vivo micro-CT scanners that provide maintenance of animal anesthesia within the scanning system may remedy this limitation. However, before using these systems, one must consider the possible adverse biological effects that may result from repeated exposure of the animals to anesthetics and relatively high doses of x-ray radiation that would occur in a sequential study. In addition, the increased image quality afforded by decalcifying specimens will not be feasible in the in vivo systems. Other potential challenges presented by this technology are development of non-toxic contrast agents that persist in the bloodstream

long enough for image acquisition and gating methods to account for heartbeat and respiratory movements during the scan.

Previous studies that involved micro-CT imaging of the vasculature predominantly have used either barium sulfate based contrast agents (129,217,218) or polymerizing compounds containing lead chromate (121-127). As shown in our preliminary studies, choice of the ideal contrast agent can be a strong determinant of image quality for some applications. We found the polymerizing agent to be far superior for the hind limb ischemia model, but it is our recommendation that both contrast agents can potentially be useful depending upon the application. In this study, the silicon polymer was shown to be ideal for imaging collateral development compared to barium sulfate because it allowed us to circumvent problems such as settling and lack of homogeneity within the vasculature, clumping during injection, and difficulty with perfusion due to high viscosity. However, the presence of bone, a similarly attenuating material, required decalcification when global thresholding was used to segment the vasculature from surrounding tissues. The ability to mix barium sulfate to higher concentrations allows the possibility to achieve a stronger attenuating contrast agent and, therefore, allows use of a higher binarization threshold. As a result, barium sulfate can provide sufficient image thresholding of large arterial vessels even without bone decalcification, but high viscosity may limit the ability to perfuse small arterioles and the venous circulation.

Micro-CT has several superior features compared to other techniques for blood vessel morphological evaluation, but ultimately, the ideal strategy for microvascular analysis may include multiple methods that allow for both anatomical and functional

measures. The micro-CT vascular imaging methodology has the flexibility and potential to be adapted to other applications where vascular structures must be analyzed in a rigorous and quantitative fashion (e.g., fracture healing, tumor angiogenesis, coronary collateral growth, etc.). The most significant limitation of micro-CT is that it is a strictly anatomical assessment. While inferences regarding physiologic function can be deduced from micro-CT images, its strength is in the quantitative anatomical information it provides. Therefore, combining micro-CT with a more powerful method for functional analysis such as laser Doppler perfusion imaging, MRA, or micro-PET may provide the most comprehensive evaluation of vascular network structure and function.

CHAPTER 4

THE ROLE OF OSTEOPONTIN IN POSTNATAL VASCULAR GROWTH

Introduction

Peripheral arterial occlusive disease (PAD) causes obstruction of flow in arteries, typically in the lower limbs, and is caused primarily by atherosclerosis. These obstructions can cause intermittent or chronic ischemia and pain in the extremities, which can lead to amputation in the most severe cases. PAD affects 17% of men and 21% of women who are 55 years or older, but prevalence is much higher in smokers and those with diabetes mellitus, with advanced disease progression being much more common in patients with these risk factors (219). Therapeutic angiogenesis, stimulation of new blood vessel formation to increase blood flow to ischemic tissues, presents a relatively new clinical approach for alleviating the deleterious effects of PAD.

Although this strategy is termed "therapeutic angiogenesis", the goal is to increase perfusion to ischemic tissues by any means possible, including arteriogenesis and vasculogenesis. The majority of studies geared toward development of therapeutic angiogenesis treatments have focused on the clinical potential of growth factor delivery (i.e. VEGF or FGF) or stem cell therapy (i.e. EPCs). Preclinical data using either VEGF or FGF have shown tremendous promise in a variety of animal models (26-30). Unfortunately, the initial human trials have not corroborated these results and have shown almost no improvement in clinical outcome (31-34). Cell therapy has also shown accelerated recovery from ischemia in animal work (59-62). By most accounts, clinical trials using cell therapy have been more favorable than those using growth factors, yet the

levels of clinical improvement have been modest (81,82). While therapeutic angiogenesis trials have shown enough clinical potential to warrant further investigation, improved efficacy will be necessary before any of these techniques can gain broad clinical use. To do so, it will be imperative that scientists are able to better define the roles of all factors involved in postnatal vascular growth, and clinicians must carefully consider the roles of other mediators, such as ECM proteins, in addition to the potential synergistic effects of using combined growth factor and cell therapies.

Previous studies have pinpointed several factors that, when studied in isolation, appear to play a significant role in the process of postnatal vascular growth. However, restoration of ischemic limb perfusion requires a precise interplay between numerous cell types, growth factors, and cues provided by the extracellular environment. In order to better develop therapeutic angiogenesis regimens, each of these areas must be better understood in isolation and more importantly, in the context of their interactions with each other. The ECM, which is probably the most neglected of these three areas, provides the structural scaffolding that maintains the organization of vascular cells into blood vessels and initiates signals that stimulate events such as cellular survival, proliferation, and migration. In order to better understand this aspect of collateral vessel formation, we have focused on the role of the ECM protein osteopontin during ischemic limb revascularization.

OPN is synthesized as a 34-kDa protein and functions in a variety of biological processes including, but not limited to, inflammatory response, immunity, wound repair, tumor formation and metastasis, cell adhesion, cell migration, and bone mineralization and remodeling. OPN has been classified by some as a “matricellular protein”, a

categorization for nonfibrillar, bioactive ECM proteins that are thought to mediate cellular functions by providing a functional link between cell surface receptors, structural ECM molecules, and cytokines, growth factors, and proteases (156). OPN interacts with as many as seven different integrins through its RGD or more novel SVVYGLR binding sequences (155,157-161). Many of these integrin interactions are regulated by thrombin cleavage, which is thought to increase accessibility of cell receptors to their binding domains and greatly enhance the cellular effects of OPN (162). Also, an intracellular form of OPN that localizes to the cell membrane where it binds to the cell surface glycoprotein CD44 has been found to be an integral component in cell migration (165,167).

Although OPN was originally isolated from bone, it has also been found to be important for normal arterial physiology (173). Albeit in the context of atherogenesis, OPN has been found to be produced by the three primary cell types traditionally thought to participate in blood vessel growth: monocytes/macrophages, endothelial cells, and smooth muscle cells (174). Previous *in vitro* studies have demonstrated that vascular cell interactions with OPN mediated through cell surface integrins regulate a variety of cellular functions that are potentially important to angiogenesis and arteriogenesis. In this context, OPN signaling through the $\alpha_v\beta_3$ integrin has been found to mediate endothelial cell survival in a process that involves the NF-κB signaling pathway (175). Also, the angiogenic growth factor VEGF has been shown to trigger an increase in $\alpha_v\beta_3$ expression, OPN expression, and thrombin cleavage of OPN, which provides a cooperative mechanism that enhances endothelial cell migration (176). In addition, OPN expression is induced by stimulation with FGF, and this cross-talk may provide a

mechanism for recruitment of monocytes and amplification of FGF-induced angiogenesis (177). OPN also mediates several processes relevant to arteriogenic collateral vessel formation including adhesion and migration of both macrophages and smooth muscle cells. (178-180). There have been a small number of *in vivo* studies that have implicated OPN in postnatal neovascularization. For example, OPN mRNA has been shown to be locally upregulated at sites of ischemia-induced retinal neovascularization in mice (3), and OPN has been found to correlate with progression of the angiogenesis-related processes tumorigenesis and metastasis (169).

Based on the observations discussed above, it is likely that the vascular effects of OPN are also relevant in recovery from limb ischemia. However, the specific function of OPN during ischemic limb revascularization has not been previously determined. In the present study, we hypothesized that OPN deficiency reduces postnatal vascular growth and delays reperfusion of ischemic tissues and recovery of limb functionality. To test this hypothesis, we have investigated *in vivo* hind limb ischemia and *in vitro* cellular function assays in wild type and $OPN^{-/-}$ mice. For the *in vivo* model, endpoints included anatomical quantification of the collateral vasculature, measurement of physiological blood perfusion, and functional assessment of exercise endurance. For *in vitro* studies, endpoints included endothelial cell sprouting and tube formation, in addition to evaluation of macrophage migration.

Methods

Mice

Male wild type C57BL/6 mice were purchased from the Jackson Laboratory. Osteopontin deficient mice were originally received from Dr. Lucy Liaw of the Maine

Medical Center, and they were subsequently backcrossed ten generations onto the C57BL/6 background. All animals were fed a standard chow and had free access to water. All protocols were approved by the Institutional Animal Care and Use Committee and done in accordance with the federal guidelines on the principles for the care and use of animals in research.

Hind Limb Ischemia Model

Animals were anesthetized by intraperitoneal injection of xylazine (10 mg/kg) and ketamine (80 mg/kg). All hair was removed from the surgical site, and the area was cleansed with sterile water followed by betadine. A unilateral incision was then made over the right medial thigh of the mouse. The superficial femoral artery and vein were ligated proximal to the caudally branching deep femoral artery, and a second ligation was performed just proximal to the branching of the tibial arteries. The femoral nerve was left intact and dissected away from the vasculature between the proximal and distal ligation. The length of the artery and vein was separated from surrounding tissues and excised between the two ligation points. The skin was then closed with interrupted silk sutures. The mice were allowed to recover on a heated pad, and, after awakening, they were returned to their cages and allowed to ambulate freely.

Micro-CT Imaging of Collateral Vessels

Novel quantitative micro-CT based methods developed in our laboratory were utilized for evaluation of ischemic limb collateralization (130). Mice were sacrificed using carbon dioxide inhalation at 7 days post surgery (wild type n=7, $OPN^{-/-}$ n=7). The vasculature of the mice was sequentially perfused at physiologic pressure using heparinized (100 units/mL) normal saline, 10% neutral buffered formalin, and then again

with heparinized saline. The vascular system was subsequently injected with a radiopaque, lead chromate based contrast agent (Flow Tech Inc.), which was then allowed to polymerize for 24 hours at 4°C. The mouse hind limbs were then dissected free from the remainder of the animal and placed in 10% neutral buffered formalin for 48 hours. Afterwards, the specimens were soaked for 48 hours in a formic acid based solution (Cal-Ex II, Fisher Scientific) for decalcification of the mineralized bone, washed thoroughly using water, and placed in 10% neutral buffered formalin until imaging. The vasculature located between the proximal ligation point and the ankle was imaged at a 30-μm voxel size, and the tomograms were globally thresholded based on x-ray attenuation and used to render binarized 3-D images of the hind limb vascular network segmented from the surrounding tissues. These 3-D images were evaluated for vascular volume.

Laser Doppler Perfusion Imaging

Laser Doppler Perfusion Imaging was completed 3, 7, and 14 days post surgery to assess perfusion to the paw of the ischemic limb (n=11-14 for each genotype at each time point). Mice were anesthetized with xylazine (10 mg/kg) and ketamine (80 mg/kg) and scanned with laser Doppler perfusion (PIM II Laser Doppler Perfusion Imager). To do so, anesthetized animals were placed in the supine position on a heating pad under the laser scanner. The lower limbs were imaged, and the footpad was chosen as the region of interest for calculation of perfusion values. To account for possible differences in ambient temperature and lighting, the ratio was calculated for the average perfusion in the foot of the ischemic leg to the foot of the control leg.

Swim Endurance Test

As a physiologic test of ischemic limb functional recovery, experiments measuring swim time until exhaustion were completed. To do so, we built a current pool that stimulates forced swimming in mice (220). This apparatus possesses a roller pump that can generate a surface current, forcing the mice to swim upstream as shown in the schematic in Figure 4.1. The water temperature was maintained at 35°C with a submersible heater (Cole Parmer), and, using the pump, flow rates of 5 L/min were generated. Prior to onset of hind limb ischemia, mice were trained for 5 minutes per day for 7 days in order to acclimate the animals to swimming. At 5 days post-surgery, maximal exercise capacity was defined as the amount of time the animal could swim against the current before experiencing 5 consecutive seconds of submersion, at which point the mouse was removed from the tank (wild type n=8, $OPN^{-/-}$ n=8).

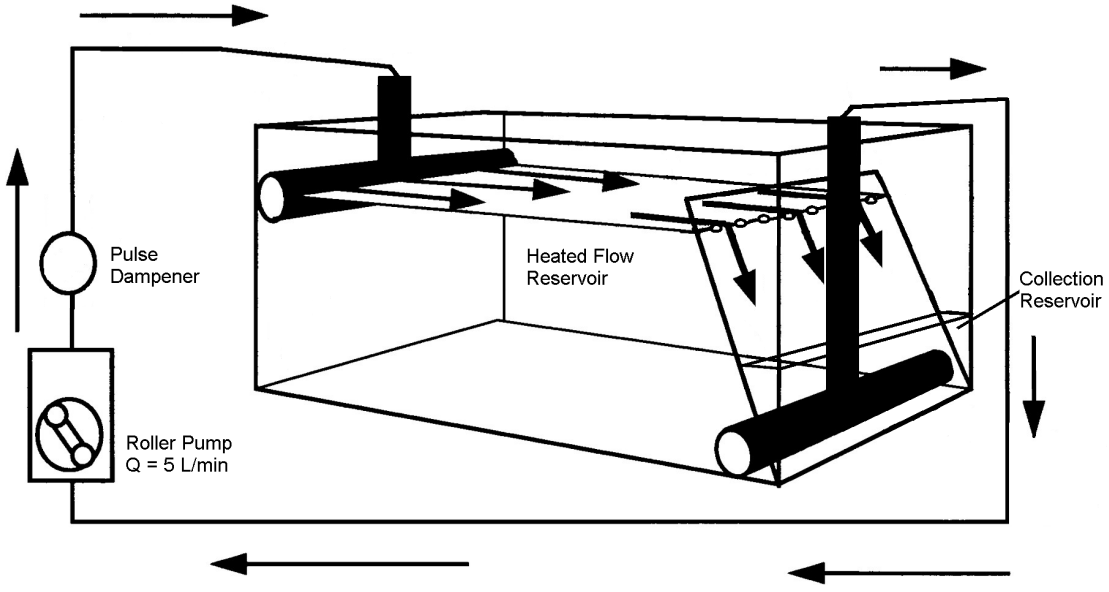

Figure 4.1. Schematic of flow tank for testing exercise endurance. In this system, a current is generated on the surface of the water in the tank. This surface current flows through a vent into the collection reservoir and recirculates to the flow reservoir.

Mouse Serum Isolation

Mice were euthanized with carbon dioxide inhalation. Blood was immediately taken from the right ventricle using a 21-gauge needle. Blood samples were left to coagulate for 45 minutes at room temperature. They were then centrifuged, and the serum supernatants were pipetted from the samples, sterilized using a syringe filter, and frozen at –80°C until use.

Aortic Ring Vascular Sprouting Assay

The mouse aortic ring assay was utilized as previously described (96). 1.5% agarose wells were created with an inner diameter of 10 mm and an outer diameter of 17 mm. Three of these wells were placed into each 60 mm bacterial culture dish. The aorta was dissected from the mouse and placed into cold serum free DMEM containing penicillin and streptomycin. The adventitial layer was carefully dissected away, and 1 mm sections were cut from the mid-thoracic region of the aorta. These rings were rinsed 2-3 times in cold DMEM and then embedded in collagen gels. In order to stain endothelial cells prior to embedding, aortic rings were incubated with fluorescently labeled low-density lipoprotein (Biomedical Technologies) for a small subset of samples. These explants were imaged with fluorescent microscopy to confirm that cells participating in tube formation were endothelial in nature.

To embed the explants, 200 µl of 1.5 mg/ml rat tail type I collagen (Serva Chemical) was initially pipetted into the bottom of each agarose well and placed into the incubator for 15 minutes to polymerize. Then, an aortic segment was placed on top of each of these collagen layers and covered with another 200 µl of type I collagen. After allowing the second collagen layer to gel for 15 minutes in the incubator, 6 mLs of

MCDB-131 containing 25 mM $NaHCO_3$, 2.5% autologous mouse serum, 1% glutamine, and penicillin/streptomycin was added to the dish. Explants were imaged microscopically at 4, 6, 8, and 10 days, and the number of vascular sprouts and length of the largest sprout from each aorta were measured.

Monocyte/Macrophage Migration Assay

Cell culture transwell chemotaxis inserts (Falcon) with a pore size of 8 μm were coated overnight at 4°C with 10 μg/ml fibronectin (Sigma) and then allowed to air dry. Resident monocytes and macrophages were isolated from wild type and OPN deficient mice by peritoneal lavage with cold PBS. Harvested cells were centrifuged, resuspended in 0.2% BSA, and counted using a Coulter counter. 720 μl of DMEM was placed in the lower well, and cells were seeded onto the tops of the inserts (400,000 cells per transwell) in 200 μl of DMEM. Dishes were placed into the incubator, and the cells were allowed to adhere for 1 hour. At this time, 80 μl of blank media or media containing chemoattractants were added to the lower reservoirs of the appropriate wells to reach a total volume of 800 μl with a final concentration of 5% homologous serum, 100 ng/ml MCP-1 (R&D systems), or negative controls with no stimulus (no stim). After incubation for 8 hours, non-migrated were removed from the top of the membrane using cotton swabs. Then, the remaining migrated cells were stained with Diff-Quick and imaged using brightfield microscopy. Cell numbers were quantified from three random fields for each insert using the Image Pro software.

Results

Micro-CT Imaging of Collateral Vessels

Micro-CT Imaging was completed at 7 days post surgery as a quantitative, anatomical measure of collateral vessel formation. Qualitative observation of the 3-D image reconstructions of the vasculature of the ischemic limbs showed decreased collateral blood vessel formation in upper thigh region of the OPN deficient mice relative to the wild types as shown in Figure 4.2 A. Quantitative analysis of these specimens determined that the OPN knockouts possessed significantly reduced vascular volume of the ischemic limb (Figure 4.2 B). We also completed a size discriminated measurement on what we deemed to be newly formed collaterals, which were defined as vessels with diameter less than or equal to 180 microns. When we completed this focused analysis, we found that the OPN deficient animals possessed significantly decreased vascular volume relative to the wild types, indicating that the difference in total vascular volume was primarily driven by a lack of smaller, newly formed collateral-sized vessels (Figure 4.2 C).

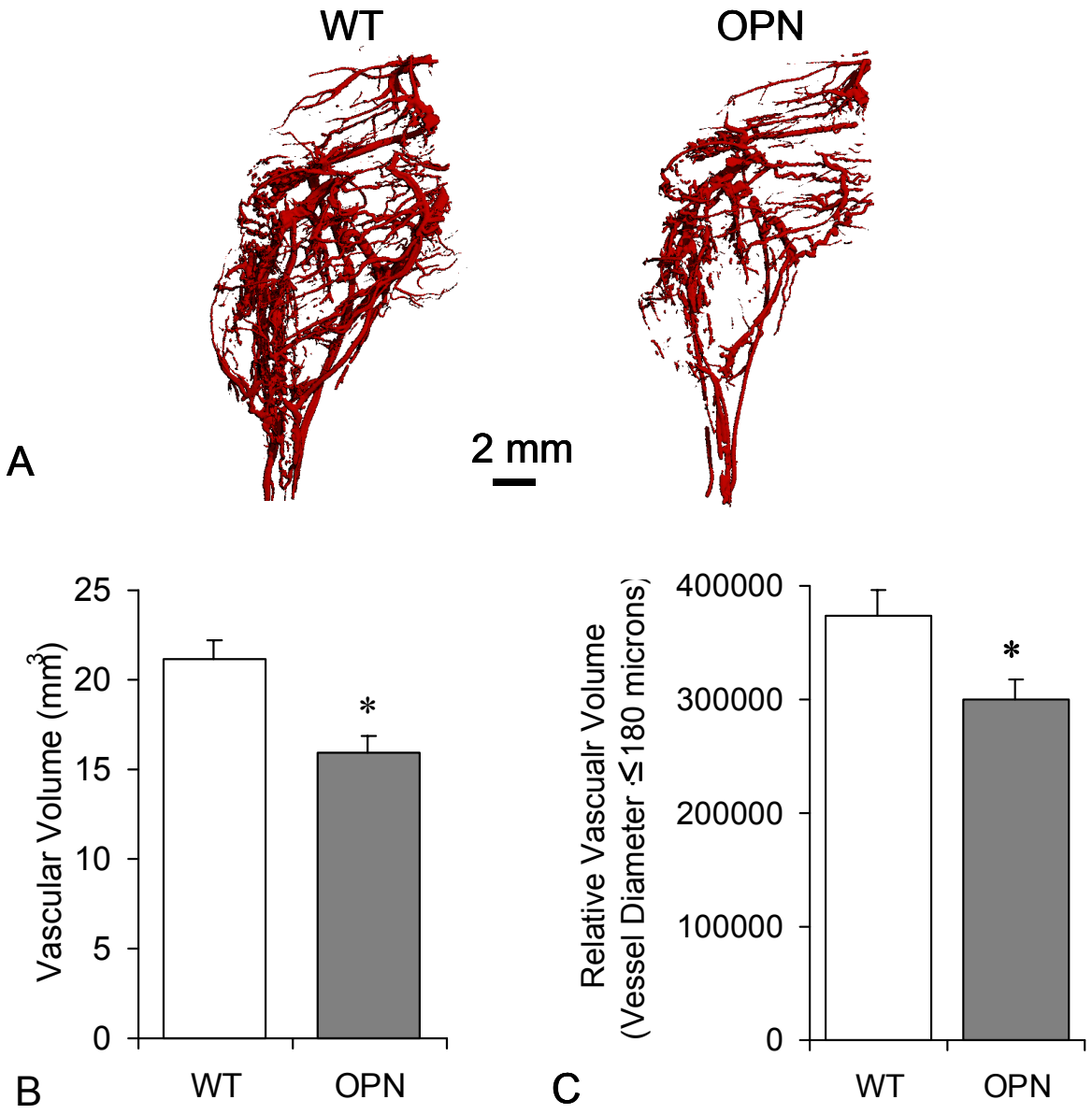

Figure 4.2. Micro-CT image analysis. (A) Micro-CT images showing decreased collateral vessel formation in OPN deficient mice. (B) Quantitative analysis shows significantly decreased vascular volume in OPN deficient mice. (C) Relative volume of vessels less than or equal to 180 microns in diameter illustrates the defect in formation of small, collateral vessels in OPN deficient mice. Data presented as mean+SEM. n=7 for all analyses. * indicates $p<0.05$ using student's t-test.

Laser Doppler Perfusion Imaging

LDPI was performed to test for recovery of distal perfusion to the ischemic limb 3, 7, and 14 days post surgery. The acquired images illustrated a gradual recovery of perfusion to the paw for both genotypes, with a visible lag in recovery seen in the OPN deficient mice (Figure 4.3 A). After calculation of average perfusion in the ischemic paw relative to the contralateral paw, we found both genotypes to have only approximately 25% perfusion by 3 days. However, by 7 days post surgery, the wild types resting perfusion values were at about 70% of normal, while the OPN mice were significantly lower at around 40%. At 14 days, this significant deficiency in perfusion recovery was even more pronounced, with wild types having nearly normal perfusion (88%) while the OPN knockouts possessed a persistent blood flow defect (45%). See Figure 4.3 B.

Swim Endurance Test

As a functional measure of ischemic limb recovery, exercise capacity was measured 5 days post surgery. At this time point, these mice, which had undergone one week of training prior to surgery, were forced to swim against a generated current until failure. Using this metric, it was determined that the OPN deficient mice had significantly hindered function of the ischemic limb, as shown by a 40% decrease in maximal swim time relative to the wild types (Figure 4.4).

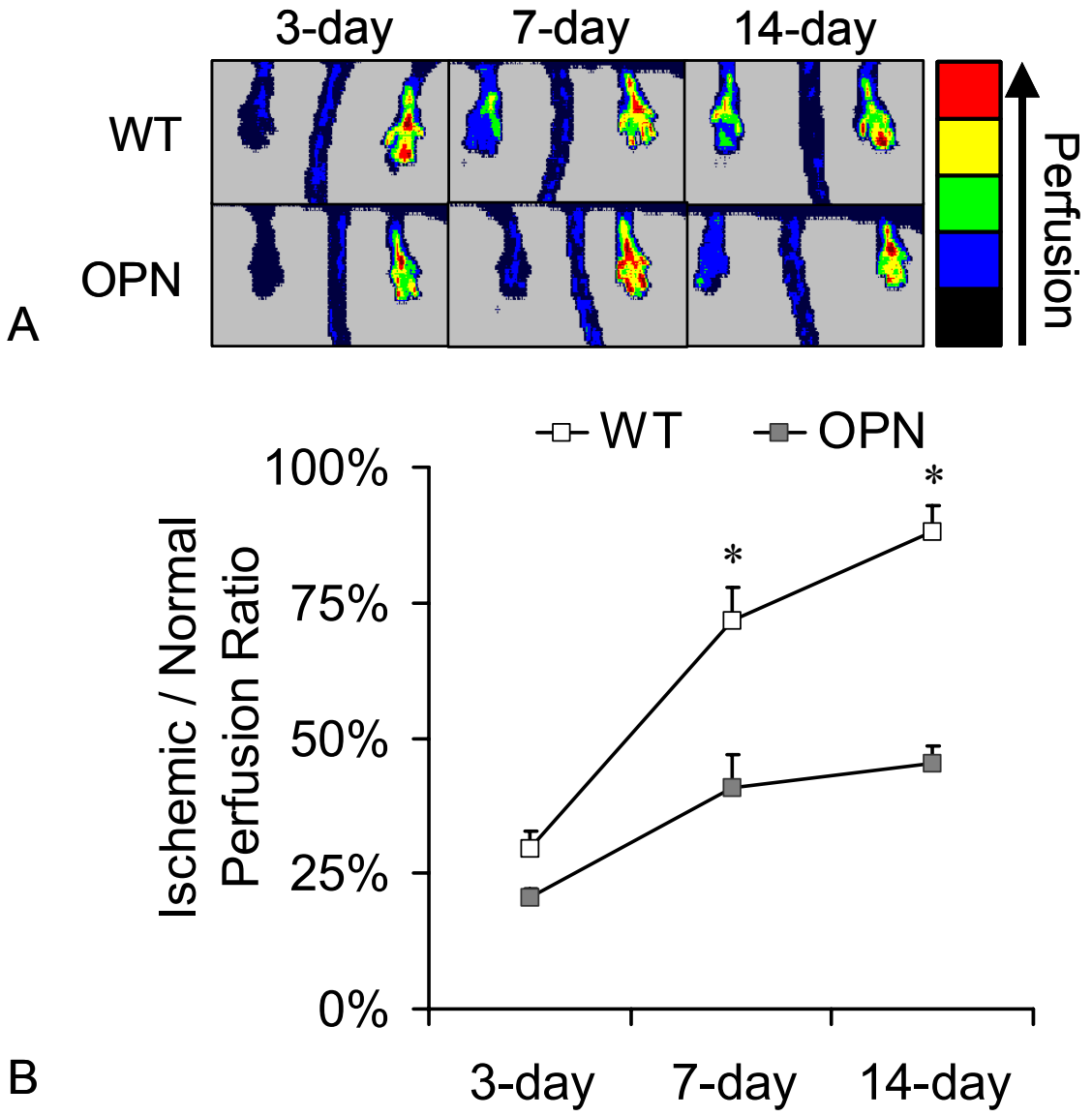

Figure 4.3. LDPI analysis. (A) Representative LDPI images display the time course of recovery of ischemic limb perfusion in OPN deficient and wild type mice. Color-coded perfusion scale shown on right. (B) Quantitative analysis (average perfusion in ischemic paw / average perfusion in normal paw) displayed a significant lag in recovery in OPN deficient mice. Data presented as mean+SEM. n=11-14 for each group. * indicates significant differences ($p<0.001$) determined using Tukey's method for pairwise comparisons between genotypes at the indicated time points.

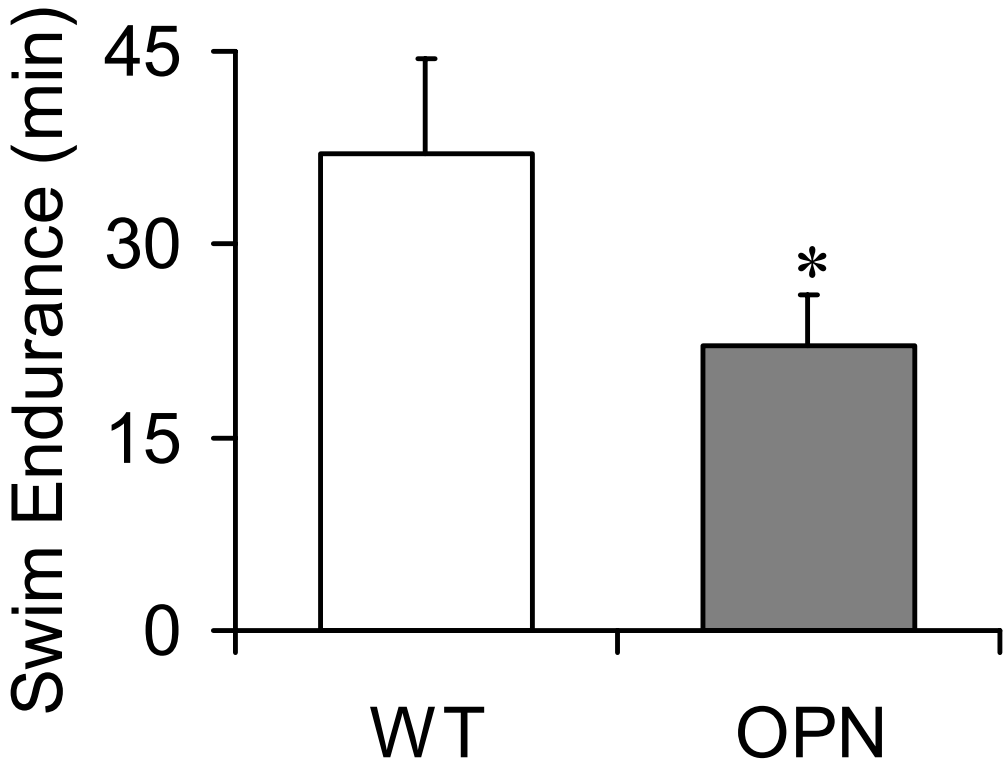

Figure 4.4. Swim endurance test. Relative to wild types, OPN deficient mice displayed significantly decreased swim endurance 5 days following onset of ischemia. Data presented as mean+SEM. For each group, n=8. * indicates $p<0.01$ using student's t-test.

Aortic Ring Vascular Sprouting Assay

The aortic ring assay was utilized to measure endothelial cell angiogenic capacity through their ability to sprout/migrate into a collagen gel and form vascular tubes. Wild type and OPN deficient aortic rings were harvested, embedded *ex vivo* in collagen gels, and assayed for neovascular sprouting every two days from 4-10 days. These rings displayed substantial sprouting, which peaked at around 1 week and could be imaged using light microscopy. There was a modest, but insignificant overall decrease in sprout number in OPN deficient specimens relative to wild types, and there was no difference between genotypes for maximum sprout length (Figure 4.5).

Monocyte/Macrophage Migration Assay

Since movement of monocytes and macrophages to sites of angiogenesis and collateralization is suspected to be a pivotal early event in these processes, we evaluated migration of these cells in response to chemoattraction. To do so, peritoneal monocytes/macrophages were harvested from wild type and $OPN^{-/-}$ mice and assayed for chemotaxis toward homologous serum and MCP-1. Homologous serum produced a strong induction in monocyte/macrophage migration for both genotypes. $OPN^{-/-}$ serum stimulated a significant increase (2.4-fold) in migration of $OPN^{-/-}$ cells. Wild type cells displayed significant migration toward homologous serum (6.8-fold increase), which was also significantly greater than the chemotactic response of the $OPN^{-/-}$ cells to serum (Figure 4.6 A). In $OPN^{-/-}$ cells, MCP-1 did not invoke significant migration above negative controls. Wild type cells exposed to MCP-1, on the other hand, migrated significantly more than cells that were not exposed to chemoattraction or OPN deficient cells that were stimulated with MCP-1 (Figure 4.6 B).

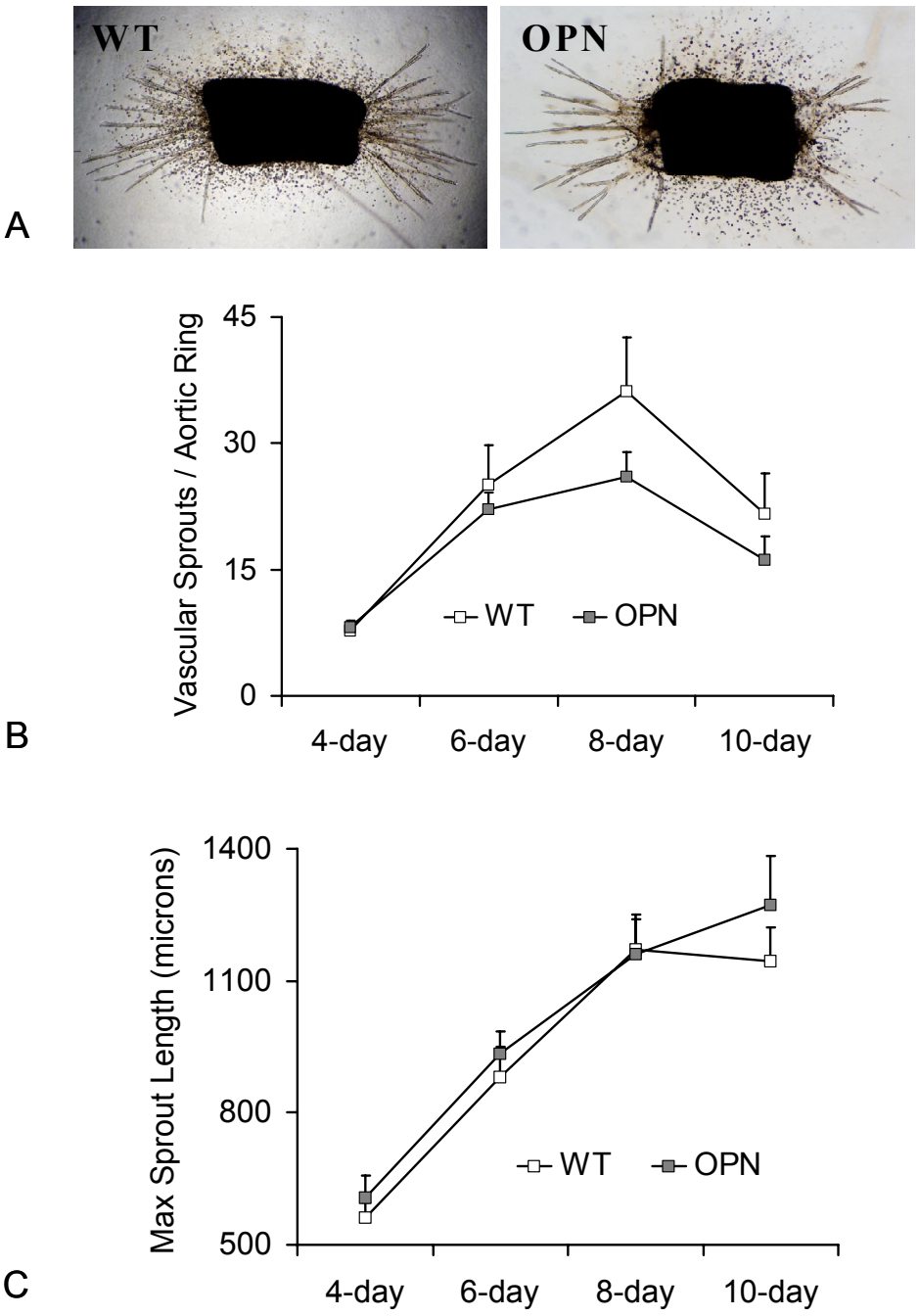

Figure 4.5. Aortic ring sprouting assay. (A) Representative aortic ring specimens displayed that the OPN deficient specimens possessed a modest decrease in angiogenic sprouting at 8 days. (B) OPN deficient mice displayed a trend towards reduction in number of vascular sprouts and (C) no difference in maximum sprout length over a 10 day time course. Genotype was not found to be a significant predictor of sprout number or maximum sprout length using ANOVA, and, using Tukey's method, it was determined that no significant differences existed in pairwise comparisons between genotypes for either measure at any time point. Data (n=9) presented as mean+SEM.

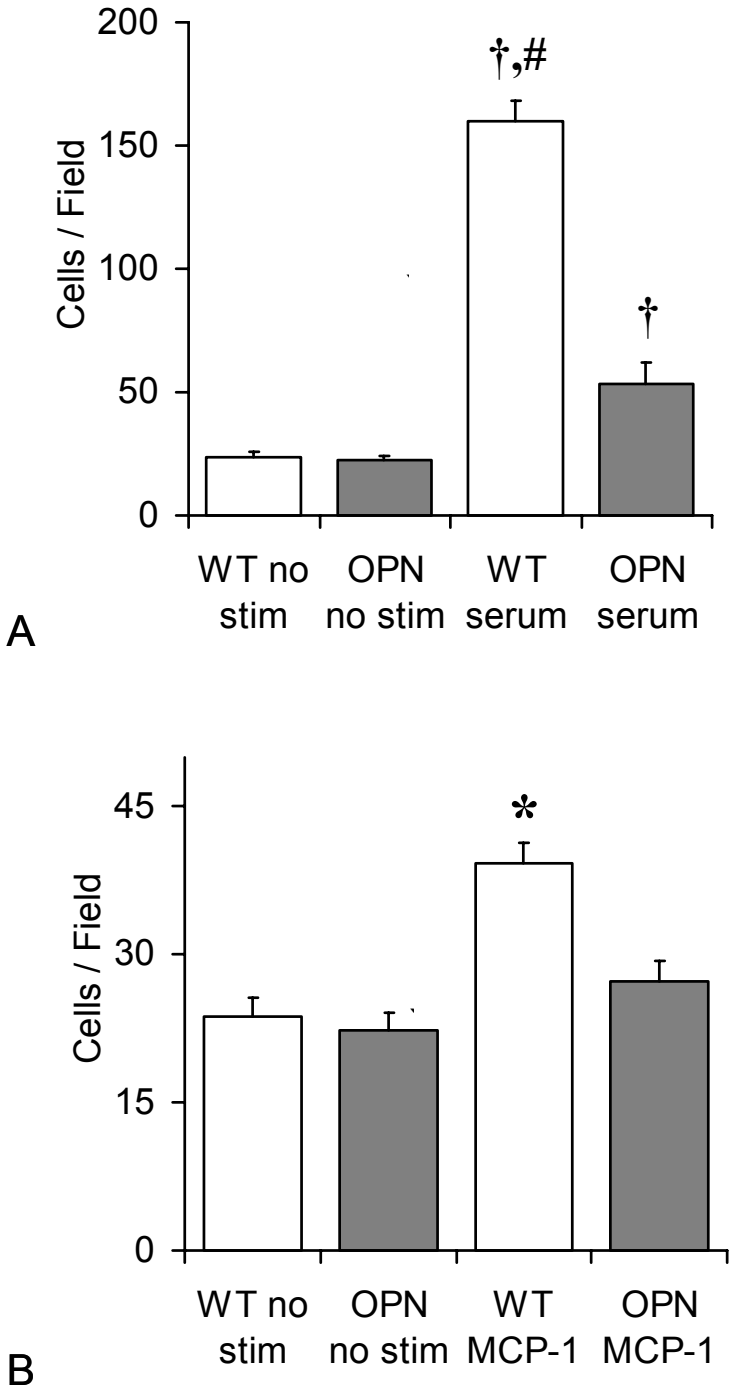

Figure 4.6. Macrophage chemotaxis assay. OPN deficient mice displayed a significant quantitative reduction in number of monocytes/macrophages that migrated across the membrane in response to chemoattraction from (A) homologous serum or (B) MCP-1. Data presented as mean+SEM. For each data point shown, n=12 (4 wells, 3 fields per well). Post-hoc comparisons done using Tukey's method. † indicates significance ($p<0.01$) versus WT no stim and OPN no stim. # indicates significance ($p<0.0001$) versus OPN serum. * indicates significantly different ($p<0.001$) from WT no stim, OPN no stim, and OPN MCP-1.

Discussion

Previous *in vitro* studies have discovered roles for OPN in controlling survival, migration, and other functions in multiple cell types involved in postnatal vascular growth. In this study, we sought to determine the *in vivo* significance of OPN in angiogenesis/arteriogenesis processes. To do so, we compared wild type and $OPN^{-/-}$ mice for their capacity to form collateral vessels and functionally recover following acute induction of hind limb ischemia. Following ligation and excision of the femoral artery, OPN deficiency was found to significantly delay collateral vessel formation, restoration of distal limb perfusion, and recovery of the functional capacity of the ischemic limb. These *in vivo* observations were found to correlate to normal *ex vivo* endothelial sprouting. In contrast, these results corresponded to a substantial decrease in migration of *in vitro* $OPN^{-/-}$ monocytes/macrophages in response to chemoattraction. These data suggest that OPN is a critical regulator of collateral vessel formation and that this effect is driven by its role in mediating monocyte/macrophage migration and functionality.

The initial endpoint of our study was based on quantitative 3-D micro-CT imaging methodologies that were established in our lab (130). Using this technique, we are able to perform high resolution, objective, and quantitative measurements of the global vascular anatomy within the mouse hind limb to a degree not afforded by immunohistochemistry, X-ray angiography, or other commonly utilized methods. Importantly, using this modality, we were able to detect significantly decreased total vascular volume, which was driven by a decrease in smaller, collateral-sized vessels in OPN deficient mice. Next, we utilized the LDPI imaging methodology as a measure of blood flow to evaluate the physiological significance of this finding. LDPI is a

commonly used endpoint in mouse hind limb ischemia studies, and it has been found to correlate with histological vessel counting (107). Using LDPI, we performed measurements on anesthetized mice and found decreased recovery of perfusion to the ischemic paw in the $OPN^{-/-}$ mice at both 1 and 2 weeks post surgery. In addition, we measured the exercise capacity of the mice as a means for functional assessment of ischemic limb recovery. We felt that it was especially important to run this full complement of studies to correlate vascular anatomy and blood flow to limb functionality, considering previous reports have indicated that measuring resting blood flow does not always accurately reflect the true flow deficit in animal models of hind limb ischemia (116). In order to measure limb functionality, we built a swimming apparatus that forced the mice to swim against a generated current (220). This technique, unlike treadmill tests, requires that the mice equally utilize both of the hind limbs and provides a useful methodology for measurement of exercise endurance and, therefore, functional recovery of the ischemic leg. Using this apparatus, we were able to measure a significant functional impairment of the ischemic limb in the $OPN^{-/-}$ mice relative to the wild types at 5 days post surgery. Taken together these data indicate an unequivocal role for OPN in revascularization and recovery from hind limb ischemia.

Endothelial cell function is generally considered to be of the utmost importance for neovascularization. Therefore, in order to better understand our *in vivo* findings, we first sought to assess the capacity for endothelial cell tube formation in aortic explants from OPN deficient mice. To do so, we employed the aortic ring vascular sprouting assay, which allows controlled measurement of neovascular sprouting from an intact vessel segment containing the full complement vessel constituents (96). In this study,

OPN null specimens showed trends toward decreased sprout number, but no significant differences were detected between genotypes for sprout number or maximum sprout length. These results indicate that OPN may not play a vital role in endothelial cell migration and tube formation during angiogenesis. However, this assay is limited by the fact that it measures the angiogenic response of the aortic endothelium rather than that of the microvasculature, which participates in the *in vivo* neovascularization process.

It is well-accepted that monocytes/macrophages bind to the vascular wall and localize to sites of angiogenesis and arteriogenesis where they play an important role in modulation of these processes (6). This finding dates back 30 years to the observation by Shaper *et al*. that large numbers of monocytes adhered to the endothelium and passed into the vessel wall of forming collaterals in the dog heart (40). Subsequent studies have shown a direct functional link between circulating monocyte concentration and arteriogenic collateral vessel formation (42,43). MCP-1 is thought to be the primary stimulus for induction of monocyte infiltration in this setting, and MCP-1 treatment has been shown to accelerate collateralization and recovery in hind limb ischemia models in a variety of animal studies (44,47-53). Conversely, animals deficient in MCP-1 or CCR2-chemokine receptor, an MCP-1 receptor, have been shown to display reduced monocyte/macrophage infiltration and collateral formation (54,55).

These studies have established monocyte and macrophage migration to the site as a pivotal event in ischemic limb revascularization and recovery. In addition, previous work has indicated that OPN helps to mediate macrophage adhesion and migration, and other studies have indicated that OPN may be important for macrophage infiltration to sites of injury *in vivo* (178). Due to this established connection between OPN and

macrophage migration, we hypothesized that OPN would play a role in macrophage infiltration and function at sites of postnatal vascular growth. In order to test this hyposthesis, we compared macrophage/monocyte migration capacity of wild type and OPN deficient mice. To do so, we utilized the transwell cell culture system to evaluate the migratory response of monocytes/macrophages that were isolated using peritoneal lavage. In these studies, we found that $OPN^{-/-}$ monocytes/macrophages displayed significantly reduced migration in response to chemoattraction. In initial experiments, we found that wild type cells exhibited a 3-fold stronger migratory response to homologous serum than $OPN^{-/-}$ cells. Next, we evaluated whether this defect in migration would be sustained using an OPN-free chemotactic stimulus, MCP-1. MCP-1 induced significant migration of wild type cells relative to controls (1.7-fold), but the response was not as strong as it was to serum. Importantly, as seen in the experiments using serum, this response was significantly higher than the $OPN^{-/-}$ cells, which did not display any significant migratory response to MCP-1 relative to cells exposed to no chemoattraction. These findings corroborate a previous study that found OPN to be important to chemotactic response of macrophages to MCP-1 *in vitro* (221). This experiment indicates that the migratory defect in the $OPN^{-/-}$ monocytes/macrophages is not dependent upon stimulation from exogenous OPN alone and that this response is driven at least in part by autocrine OPN stimulation.

The significance of our *in vitro* findings showing decreased migration of $OPN^{-/-}$ mononctyes/macrophages toward MCP-1 is strengthened by the fact that MCP-1 has been shown by numerous studies to play an important role in *in vivo* stimulation of monocyte homing and activity at sites of collateralization. It is believed that once these

cells have arrived at the site of angiogenesis/arteriogenesis, they produce growth factors and proteases that induce vascular endothelial and smooth muscle cell proliferation and stimulate remodeling of the vascular wall in order to satisfy increased blood flow demands. In addition to providing paracrine stimulation of other cells types, monocytes have also been reported to tunnel through ischemic myocardium and form physical conduits that could be subsequently endothelialized and incorporated into the preexisting vasculature (222). Therefore, defective migratory response to chemoattraction and the subsequent reduction in activity of monocytes and macrophages at the site of collateralization likely has significant, detrimental effects on revascularization and recovery of the ischemic limb in the $OPN^{-/-}$ animals.

In this study, we have presented evidence suggesting that a definitive biological role exists for OPN in the vascular response in the mouse hind limb ischemia model. We were able to confirm this finding using a range of anatomical, physiological, and functional measurements on the ischemic limb. We have also reported evidence that suggests that this defect in angiogenesis/arteriogenesis could be driven by alterations in macrophage migration and function in the OPN null mice. These findings represent the first evidence that OPN may be a key regulator for postnatal vascular growth and that OPN may be an important mediator of macrophage function in this setting.

CHAPTER 5

IMPAIRED ANGIOGENESIS, EARLY CALLUS FORMATION, AND LATE STAGE REMODELING IN FRACTURE HEALING OF OSTEOPONTIN DEFICIENT MICE

Introduction

Bone fracture healing involves a well-characterized cascade of events that includes hematoma formation, inflammation, soft cartilaginous callus formation, neovascularization, osteoblastic callus mineralization, and osteoclastic remodeling of the hard callus back to mature lamellar bone (144). This complex sequence of biological processes is orchestrated by a variety of growth factors and matricellular proteins that regulate differentiation, chemotaxis, and haptotaxis of the cell types responsible for mediating these events. For example, the family of BMPs has been thoroughly characterized for induction of osteogenesis at fracture sites and is utilized clinically to promote bone regeneration (147). In addition, Street *et al* have shown that VEGF, a known promoter of angiogenesis, stimulates neovascularization and promotes fracture healing, while treatment with angiogenesis inhibitors that specifically target vascular cells blocks fracture healing and produces atrophic nonunions (151,152). Furthermore, as reviewed by Alford *et al*., ECM proteins, while not always vital for normal embryonic bone development, play an important role in mediating cellular function and serve as important modulators of bone regeneration (154). Further understanding of the intricate interplay between this diverse set of cell types, endogenous factors, and matrix proteins is

a necessity for the development of improved therapeutic strategies for promoting bone repair.

Osteopontin is one of the major non-collagenous ECM proteins in bone. It has been studied based on its role in a diverse range of biological processes including inflammation, immunity, angiogenesis, wound repair, tumor formation and metastasis, cellular survival and migration, and osteoclastic bone remodeling. Although now known to also be present in a number of nonmineralized tissues, OPN was originally cloned from bone where it has been shown to have a functional role in controlling mineralization and remodeling. OPN inhibits mineral crystal formation and growth (188,189), and OPN deficient mice have been found to possess increased mineral content and crystallinity (190). In addition, OPN is known to be a major ligand for CD44 on bone cells, which is important in mediating osteoclast recruitment and function (187,191,192). The *in vivo* importance of OPN in bone remodeling has been further demonstrated by the finding that OPN deficient mice undergo significantly less bone resorption than wild type mice in response to reduction in mechanical loading, ovariectomy, stimulation by parathyroid hormone, or administration of a high phosphate diet (193-196).

While many researchers have studied the role of OPN in bone, it is also important for normal arterial physiology (173) and is produced by the primary cell types involved in blood vessel growth and remodeling: monocytes/macrophages, endothelial cells, and smooth muscle cells (174). In addition to its interactions with CD44, OPN also contains an RGD motif, which allows it to interact with the integrin family of cell-adhesion molecules including $\alpha_4\beta_1$ (158) and $\alpha_v\beta_3$ (176). Previous *in vitro* studies have demonstrated that cellular interactions with OPN mediated through these integrins

regulate a wide variety of cellular functions relevant to angiogenesis including vascular cell adhesion and spreading (179), macrophage adhesion and migration (178), endothelial cell migration (176), endothelial cell survival (175), chemotactic response of smooth muscle cells (179), and smooth muscle cell migration (180). Other *in vivo* studies have also implicated OPN in neovascularization and remodeling of the vessel wall. For example, OPN mRNA has been shown to be locally upregulated at the site of ischemia-induced retinal neovascularization in mice (3), and OPN deficiency has been found to decrease angiogenesis around ectopic bone implants and to diminish arterial remodeling (2,173). Based on these observations, it is likely that the vascular effects of OPN are also relevant to vessel formation and maturation during fracture healing.

The role of OPN in a diverse set of processes including macrophage function, angiogenesis, ECM mineralization, and osteoclastic bone remodeling suggests that OPN may be important during multiple stages of fracture healing. Previously, *in situ* hybridization studies have noted OPN expression in the fracture callus by osteoprogenitors in woven bone, hypertrophic chondrocytes in the cartilage to bone transitional region, and in the osteocytes, osteoblasts, and osteoclasts of the hard callus (144,197,198). However, the specific function of OPN during bone healing has not been previously determined. In the present study, we hypothesized that OPN deficiency alters neovascularization, mineralization, remodeling, and the restoration of mechanical properties during fracture healing. To test this hypothesis, we have investigated fracture repair in wild type and $OPN^{-/-}$ mice.

Methods

Animals

Male wild type C57BL/6 mice were purchased from the Jackson Laboratory. Osteopontin deficient mice were originally received from Dr. Lucy Liaw of the Maine Medical Center (170), and they were subsequently back-crossed ten generations onto the C57BL/6 background. All animals were fed a standard chow and had free access to water. All protocols were approved by the Institutional Animal Care and Use Committee and done in accordance with the federal guidelines on the principles for the care and use of animals in research.

Intact Bone Biomechanics

The baseline biomechanical consequence of OPN deficiency in intact bone was assessed by testing femora from 10-week-old wild type (n=5) and $OPN^{-/-}$ (n=7) mice. Soft tissues were removed, and the bones were wrapped in PBS soaked gauze and frozen at –20°C. The left femora from these mice were tested in three-point bending, and the right femora were testing in torsion. All bones were thawed in PBS at room temperature for 3 hours prior to mechanical testing. While thawing, the specimens were imaged using the VivaCT 40 micro-CT imaging system (Scanco Medical) at a voxel size of 21 μm. The micro-CT images were utilized to determine moment of inertia within the mid-diaphyseal region, which was used to calculate bone material properties.

For three point bending tests, specimens were loaded onto a three-point bending setup with a 6.2 mm distance between lower supports. An 858 Mini Bionix II testing system (MTS) was then used to load the femora to failure at a rate of 0.05 mm/sec with

the anterior side in tension and posterior side in compression. Maximum load, elastic modulus, work to failure, and post yield displacement were determined from the recorded force-displacement data.

For torsional testing, we designed fixtures and a custom potting apparatus that allowed us to reproducibly align and pot the femora in Wood's metal with a gauge length of 6.5 mm. After the femora were potted, they were loaded in torsion at a rate of 3 degrees per second until failure using an ELF 3200 testing system (Bose Corp.). Using the recorded test data, maximum torque, shear modulus, work to failure, and post yield rotation were determined.

Bone Fracture Healing Model

A well-established, unilateral femoral fracture model (4) was utilized to study bone repair in 10-week-old male wild type and $OPN^{-/-}$ mice. Animals were anesthetized by intraperitoneal injection of xylazine (10 mg/kg) and ketamine (80 mg/kg). All hair was removed from the surgical site, and the area was cleansed with sterile water followed by betadine. A 25-gauge needle was inserted in a retrograde manner into the intramedullary canal of the right femur. Subsequently, a mid-diaphyseal fracture was created in this leg, and the contralateral leg was left intact. The mice were allowed to recover on a heated pad, and, after awakening, they were returned to their cages and allowed to ambulate freely. Upon sacrifice, any animals that displayed intramedullary pin displacement, fractures that were not transverse, or fractures not in the mid-diaphyseal region were removed from the study.

Micro-CT Analysis of Fracture Site Neovascularization

Recently developed quantitative micro-CT based methods (130) were utilized for evaluation of fracture callus vascularity. Mice were sacrificed using carbon dioxide inhalation at 7 days (wild type n=10, $OPN^{-/-}$ n=10) or 14 days (wild type n=9, $OPN^{-/-}$ n=6) post surgery. The vasculature of the mice was sequentially perfused at physiologic pressure using heparinized (100 units/mL) normal saline, 10% neutral buffered formalin, and then again with heparinized saline. The vascular system was then injected with a radiopaque, lead chromate based contrast agent (Flow Tech Inc.), which was then allowed to polymerize for 24 hours at 4°C. The fractured femora were isolated from the surrounding musculature under a dissecting microscope, and the intramedullary pins were carefully removed. The femora were stored at 4°C for 48 hours in 10% neutral buffered formalin, soaked 48 hours in a formic acid based solution for decalcification of the mineralized bone, washed thoroughly using water, and placed in 10% neutral buffered formalin until imaging. The decalcification procedure is a vital step that allows radiodensity-based segmentation of the contrast-filled vessels from the surrounding mineralized tissues, and, therefore facilitates calculation of vascular morphology parameters. The specimens were imaged at a 10.5 μm isotropic voxel size, and two-dimensional (2-D) tomograms were reconstructed. The volume of interest was defined by drawing contour lines along the borders of the callus in the 2-D slices. Then, within this VOI, the 2-D images were globally thresholded based on x-ray attenuation and used to render binarized 3-D images of the radiopaque, contrast-filled vascular network segmented from the surrounding tissues. These 3-D images were evaluated for vessel volume, volume fraction, and average diameter.

Micro-CT Analysis of Fracture Callus Formation and Mineralization

Mice were euthanized post-operatively for micro-CT imaging at 7 (wild type n=7, $OPN^{-/-}$ n=6), 14 (wild type n=7, $OPN^{-/-}$ n=6), 28 (wild type n=5, $OPN^{-/-}$ n=8), and 56 (wild type n=7, $OPN^{-/-}$ n=6) days. The femora were removed and dissected free from surrounding musculature under a dissecting microscope. The intramedullary pins were removed, and the bones were wrapped in PBS soaked gauze and frozen at –20°C. Upon removal from the freezer, the bones were placed in PBS to thaw at room temperature.

While thawing in PBS, the specimens were imaged using micro-CT at a voxel size of 21 μm. The newly formed fracture callus tissue was spatially segmented from the native cortical bone in the 2-D tomograms. Prior to generation of 3-D images of the mineralized callus, we scanned a set of hydroxyapatite (HA) phantoms (0-800 mg HA) in order to define our mineralization threshold. Based on the precedent set in a similar fracture healing study (151), we defined the fracture callus mineralization threshold (295 mg HA/cm^3) as 50% of the mineral density that we utilized to segment intact cortical bone. Using this threshold, three-dimensional images of the mineralized callus were rendered, and total volume, percent mineralization, and average mineral density were measured on the digitally extracted callus tissue.

Fracture Specimen Biomechanical Testing

Specimens were thawed in PBS at room temperature for a total of 3 hours prior to mechanical testing, during which time micro-CT imaging was completed as discussed above. For three-point bending tests, a pilot set of 28 day post fracture specimens were loaded onto a three-point bending setup as described for intact bone biomechanics (wild

type n=8, $OPN^{-/-}$ n=8). Ultimate load, work to maximum load, and displacement at maximum load were determined from the recorded force-displacement data.

For torsional mechanical testing, the fracture calluses were loaded to failure using the same testing setup described for intact bone biomechanics. Stiffness, yield point, maximum torque, work to failure, rotation at failure, and post yield rotation were determined for the fracture specimens. Specimens collected at the earliest time point (7 days) were too fragile to test, so this analysis was only completed on specimens 14, 28, and 56 days post fracture (14 days wild type n=7, $OPN^{-/-}$ n=6; 28 days wild type n=5, $OPN^{-/-}$ n=8; 56 days wild type n=7, $OPN^{-/-}$ n=6).

Real-time RT-PCR

RNA was isolated from the mid-diaphysis of intact bones and from fracture callus tissues at 3, 7, and 14 days post surgery. The tissue was snap frozen and homogenized in QIAzol lysis reagent (Qiagen). RNA was purified using a commercial kit (Qiagen) and then reverse transcribed into cDNA using the SuperScript™ III First Strand Synthesis System (Invitrogen), which was subsequently purified using a commercially available kit (Qiagen). Primers were designed using the ABI Primer Express software (Table 5.1), and SYBR Green intercalating dye (Applied Biosystems) was used to perform real time PCR with the ABI Prism 7700 Sequence Detection System (Applied Biosystems). Standards for each gene were amplified from cDNA and purified. Standard concentrations were determined using spectrophotometric measurement at 260 nm, and standards were serially diluted to an appropriate range of concentrations. Transcript concentration in template cDNA solutions was quantified from the linear standard curve and expressed as 10^{-18} moles of transcripts per μg of total RNA.

Table 5.1. Oligonucleotides for quantitative RT-PCR

Target Gene (Accession No.)	Sense Primer	Antisense Primer
Osteopontin (AF515708)	5'-CCCTCGATGTCATCCCTGTT-3'	5'-CCCTTTCCGTTGTTGTCCTG-3'
Fibronectin (M18194)	5'-TCTCGGAGCCATTTGTTCCT-3'	5'-TTGTCACAGCGCCAGCC-3'
Bone Sialoprotein (L20232)	5'- TCCTCCTCTGAAACGGTTTCC-3'	5'-GGAACTATCGCCGTCTCCATT-3'
Col1α1 (U08020)	5'-TGGATTCCCGTTCGAGTACG-3'	5'-TCAGCTGGATAGCGACATCG -3'
Lysyl Oxidase (NM_010728)	5'-TAGCGAAGCACATAGCATTG-3'	5'-TGCAGCAATGAGTCTACAGC-3'
Col2α1 (NM_031163)	5'-CCAGGGCTCCAATGATGTAGAG-3'	5'- TGTTTCGTGCAGCCATCCT -3'
Col10α1 (NM_009925)	5'-CAAGCTCATCCTATTCTCCGCT-3'	5'-CCAAATGCATCTCCAGGGA-3'
Osteoprotegerin (U94331)	5'-GAAAGCAGCGTGCAGCG-3'	5'-TCAAGGCAAGAAGCTGCTCTG-3'
RANKL (NM_011613)	5'-GGATGTGGCCCAGCGAG-3'	5'-GCAGCATTGATGGTGAGGTG-3'
TRAP (AK008391)	5'-CAGCCCAAAATGCCTCGA-3'	5'-GCTTTTTGAGCCAGGACAGC-3'
Cathepsin K (AK003425)	5'-TTGGTGGCTTTGGAAGGG-3'	5'-TTAGTTAGCATCGCTGCGTCC-3'

Histological Analysis

Mice were perfused with heparinized 0.9% normal saline, followed by 10% neutral buffered formalin. Tissues were decalcified using a formic acid based agent (Cal-Ex II, Fisher Scientific), embedded in paraffin, and cut into 5 μm thick longitudinal sections. Images shown are representative of sections taken from n≥4 different animals. Immunostaining was done with antibodies to OPN (Immuno-Biological Laboratories), fibronectin (Chemicon), and bone sialoprotein (University of Iowa Developmental Studies Hybridoma Bank). Primary antibodies were detected using an avidin-biotin-alkaline phosphatase method from a commercially available kit (Vector Laboratories), and the sections were counterstained with hematoxylin. Using commercially available kits (Sigma-Aldrich), safranin O staining was completed for detection of cartilage, and multinucleated osteoclasts were identified based on staining for tartrate resistant acid phosphatase (TRAP).

Picrosirius red staining was done using standard methods (223). Briefly, specimens were deparaffinized, rehydrated, stained for 1 hour in 0.1% sirius red F3B in saturated picric acid, washed in 0.5% acetic acid, dehydrated, cleared in xylene, and

mounted for imaging using planar polarized light microscopy. Samples were aligned approximately 45 degrees from the transmission axis of the polarizing filters in order to maximize brightness of the images from each sample and provide a consistent assessment. Using this technique, one can qualitatively assess collagen fiber organization based on polarization color (224).

Measuring Total Collagen Content

For analysis of total collagen content, the hydroxyproline assay (225) was performed on fracture calluses. Briefly, the tissue was lyophilized and dry weight measurements were recorded. The samples were decalcified in 10% formic acid, diced into small pieces, digested in proteinase K, hydrolyzed in 6N HCl at 110°C, and assayed for hydroxyproline content using a standard colorimetric assay (225).

Statistical Analysis

All data are presented as mean ± SEM. Statistical analyses were performed using the Minitab software. ANOVA was used to model the effect of genotype on all response variables. $P<0.05$ was interpreted as significant in all analyses.

Results

Intact Bone Biomechanics

To determine the baseline biomechanical phenotype in intact bone, we tested two matched sets of intact wild type and $OPN^{-/-}$ femora in torsion and in three-point bending. We found consistent results for the two testing methods, confirming that $OPN^{-/-}$ bones possessed higher elastic/shear modulus, lower maximum load/torque, and reduced work to failure and post yield deflection/rotation (Table 5.2).

Table 5.2. Intact bone mechanics. Comparison of wild type (n=5 for both testing setups) and OPN deficient (n=7 for both testing setups) intact bone properties. [a]$p<0.05$, [b]$p<0.005$.

	3-Point Bending		Torsion	
	WT	$OPN^{-/-}$	WT	$OPN^{-/-}$
Modulus (GPa, GPa)	3.82 ± 0.24	5.28 ± 0.12[b]	2.22 ± 0.15	3.02 ± 0.13[b]
Max Load / Torque (N, N-mm)	18.4 ± 0.8	16.3 ± 0.3[a]	31.9 ± 2.9	21.5 ± 0.7[b]
Work to Failure (N-mm, N-mm-deg)	14.7 ± 2.1	8.8 ± 0.5[a]	327 ± 17	167 ± 9[b]
Post Yield Displacement (mm, degrees)	1.01 ± 0.61	0.61 ± 0.06[a]	14.5 ± 1.3	8.9 ± 0.7[b]

Expression and Immunolocalization of ECM Proteins in $OPN^{-/-}$ mice

Quantitative RT-PCR measurement of OPN expression in wild type and $OPN^{-/-}$ intact and fractured femora at 3, 7, and 14 days post-surgery illustrated increased OPN expression in the setting of fracture healing in the wild type animals. In addition, it validated the complete absence of OPN mRNA in the knockout animals. Immunohistochemical staining of 28 day post surgery tissue sections taken from the fracture callus corroborated this finding, illustrating the lack of OPN at the protein level in the knockout animals and the localization of OPN in the fractured wild type bones (Figure 5.1).

It has been hypothesized that the relatively mild bone phenotype seen in $OPN^{-/-}$ mice without external stimulation could be due to compensatory activity of other, similar ECM proteins. Here we measured the gene expression and protein localization of

fibronectin and bone sialoprotein (BSP), two bone ECM proteins that possess similar recognition sequences and properties to OPN. These genes displayed intense upregulation in fractures relative to intact bones for both genotypes, but, other than a significant but modest deficiency in BSP expression at 14 days, we found that OPN deficient mice displayed no aberrant expression of these genes relative to the wild type animals. Using immunohistochemistry, we further observed apparently normal localization of these related proteins within the calluses of $OPN^{-/-}$ mice at 14 days post fracture (Figure 5.1).

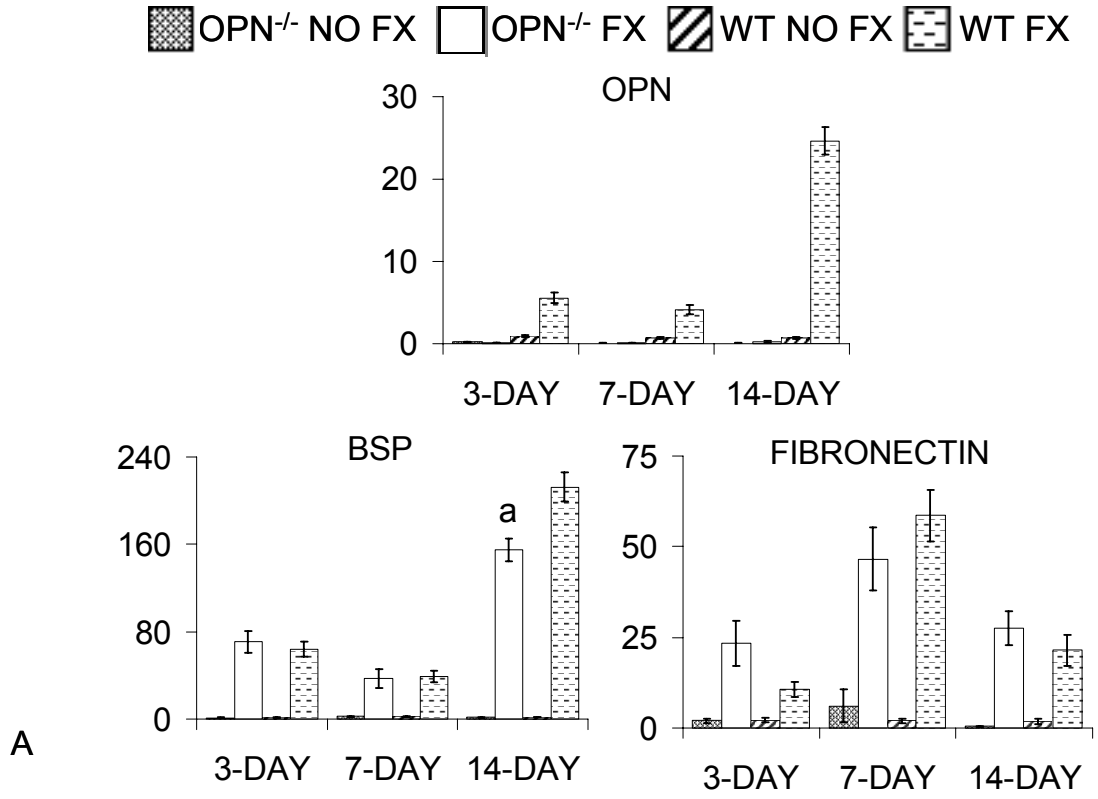

Figure 5.1. Validation of OPN deficiency and evidence that no compensatory changes in gene expression or protein localization of bone sialoprotein and fibronectin occur in $OPN^{-/-}$ mice. (A) Quantitative RT-PCR measurement of OPN, BSP, and FN expression in OPN deficient and wild type (WT) intact (No Fx) and fracture healing (Fx) bone samples 3, 7, and 14 days post-surgery expressed as 10^{-18} moles of transcripts per µg of RNA ($^{a}p<0.05$).

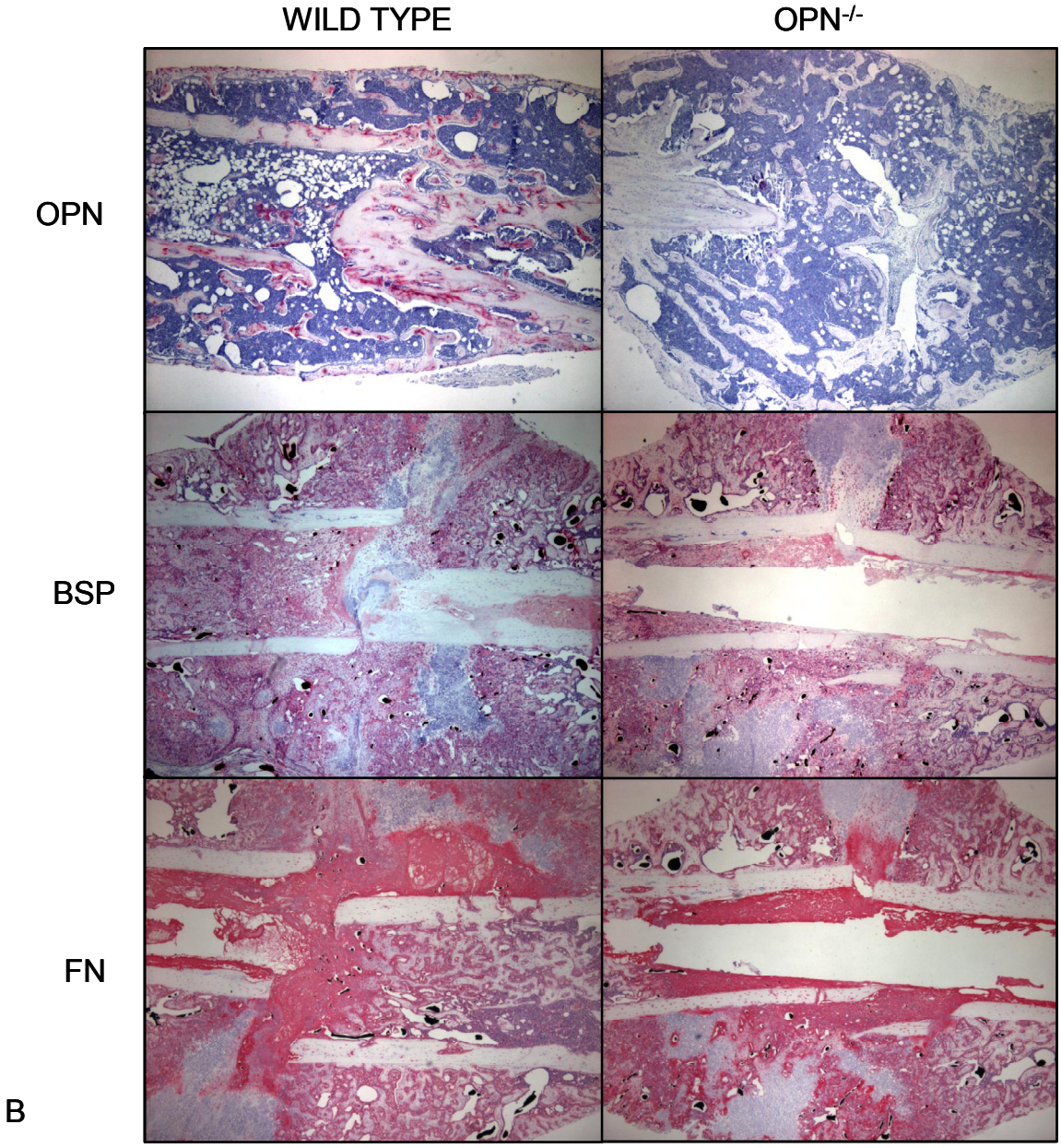

Figure 5.1 (B) Representative immunohistochemistry photomicrographs of the fracture sites from WT and OPN deficient mice identifying OPN at 28 days post fracture and BSP and fibronectin at 14 days post fracture. These data illustrate increased OPN expression in the setting of fracture healing and the absence of OPN mRNA in the knockout animals, in addition to the lack of OPN at the protein level in the $OPN^{-/-}$ mice and the localization of OPN in the wild types. BSP and fibronectin were upregulated in the setting of fracture healing, and, other than a modest decrease in BSP expression in $OPN^{-/-}$ fractures at 14 days, no alterations were seen in gene expression or protein quantity or localization of these ECM proteins in the fracture callus due to OPN deficiency.

Micro-CT Analysis of Fracture Site Neovascularization

We utilized micro-CT imaging of contrast perfused, decalcified specimens for visualization and quantification of vascular growth within the fracture callus (Figure 5.2 A). Significantly reduced vessel volume and vessel volume fraction, along with a trend toward decreased average vessel diameter ($p=0.071$), were detected in the fracture calluses of $OPN^{-/-}$ mice compared to wild types at 7 days post surgery (Figure 5.2 B). At 14 days post surgery, while there was a significant reduction in average vessel diameter in $OPN^{-/-}$ mice, significant differences for other vascular parameters were no longer present (Figure 5.2 C).

Micro-CT Analysis of Fracture Callus Formation and Mineralization

Micro-CT imaging was utilized to measure volume, percent mineralization, and average mineral density within the newly formed fracture callus that was outside the periphery of the pre-existing cortical bone structure (Figure 5.3 A). The $OPN^{-/-}$ mice displayed a significant reduction in callus volume relative to the wild types at days 7 (-27%) and 14 (-30%). No differences were seen in callus volume between genotypes at 28 days, and callus volume was significantly increased (46%) in the OPN deficient mice compared to wild types at 56 days post fracture (Figure 5.3 B). The $OPN^{-/-}$ mice displayed accelerated early mineral formation and had significantly higher percent callus mineralization at 14 days. However, no differences were seen in percent callus mineralization at other time points (Figure 5.3 B). Lastly, the average density of the mineralized portion of the fracture callus was significantly lower in the OPN deficient mice at 28 days, and this trend persisted but was no longer significant at 56 days (Figure 5.3 B).

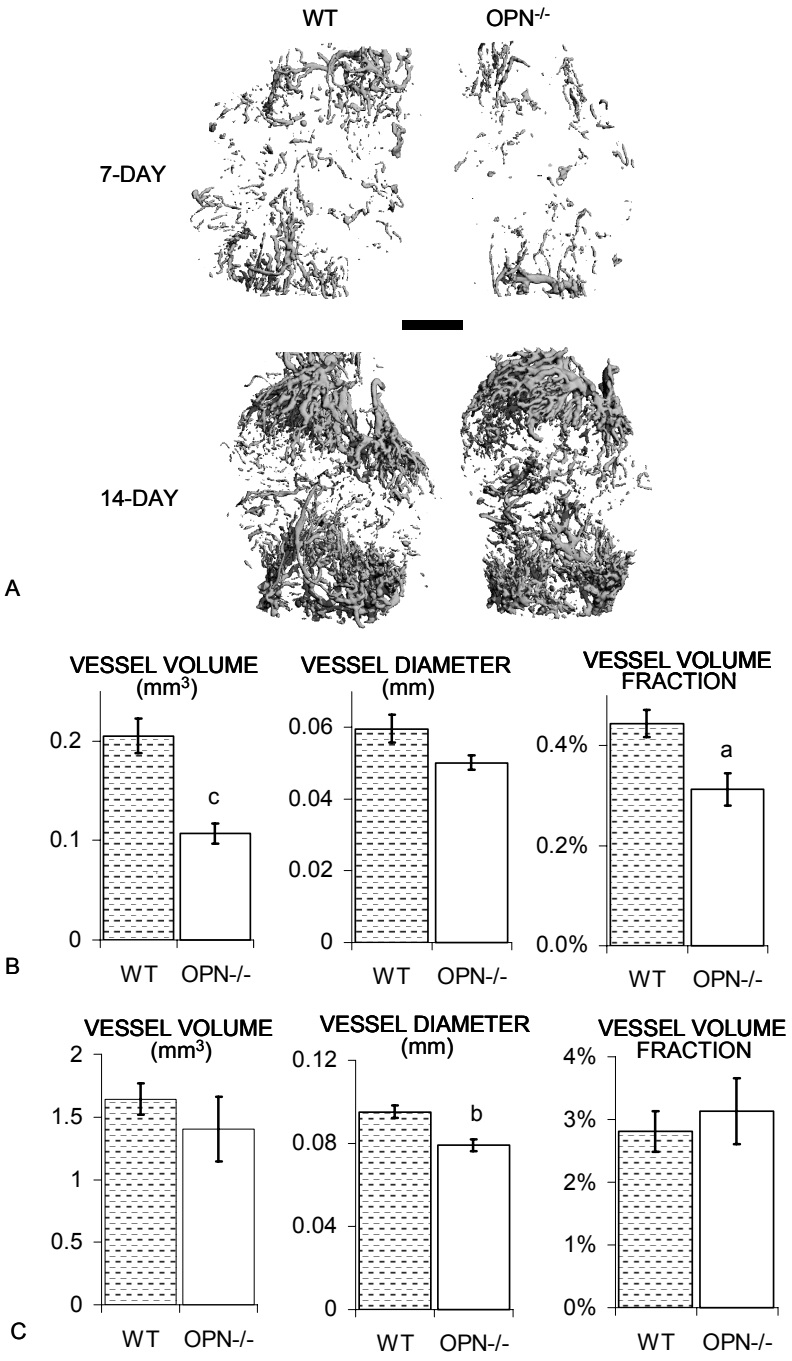

Figure 5.2. Reduced early stage neovascularization in OPN deficient mice was recovered at later time points. (A) 7-day and 14-day post surgery micro-CT images visibly showed reduced early neovascularization in OPN deficient mice that appeared to be recovered by 14 days. (B) At 7 days, this angiogenic deficiency was found to be significant in quantitative 3-D image analyses of vascular volume and volume fraction (wild type n=10, $OPN^{-/-}$ n=10). (C) At 14 days post surgery, micro-CT images and quantitative analysis revealed reduced average vessel diameter but an overall recovery of the early vascular defect seen in the OPN deficient mice (wild type n=9, $OPN^{-/-}$ n=6). Scale = 1 mm. $^{a}p<0.05$, $^{b}p<0.005$, and $^{c}p<0.0005$.

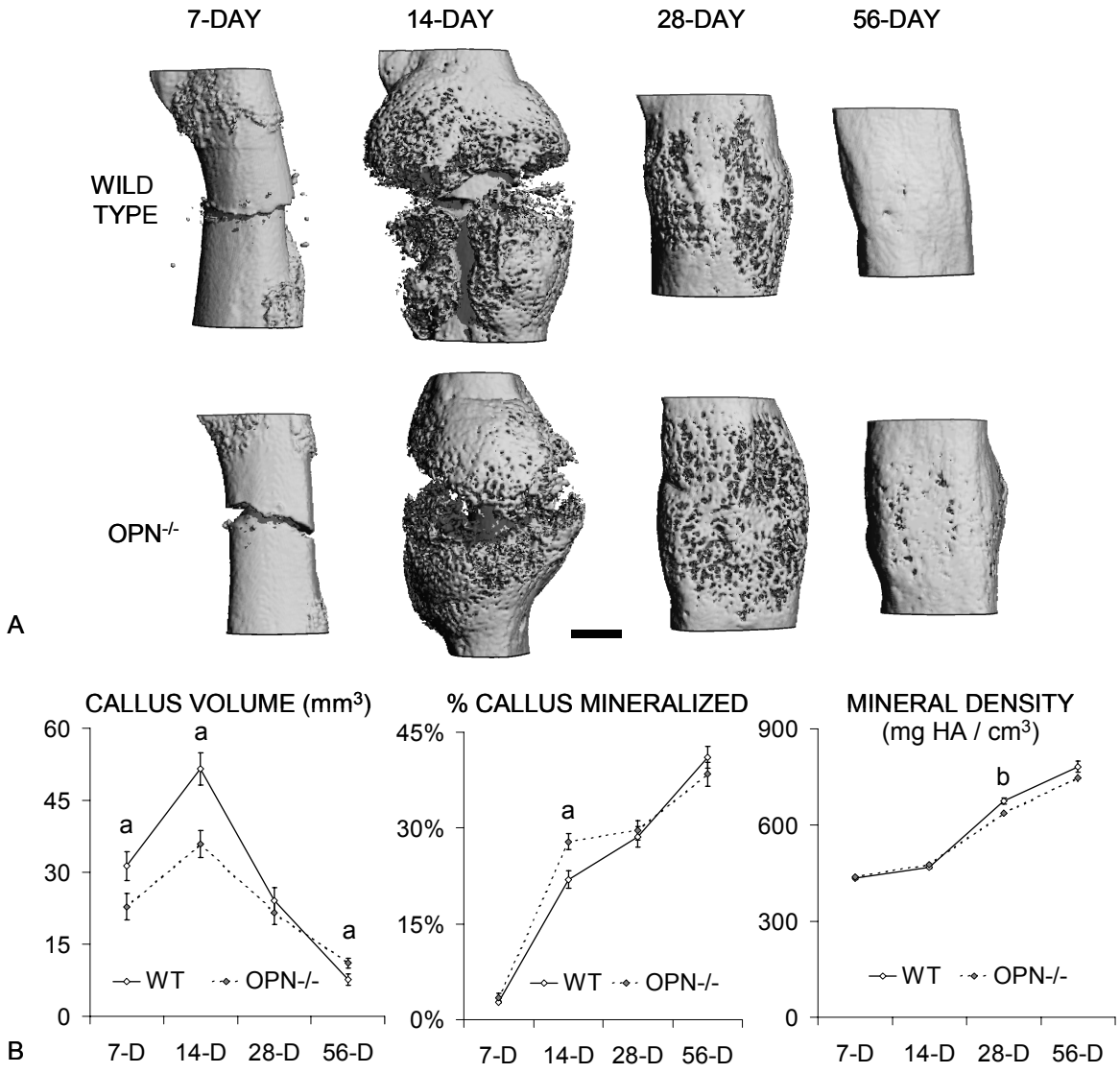

Figure 5.3. OPN deficient mice displayed reduced early stage callus size, increased early mineralization, and delayed late stage remodeling. (A) Micro-CT imaging captured the time course of mineralized callus formation and remodeling in the wild type and $OPN^{-/-}$ mice. (B) Quantitative image analysis revealed that $OPN^{-/-}$ mice possessed reduced callus size 7 and 14 days post surgery but increased callus volume 56 days post surgery. $OPN^{-/-}$ mice also displayed increased percent callus mineralization at 14 days. Analysis of average mineral density within the newly formed callus found that this parameter increased significantly over time post fracture, and it was found that OPN deficiency resulted in a small but significant decrease in average mineral density at 28 days post fracture. 7-day (wild type n=7, $OPN^{-/-}$ n=6), 14-day (wild type n=7, $OPN^{-/-}$ n=6), 28-day (wild type n=5, $OPN^{-/-}$ n=8), and 56-day (wild type n=7, $OPN^{-/-}$ n=6). Scale = 1 mm. $^{a}p<0.05$, $^{b}p<0.005$.

Fracture Specimen Biomechanical Testing

In initial three-point bending tests done at 28 days post surgery, fractured $OPN^{-/-}$ femora displayed reduced deflection and work to ultimate load relative to wild types (data not shown). However, in this pilot experiment, we found that the three-point bending setup resulted in artifacts from fracture callus indentation by the middle support. This affected the initial portion of the tests and made it difficult to accurately determine the stiffness and yield point, so, as a result, we switched to the torsional testing modality for biomechanical assessment. Using torsional testing, we found that $OPN^{-/-}$ fractures possessed significantly reduced maximum torque at 14 and 28 days, but this difference did not persist at 56 days post fracture (Figure 5.4 A). $OPN^{-/-}$ calluses required significantly less work to failure at 14 and 28 days post surgery (consistent with our pilot study using 3-point bending) but were similar to the wild types at 56 days (Figure 5.4 B). Furthermore, OPN deficient mice tended to have reduced post yield deformation at all time points, but ANOVA analysis did not find genotype to be a significant predictor ($p=0.054$) of this parameter (Figure 5.4 C). Finally, stiffness was similar between genotypes at 14 and 28 days, but it was significantly higher in $OPN^{-/-}$ mice at 56 days post fracture, consistent with the observed increase in callus size at that time point (Figure 5.4 D).

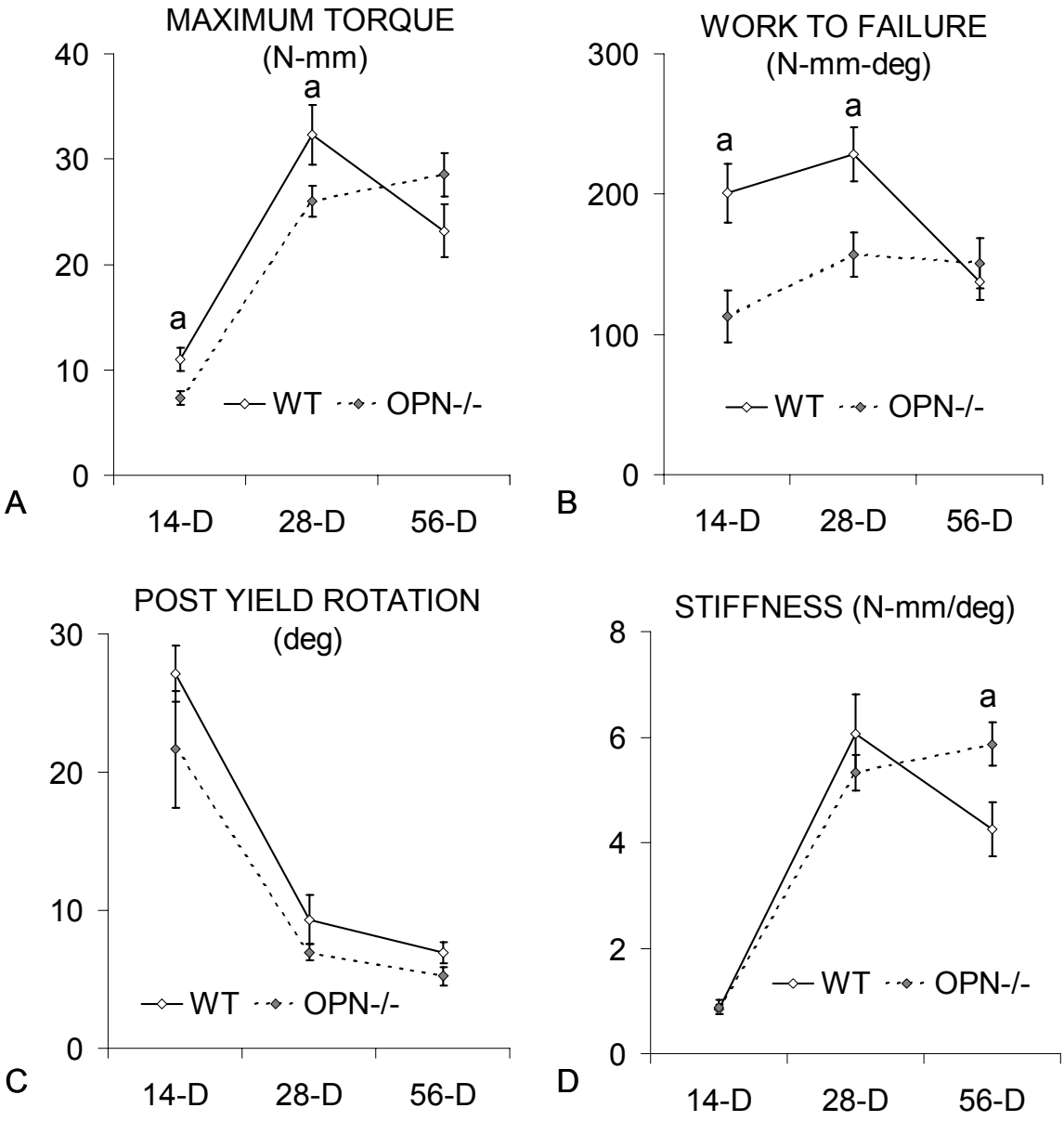

Figure 5.4. Altered fracture callus mechanics in $OPN^{-/-}$ mice. $OPN^{-/-}$ mice had significantly reduced (A) maximum torque and (B) work to failure at 14 and 28 days post fracture. The OPN deficient mice also showed a strong trend toward (C) decreased overall post yield deformation ($p=0.054$) as determined by ANOVA analysis and displayed (D) increased stiffness at 56 days. 14-day (wild type n=7, $OPN^{-/-}$ n=6), 28-day (wild type n=5, $OPN^{-/-}$ n=8), 56 day (wild type n=7, $OPN^{-/-}$ n=6). $^{a}p<0.05$.

Gene Expression and Histology

Cartilage Callus Formation

Due to the reduction in fracture callus size at early time points, we hypothesized that the OPN deficient mice had defective development and hypertrophy of chondrocytes for formation of the early cartilaginous callus. To test this hypothesis, we measured relative gene expression of type II and type X collagen, early and late markers of chondrocyte differentiation, respectively. Quantitative RT-PCR measurement revealed that these genes were upregulated by 7 days post fracture, and there appeared to be a slight lag in chondrogenesis in the OPN deficient mice, which tended to have stronger persistence of cartilage markers at 14 days. However, there was no significant difference in expression between genotypes (Figure 5.5 A), indicating that OPN deficiency does not significantly hinder chondrocyte formation and maturation at the fracture site. Safranin O staining revealed similar staining patterns for the presence of cartilage in fracture callus sections from the two genotypes at 14 days post fracture, confirming this finding (Figure 5.5 B).

Bone Remodeling

Next, due to the larger residual fracture callus seen in OPN deficient mice at the latest time point, we hypothesized that OPN plays a critical role in osteoclastogenesis. To test this hypothesis, we first measured expression of RANKL and OPG, two of the most prominent proteins involved in regulation of osteoclast formation (226). In addition, we measured expression of TRAP and Cathepsin K, two enzymes produced by mature osteoclasts to digest the mineralized bone matrix during remodeling. Quantitative RT-PCR illustrated no significant differences in expression of these markers of

osteoclastogenesis between genotypes (Figure 5.6 A-B). Furthermore, histological staining for TRAP activity indicated that the OPN deficient mice displayed similar levels of TRAP positive osteoclasts as their wild type counterparts at 28 days post fracture (Figure 5.6 C). These data indicate that there is no defect in the basic machinery required for mature osteoclast formation and activity in the OPN$^{-/-}$ mice.

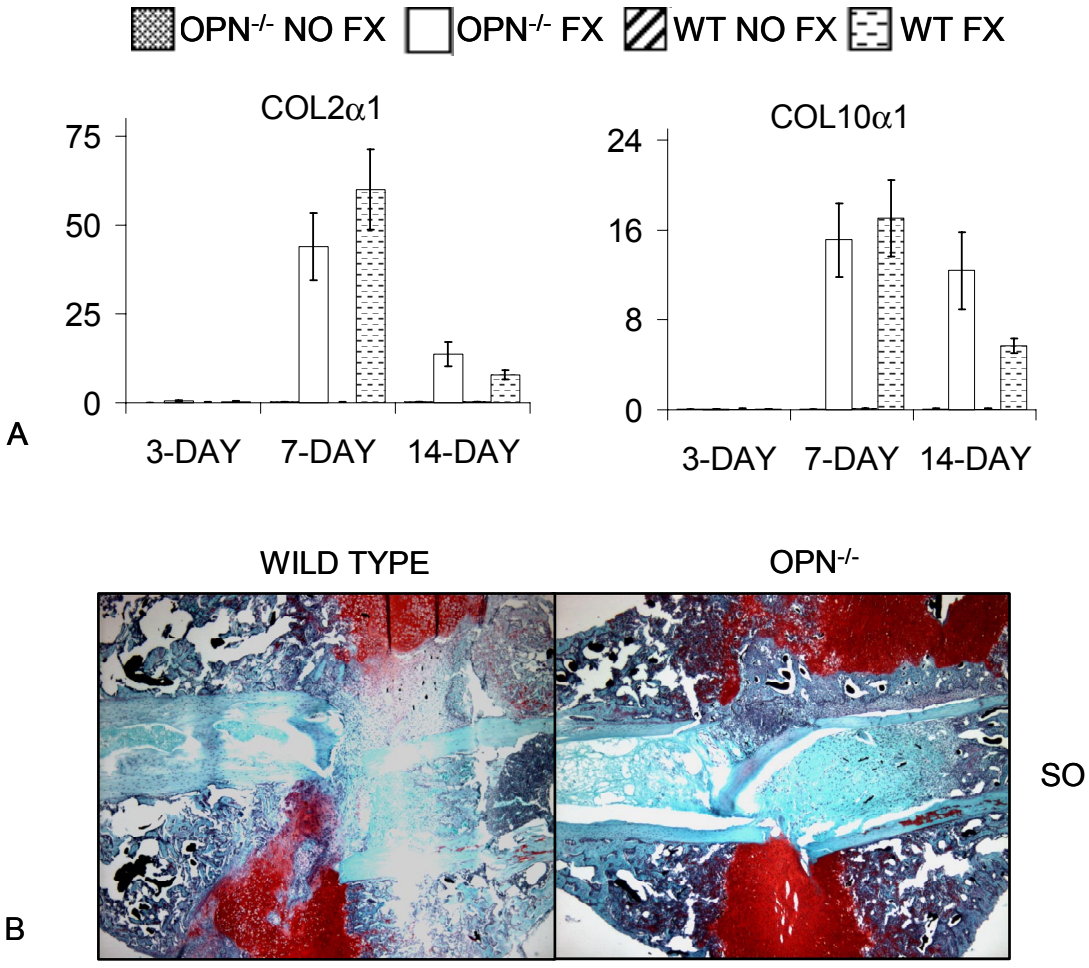

Figure 5.5. Chondrocyte formation and maturation was not altered in the absence of OPN. (A) Quantitative RT-PCR measurement of collagen II and collagen X, markers of chondrocyte formation and maturation, did not reveal differences in expression of these genes in the OPN deficient mice, indicating chondrogenesis was not altered in the absence of OPN. Data are expressed as 10^{-18} moles of transcripts per µg of RNA. (B) Safranin O staining confirmed normal cartilaginous callus formation at the fracture site in OPN deficient mice.

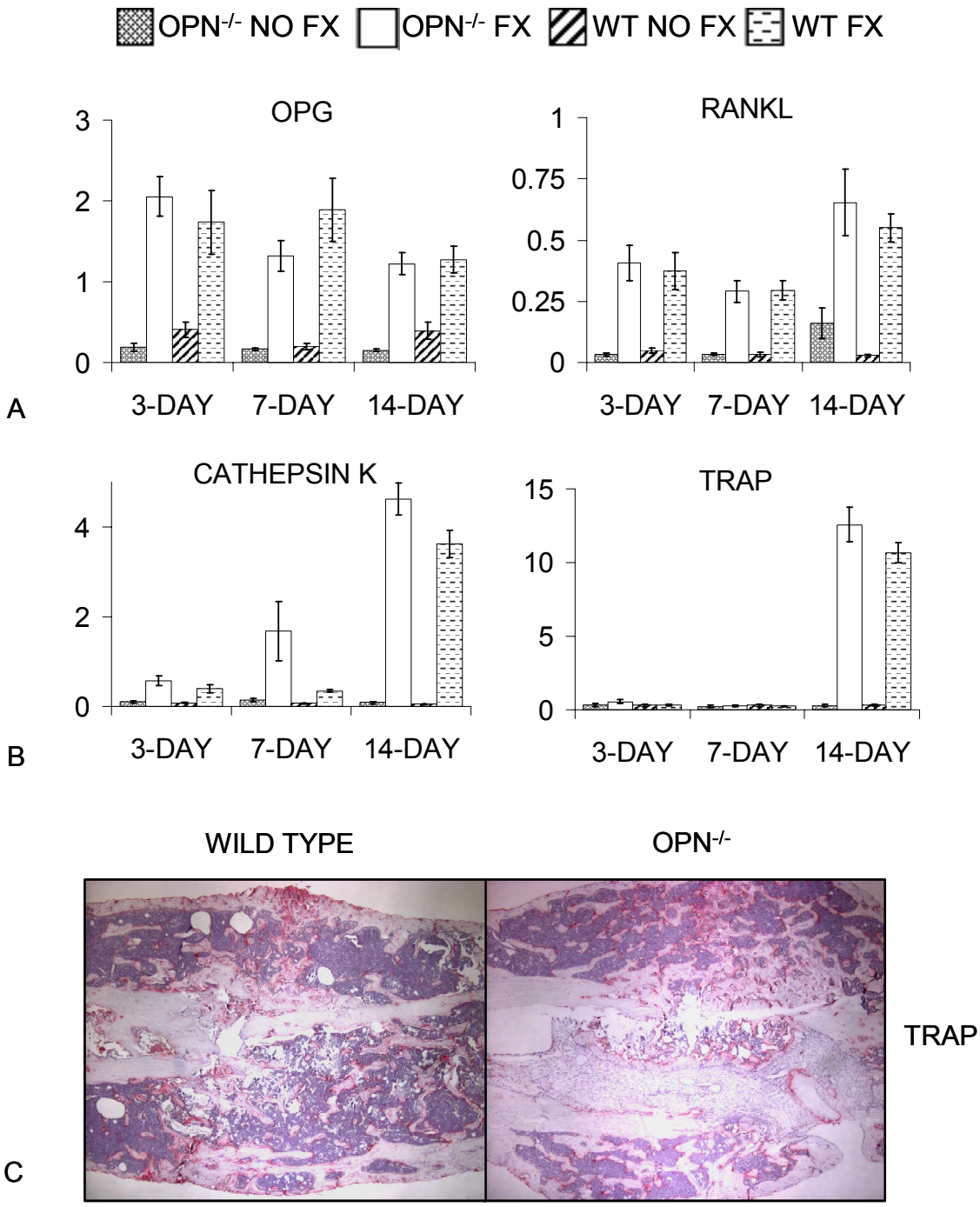

Figure 5.6. Osteoclast differentiation is not altered in the absence of OPN. Quantitative RT-PCR (expressed as 10^{-18} moles of transcripts per µg of RNA) showed OPN deficient mice had no alteration in the expression of (A) OPG and RANKL, regulators of osteoclast maturation, or (B) cathepsin K and TRAP, markers of osteoclast activity. (C) Staining for TRAP activity showed similar osteoclast number and activity in the $OPN^{-/-}$ mice compared to wild types. These results suggest that osteoclast differentiation is not altered in the absence of OPN.

Type I Collagen Content and Organization

OPN has been postulated to bind to other ECM proteins and to be important in matrix reorganization after injury (170). Therefore, we measured gene expression of type I collagen, the most abundant bone ECM protein, and lysyl oxidase (LOX), an enzyme that cross-links collagen fibers. Results indicated that these genes undergo rapid upregulation in the setting of fracture healing, but no differential expression between genotypes was detected (Figure 5.7 A). In addition, we measured total collagen content at the protein level in 56-day post surgery fracture callus specimens as determined by the hydroxyproline assay. At this late time point, the bony callus is primarily composed of type I collagen, but a well-known limitation of this assay is its inability to distinguish between different collagen types. Based on this assumption, results indicated that total collagen content (collagen weight / total dry weight) in the fracture callus was not different between genotypes with an average of 12.7±0.3% for wild types and 12.3±0.3% for $OPN^{-/-}$ mice. Next, we utilized picrosirius red staining combined with polarized light microscopy for qualitative determination of collagen fiber organization. This imaging technique suggested that, while there is no difference in collagen content, the newly formed bone in the OPN deficient mice contained abnormal collagen organization relative to their wild type counterparts at 56 days post fracture (Figure 5.7 B).

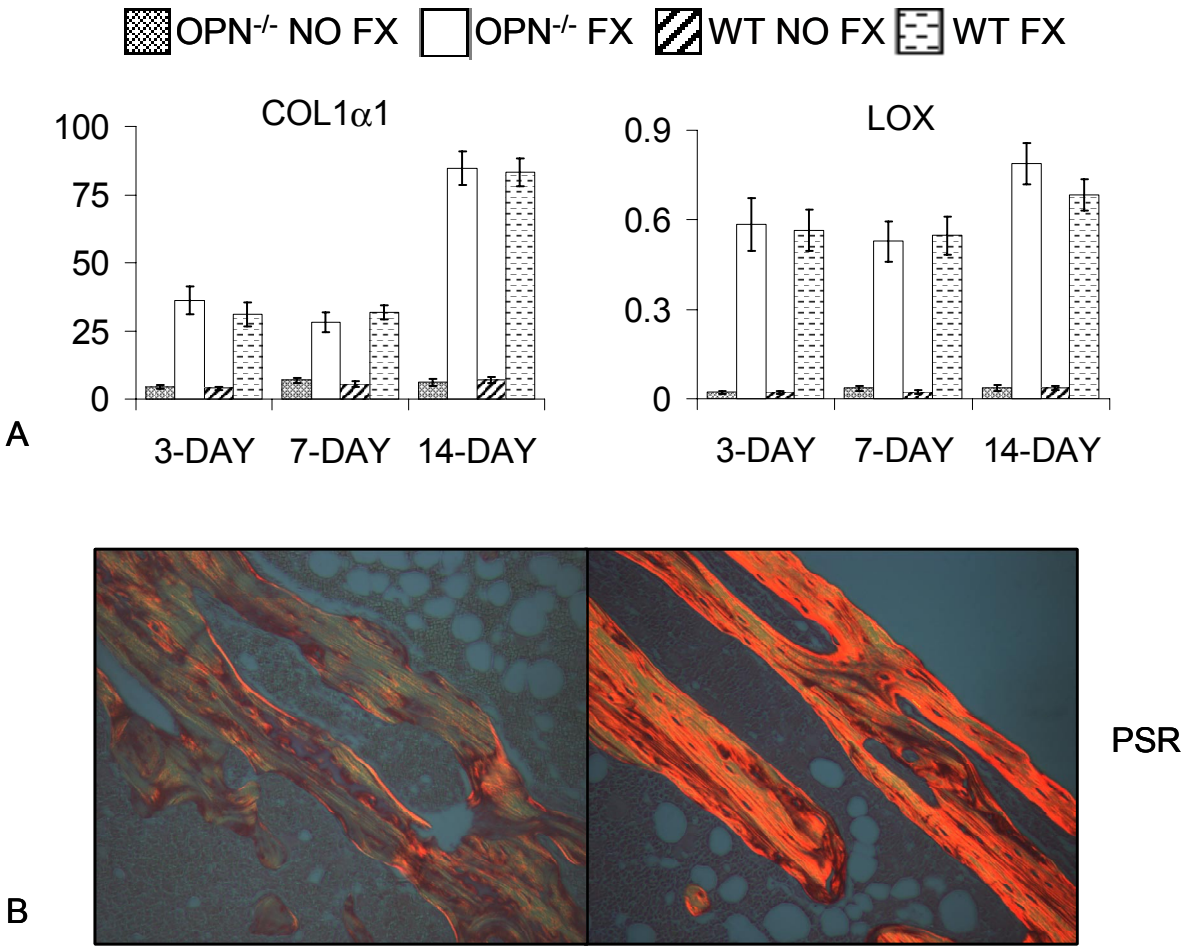

Figure 5.7. Collagen I and lysyl oxidase expression was unchanged but collagen fiber arrangement was qualitatively different in OPN$^{-/-}$ mice. (A) Quantitative RT-PCR measurement of type I collagen and lysyl oxidase was normal in OPN deficient mice as shown here expressed as 10^{-18} moles of transcripts per μg of RNA. However, (B) polarized light microscopy of picrosirius red stained sections revealed a qualitative difference in polarization colors, suggesting altered collagen organization between genotypes.

Discussion

In this study, we compared wild type and $OPN^{-/-}$ mouse femoral fracture callus formation, neovascularization, mineralization, and mechanical properties. OPN deficiency was found to significantly alter but not prevent bone regeneration and remodeling of fractures in mice. No compensatory overexpression of other ECM components was found, suggesting that there may be redundant mechanisms that allow fracture healing to occur (albeit delayed) in the absence of OPN due to common cellular binding sites (i.e. RGD sequence) and functional overlap between OPN and other ECM proteins. Specifically, our data indicate that the presence of OPN is essential for normal early callus formation, neovascularization, and biomechanical strength and ductility. Additionally, OPN deficiency was found to delay the time course of remodeling of the fracture callus during the later stages of healing. Lastly, while ECM content seemed generally unchanged, abnormal collagen organization was observed within the remodeling calluses of $OPN^{-/-}$ mice.

At early stages of healing, OPN was found to play an important role in callus formation and to have a significant but transient effect on neovascularization. The reduction in early vascular volume within the fracture callus at 7 days was recovered by 14 days. However, a significant decrease in average vessel diameter persisted indicating that OPN may also play a role in vessel maturation. This may be related to the stimulatory role that OPN has on smooth muscle cell migration and chemotaxis (179,180), or it could be a consequence of the $OPN^{-/-}$ mouse macrophage phenotype, which has been linked to abnormal vascular remodeling (173). Relevant to the latter hypothesis, OPN deficiency has been found to result in normal macrophage numbers but

decreased levels of macrophage activation in skin wounds, and intradermal injection of exogenous OPN has been found to stimulate macrophage infiltration (170,178). The prior study was consistent with our findings, which indicated normal macrophage numbers (data not shown) but evidence that there may be defective functionality of these cells at the site of injury in the $OPN^{-/-}$ mice. Therefore, in addition to the direct effects of OPN on endothelial and smooth muscle cell survival and migration, a reduced inflammatory response likely has secondary effects on callus neovascularization, vessel maturation, and ECM formation due to decreased reorganization of damaged tissue and cytokine production during the early stages of fracture healing.

One interesting observation from this study is that, while the $OPN^{-/-}$ mice displayed a reduction in callus volume at 1 and 2 weeks post fracture, they possessed 46% larger fracture calluses at 8 weeks. The observed time dependent phenotype provides further evidence for the multifunctionality of OPN during fracture healing. The increased residual fracture callus present in the $OPN^{-/-}$ mice at 56 days is likely due to the well-documented role that OPN has in mediating activity of mature osteoclasts during bone remodeling (187,191,192). This defect, as was shown here, is not a result of inhibition of osteoclast differentiation or production of proteolytic enzymes. Previous studies have also shown that osteoclastogenesis is not inhibited in the setting of OPN deficiency, and, in fact, a compensatory increase in osteoclast number has been reported in the bones of $OPN^{-/-}$ mice under basal conditions in some studies (191,194). As elegantly shown by Chellaiah and co-workers, the reduction in functionality of OPN deficient osteoclasts can be attributed to decreased motility caused by a lack of cell surface expression of CD44 and activation of the $\alpha_v\beta_3$ integrin (191).

In the aforementioned study, Chellaiah and authors were the first to link $OPN^{-/-}$ osteoclast dysfunctionality to an observable *in vivo* bone phenotype in OPN deficient animals at baseline. Although neither Rittling or Liaw found any abnormal bone phenotype upon initial development of the OPN knockout mouse (170,187), this group more recently reported larger femoral moment of inertia and, as determined by four-point bending, increased elastic modulus, ultimate moment, and energy to failure in $OPN^{-/-}$ mice (191). In the present study, as verified using independent three point bending and torsional mechanical testing modalities, we found results that are partially contradictory to these previously published data. Similar to Chellaiah *et al*., we observed an increase in the elastic modulus of $OPN^{-/-}$ bone. However, the OPN deficient mice used for our study did not display increased femoral moment of inertia, and we found decreased maximum load and energy to failure relative to bones from wild type mice. In addition, we found the $OPN^{-/-}$ mice to have an approximately 40% decrease in post yield deformation, a parameter that was not reported in previous studies. Taken together, these biomechanics data indicate that OPN deficiency increases the material stiffness of the bone tissue and also causes it to be more brittle. A few possible explanations exist for the discrepancy between our data and the previously published results. The slightly older mice used in the Chellaiah publication could have displayed a phenotype that develops as the mice age due to a mild, but prolonged defect in osteoclast functionality. These divergent results could also be a function of the difference in genetic background. The previous study was completed with mice on a hybrid background, while the mice used here were backcrossed onto a C57BL/6 genetic background. The potential relevance of this cannot be ignored considering the significantly dissimilar baseline bone phenotype between background

strains (227) and the different susceptibility of each mouse strain to a variety of pathologies including osteoporotic bone loss, femoral artery blockage, and atherosclerosis (228-231). The final difference of note is that the mice used in our study were derived from the OPN deficient mouse population developed by Liaw *et al*., rather than the Rittling mouse. The two different OPN knockouts were derived using slightly different methodologies, and the Rittling mouse has been found to express a small but likely non-functional fragment of the OPN protein (170,187).

Significant functional effects of OPN deficiency were also evident in the biomechanical tests on the fracture callus specimens. The physical significance of altered callus size was evident in the torsional tests, which showed that the smaller $OPN^{-/-}$ calluses at 14 days post fracture possessed significantly reduced maximum torque and work to failure. Interestingly, significantly reduced mechanical properties (maximum torque, work to failure) were also found in the OPN deficient mice at 28 days post fracture, but no differences were seen in callus size or percent mineralization between genotypes at this endpoint. These data, in addition to the strong overall trend toward decreased post yield behavior in the $OPN^{-/-}$ mice, indicate the existence of fracture callus material property differences as a result of OPN deficiency. The observed brittle material behavior in the $OPN^{-/-}$ fracture specimens corroborates the observation of decreased ductility in $OPN^{-/-}$ intact bone, and this consistent decrease in bone quality may be the result of altered organization of the ECM within the callus of the $OPN^{-/-}$ mice. The biological relevance of the callus volume was also evident at 56 days, at which point the $OPN^{-/-}$ specimens possessed significantly increased stiffness. It should be noted, however, that at 56 days, the geometry of the fracture callus had undergone significant

remodeling in both genotypes and was relatively small compared to callus size measurements at earlier time points. However, even at 56 days, it seemed that neither group had achieved a remodeling equilibrium or completely regained the mechanical properties of intact bone. This incomplete restoration of bone quality can be readily explained by the fact that, while the bone geometry is approaching baseline, mineral density of the fracture callus has only reached approximately 60% of the mineral density of normal intact bone at this endpoint (data not shown).

Despite alterations in size and biomechanical strength of the fracture callus, other than a modest change found in BSP mRNA levels, measurement of gene expression, immunohistochemical protein localization, and quantitative measurement of collagen content does not indicate compensatory changes in other ECM proteins in $OPN^{-/-}$ mice. However, while no differences were seen in total collagen content, picrosirius red staining suggested abnormal collagen organization within remodeling $OPN^{-/-}$ fracture calluses, which could be a result of alterations in collagen fibrillogenesis or turnover in OPN deficient mice. This interpretation agrees with previous observations that OPN deficiency results in altered collagen fibril diameter and organization in skin wounds (170) and increased collagen maturity in bone (190). Considering these observations, in conjunction with the fact that OPN has a high affinity for binding collagen (232), it is possible that the absence of an OPN-collagen interaction could result in aberrant fibril organization and contribute to the reduced mechanical integrity detected here for both intact and fractured $OPN^{-/-}$ bones. Altered collagen organization may have a detrimental effect on the ability of the bone tissue to dissipate energy as mineralized fibrils begin to move relative to each other during post yield deformation of the tissue. Consistent with

this interpretation, Hansma and co-workers have recently hypothesized that the mechanical behavior of bone is greatly influenced by nonfibrillar matrix proteins that form sacrificial bonds between mineralized collagen fibers. They specifically suggest that OPN and related proteins may be important components of the "glue" that resists separation of collagen fibers and propagation of cracks during mechanical failure (233,234). This recent work may provide a mechanistic explanation for both the alteration in collagen organization and the observed brittle behavior in the bones of the $OPN^{-/-}$ mice.

In conclusion, OPN deficiency significantly alters several stages of the bone healing process but does not prevent bone union. More specifically, this study indicates that OPN plays multiple roles during early callus formation, neovascularization, and late stage remodeling. In addition, our extensive biomechanical analyses suggest that OPN functions to enhance bone strength and its ability to dissipate energy prior to failure. The fact that no alterations in content of other ECM proteins were found suggests that the phenotype could be driven by altered matrix turnover and collagen organization, which appears to span multiple organ systems. Therefore, we believe that a unifying link between the vascular and bone related defects found here may be related to diminished collagenous matrix organization and remodeling. Hypothetically, this defect could decrease the ability of cells to bind to ECM and respond appropriately to environmental cues in the absence of OPN. However, future studies are necessary to more definitively determine whether diminished ECM integrity is a primary effect of OPN deficiency or secondary to altered cellular functionality in the absence of OPN. These findings contribute to an improved understanding of the role of OPN *in vivo* and provide new

insight into bone biomechanics and mechanistic control of vascularization and bone regeneration during fracture repair.

CHAPTER 6

SUMMARY AND FUTURE CONSIDERATIONS

Micro-CT Vascular Imaging

The micro-CT vascular imaging techniques developed in Aim 1 provided great utility in subsequent aims of this thesis project. In addition, we have been able to collaborate with researchers within and outside of our institution to assist in implementation of this technique for a number of ongoing studies. As discussed in detail in chapter 3, this technique has broad applicability to studies involving analysis of vasculature anatomy within small animal models. However, some aspects of this methodology still have room for improvement.

A continued obstacle during implementation of this technique is choosing the appropriate threshold value for vascular segmentation. As mentioned, this part of the process is somewhat subjective, and choosing the appropriate global threshold involves balancing the tradeoff between omission of small vascular structures and overestimation of the larger vascular structures in the final 3-D images. This tradeoff introduces artifacts into the quantitative analyses as well, since omission of small vessels has effects such as decreased vessel number, connectivity, etc, as shown in the threshold parameter sensitivity analysis in Chapter 3 (Figure 3.3). In general, this technique provides a simple and useful platform for testing and implementation of micro-CT applications. However, many researchers have developed segmentation methods that are specifically designed for 3-D visualization of blood vessel networks. Implementation of one of these algorithms may help to overcome some of the negative tradeoffs associated with global thresholding and thus yield more accurate 3-D renderings.

Over the past 15 years, dozens of new vascular segmentation algorithms have been developed, and these varied techniques have employed many different image-processing strategies such as filtering, differential analysis, statistical methods, and even artificial intelligence concepts. One example, which was specifically designed for improved segmentation of small diameter vessels, is the curve evolution for vessel segmentation (CURVES) algorithm (235). CURVES falls into the deformable models category of segmentation methods and utilizes a "level-set approach" which determines the vessel axes before estimating their radii. The CURVES algorithm was primarily designed for segmentation of magnetic resonance angiography (MRA) images for use in pre-planning and performing image-guided neurosurgery, but this technique can be applied to 3-D CT data as well. Figure 6.1 compares MRA vascular image segmentations using global thresholding and the CURVES algorithm. Here, maximum intensity projection (MIP) images are shown as a standard with which to compare the binarized, segmented images. MIP is a technique that depicts the brightest pixel value that is encountered along a viewing ray that travels through the stacked tomographic images. MIP is computationally fast, but the 2-D results do not provide a good sense of depth or a means for further 3-D computational analysis. Figure 6.1 illustrates the increased capacity for resolving smaller caliber vessels using the CURVES algorithm, but also shows that this methodology introduces artifactual "thinning" of larger diameter vessels in MRA data. However, this artifact does not persist in CT data due to differences in the nature of the vessel intensity profile between imaging modalities, and the authors exemplify this through an apparently more accurate segmentation of bronchi from a lung CT scan (Figure 6.2). Incorporation of this or a similar vascular-specific segmentation

algorithm would improve the accuracy of the rendered 3-D images and subsequent quantitative analysis.

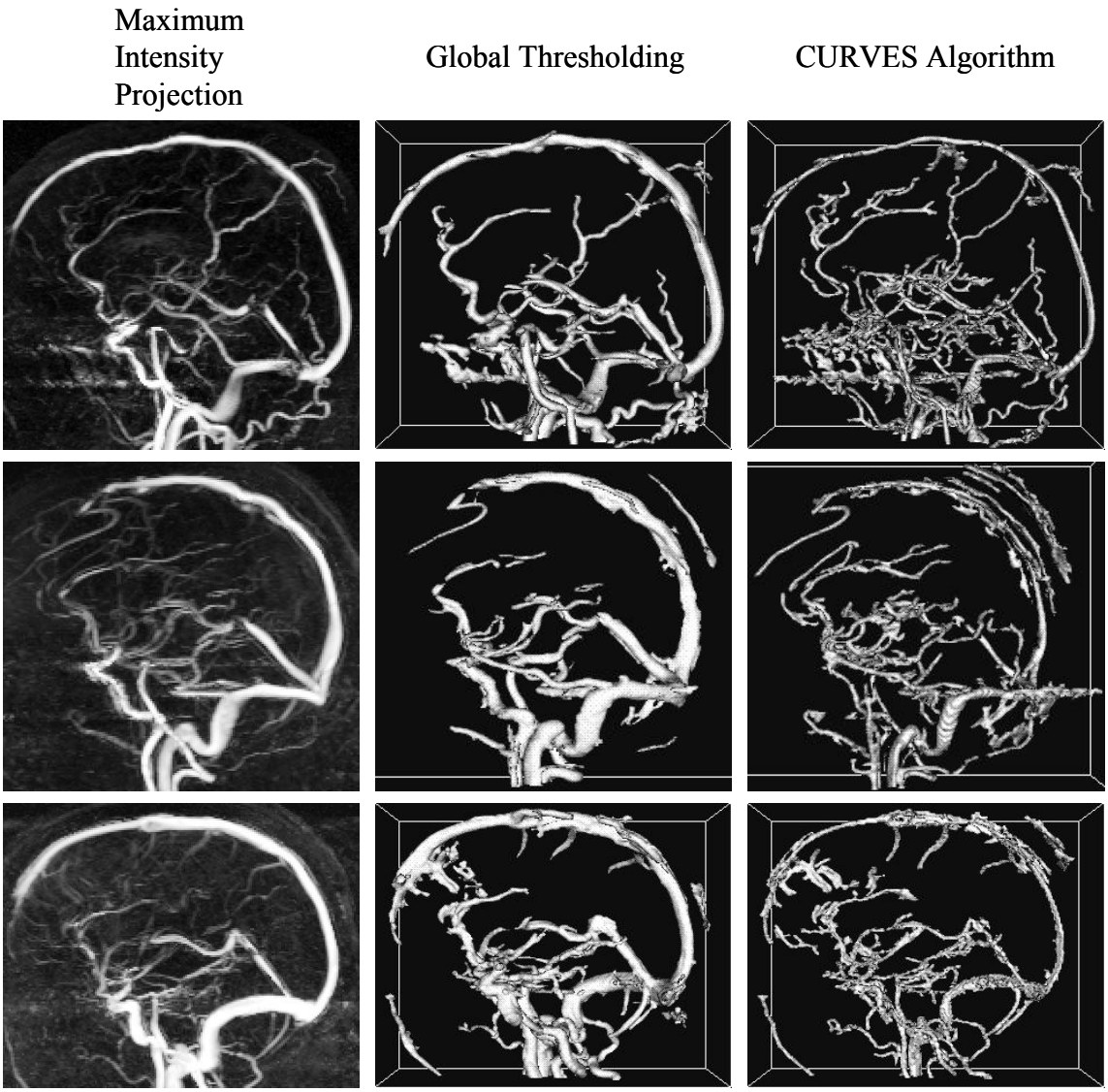

Figure 6.1. Comparison of global thresholding to CURVES algorithm for vascular segmentation. Note that, compared to thresholding, the CURVES algorithm is able to better depict the connectedness and fine detail of the smaller vascular structures. The authors note that the apparent "thinning" of the larger vessels is an artifact that occurs due to the Gaussian vessel intensity profile that exists in MRA images. Images borrowed from (236).

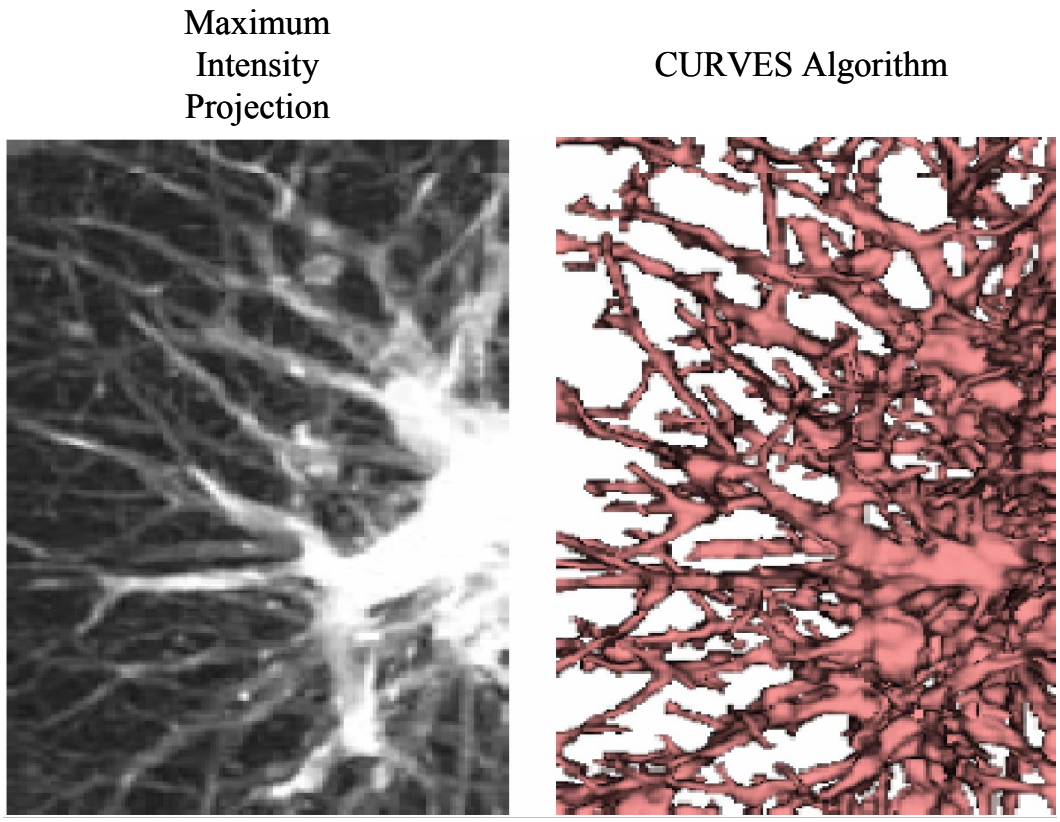

Figure 6.2. CURVES algorithm segmentation of CT data from a lung scan. Note that the artifactual thinning of the larger vessels does not occur in CT data since its intensity profile is not Gaussian. Images modified from (235).

Development of new *in vivo* contrasts and imaging techniques is another area with vast room for expansion in vascular micro-CT imaging. Improvement in this area would grant the opportunity to perform longitudinal analyses within a given experimental animal. This would allow for more information to be gathered from each experiment and spare animal lives and research time required to complete a given study. Investigators in this area have concentrated on development of contrasts with longer circulation times based on slower clearance from the blood pool, allowing more time for imaging of the

anesthetized animal (237). In our limited experience, these agents have provided insufficient contrast from surrounding tissues, but increasing the attenuation of the contrast or simply optimizing delivery to the circulation could make this a feasible methodology. However, longitudinal *in vivo* scans on a single animal increase the amount of total X-ray exposure, and the potential biological effects of this amplified radiation dose must be considered. Additionally, *in vivo* imaging would eliminate the possibility of decalcifying bone tissue, thus decreasing the ease of analyzing vascular networks in proximity to bone structures. Therefore, as *in vivo* vascular contrasts and imaging techniques evolve, researchers must be cognizant of the new difficulties that may be encountered upon their implementation.

Biological Functions of OPN

In chapters 4 and 5, we described studies that, for the first time, addressed the *in vivo* relevance of OPN for its role in postnatal vascular growth and bone healing. As part of these studies, we utilized picrosirius red staining combined with polarized light microscopy to uncover an alteration in collagen fiber organization within the fracture calluses of OPN deficient mice. In future work, it would be important to further understand this finding and to better determine the role of OPN in tissue remodeling following injury and for its contributions to normal and healing bone mechanics. Along these lines, using electron microscopy and other mechanics techniques, one could provide valuable insights into the role of OPN in determining the ultrastructure of bone and other tissues and how this organization functionally affects the mechanical properties.

As discussed in Chapter 5, we have found that OPN is an important contributor to post yield behavior, and OPN deficient bone was found to be more brittle in nature. As

has been elegantly studied by Hansma and colleagues, sacrificial bonds or glue-like filaments are thought to bridge mineralized collagen fibrils and have substantial effects on the fracture resistance of bone (233,238-240). As illustrated in Figure 6.3, these bridging molecules can be imaged with scanning electron microscopy (SEM) and their mechanical role can be measured with atomic force microscopy (AFM). However, the constituents and nature of the sacrificial bonds between collagen fibrils remain unknown. As mentioned in Chapter 2, OPN possesses a high level of phosphorylation and thus, negative charge at physiologic pH. As a result of its negative charge, OPN binds strongly to multivalent, positively charged ions such as calcium. Due to this property, it has been hypothesized that OPN binds to the calcium ions within the hydroxyapatite component of mineralized collagen fibrils. Based on this idea, OPN is suspected to be a prime candidate to participate in the "glue" between mineralized collagen fibrils in bone. Using SEM and AFM techniques, comparison of wild type and OPN deficient bone specimens could further unravel the interactions of OPN with other ECM constituents and better elucidate the mechanism by which OPN contributes to bone mechanical behavior.

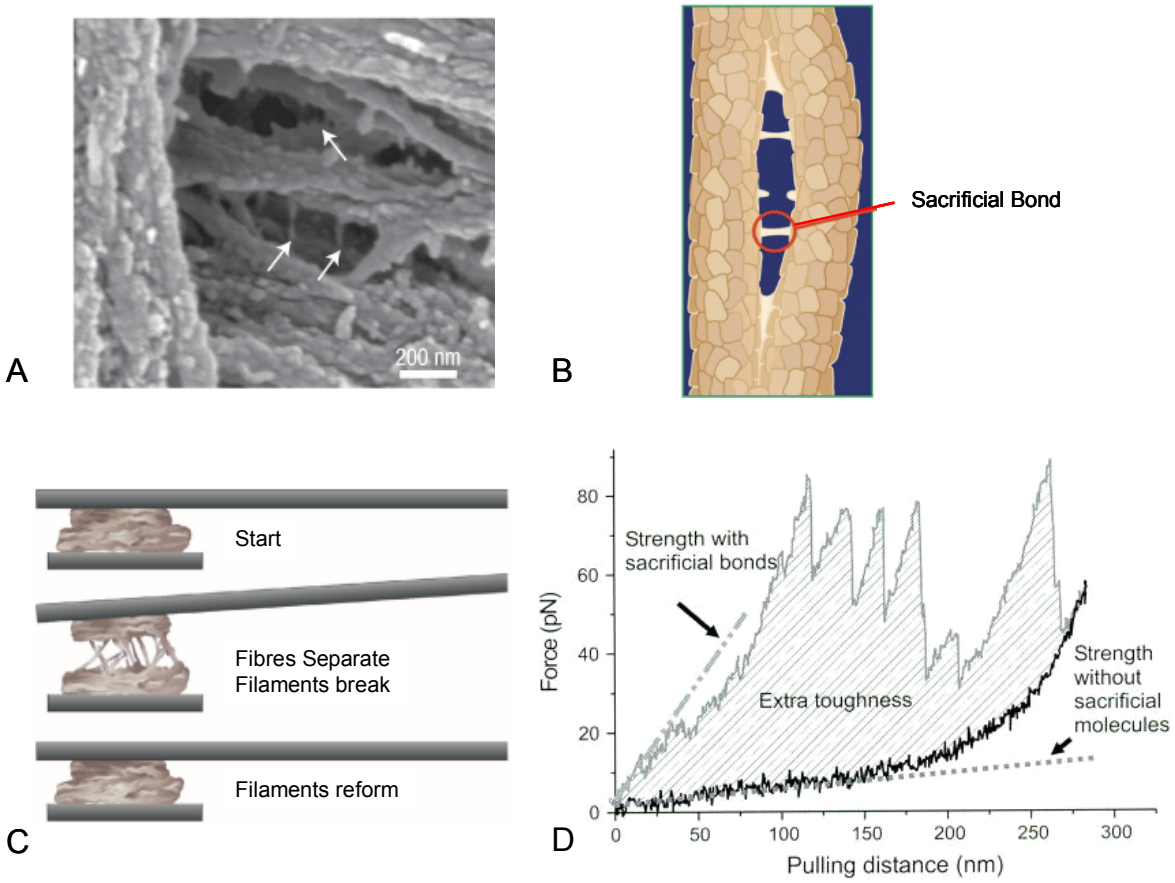

Figure 6.3. Visualization and mechanical measurement of glue-like filaments that resist separation of collagen fibrils. (A) SEM images illustrating sacrificial bonds or "glue-like" filaments that bind together collagen fibrils and potentially resist their separation. (B) Schematic depiction of these filaments resisting separation of collagen fibrils during propagation of a bone crack. (C) Illustration of an AFM setup that can be used to measure the forces that resist mineralized collagen fibril separation in bone. (D) Graph displaying the contribution of sacrificial bonds to material properties by showing representative force measurements of a material with and without sacrificial bonds. The slope of the force-displacement recordings (dashed and dotted lines) show that these bonds can contribute to increased initial stiffness. The shaded area between the recorded force-displacement data sets represents the significant enhancement of fracture toughness when sacrificial molecules are present. Modified from (233,240).

As previously mentioned we postulate that altered ECM organization and remodeling across multiple organ systems could be the unifying characteristic that drives the bone and vascular phenotypes that we have found in the OPN null mice. It has been previously reported that OPN deficient mice possess altered vascular ECM organization, which is apparent even at baseline (see Figure 6.4). This study by Myers *et al.* also found that OPN knockouts displayed reduced remodeling of the vessel wall following carotid artery ligation, a defect that the authors attributed to altered ECM organization and reduced leukocyte invasion (173). Many of the same mechanisms that control vascular remodeling in the pathological sense (i.e. neointima formation following vascular injury) also direct vessel formation and remodeling in more beneficial circumstances (i.e. revascularization of ischemic tissues). To this end, in Chapter 4, we described findings that paralleled the results from the work of Myers *et al.* This study indicated that $OPN^{-/-}$ mice also displayed delayed revascularization and functional limb recovery following onset of hind limb ischemia and reduced monoctye/macrophage chemotaxis. We postulate that these *in vivo* hind limb ischemia results are a manifestation of a defect in arteriogenic vascular remodeling, a process thought to be mediated by monocytes and to be the most important contributor to reperfusion of ischemic tissues. Likewise, in Chapter 5, bone fracture studies indicated that OPN deficiency resulted in diminished early neovascularization and a persistent decrease in vessel diameter, which could be further indicative of a role for OPN in vessel wall remodeling and maturation.

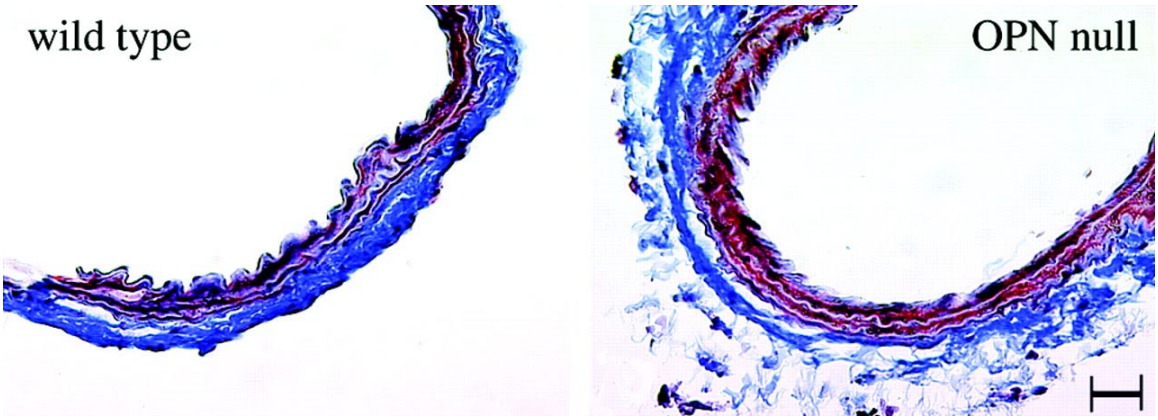

Figure 6.4. Histological images displaying loosely organized collagen matrix in OPN deficient mice. This observation is particularly evident in the adventitial layer and was found to result in increased vascular compliance and possibly contribute to reduced vascular remodeling following carotid artery injury. Images borrowed from (173).

Taken together, previous work and our own studies point to OPN playing an important role in formation and maintenance of organized ECM and in mediating monocyte/macrophage functionality. However, it isn't completely clear that these effects are primarily driven by the lack of OPN behaving as a structural component within the ECM. For example, as mentioned previously, it was recently determined that interactions with an intracellular form of OPN plays an integral role in cell migration and activity of multiple cell types, including activated macrophages (167). Therefore, it is also possible that the absence of OPN has a more direct effect on cellular functionality and that disorganized collagenous matrices in $OPN^{-/-}$ mice are a secondary effect of the cells' ability to remodel and organize the ECM appropriately.

To gain insight into the functional importance of cell-mediated effects of OPN versus those due to ECM structural alterations, bone marrow transplant (BMT) studies could be performed. In these studies, wild type bone marrow (BM) would be

transplanted into irradiated $OPN^{-/-}$ mice and vice versa. After approximately 5 weeks are given for the donor BM cells to engraft into the irradiated recipient mice, this procedure would yield two sets of experimental animals. One set of animals would only produce OPN in BM-derived cells such as monocytes/macrophages and, therefore, have no OPN in the ECM peripheral to the BM. Conversely, the other set of animals would possess OPN in the ECM and tissue resident cells but have no OPN expression in BM-derived cells. Then, it would be important to challenge these animals with hind limb ischemia or bone fracture and compare their responses relative to "control animals", which in this case would be irradiated wild type mice receiving wild type BM and irradiated $OPN^{-/-}$ mice receiving $OPN^{-/-}$ bone marrow. Using this experimental design, one could measure the relative importance of the contribution of OPN to ECM structure versus functionality of BM-derived monocyte / macrophage cells. While this experimental design could potentially lend a great deal of insight into the mechanisms behind OPN functionality, it is not without significant assumptions. For example, as mentioned in Chapter 2, EPCs are also believed to be derived from the bone marrow and to be important participants in neovascularization. Therefore, the effects of BMT and the formation of the described chimeric mice on EPC activity could not be ignored.

Along those lines, it is also noteworthy to revisit two recent studies which have indicated that OPN plays a role in regulation of the hematopoietic stem cell (HSC) niche (171,172). These investigators found aberrant localization and increased cycling of HSC in OPN-/- mice, and both studies, which were published within a few months of each other, independently concluded that OPN participates in HSC localization and as a negative regulator of HSC proliferation. Functional effects of the role of OPN in

regulation of the HSC niche have yet to be determined. As more completely discussed in Chapter 2, EPC mobilization and homing to sites of neovascularization are thought to be a vital part of the physiological response to pro-angiogenic cues. These cells are believed to be derived from the HSC niche, and, therefore, their functionality could be affected by the absence of OPN. Thus, one could hypothesize that EPC numbers, homing, or ability to incorporate into functional vasculature could be altered in the absence of OPN, and this could prove to be an important area for future studies.

Chapter 2 of this thesis summarized a number of *in vitro* cell signaling studies characterizing the multifaceted properties of OPN. These previous studies have implicated OPN in cell survival, migration, and functionality of numerous cell types, and these effects are believed to be mediated through a wide variety of integrin and CD44 receptors via intact OPN or cleavage fragments. The importance of OPN in this sense has been well established. However, the inherent complexity of this system has made it difficult to directly translate findings from studies in cells to a net effect *in vivo*. The current thesis is comprised of many of the first studies that have carefully examined the overall importance of OPN on postnatal vascular growth and bone healing in living animals. As summarized in Figure 6.5, these studies have allowed us to uncover significant, new findings and have allowed us to further speculate on what we believe to be the prominent mechanisms by which OPN exerts its effects. However, as discussed in this chapter, much remains to be understood. To this end, it is anticipated that the results of this work will spur further efforts that will lead to an even better understanding of both OPN functionality and the overall physiological control of postnatal vascular growth,

development and homeostasis of bone tissue mechanical integrity, and bone healing processes.

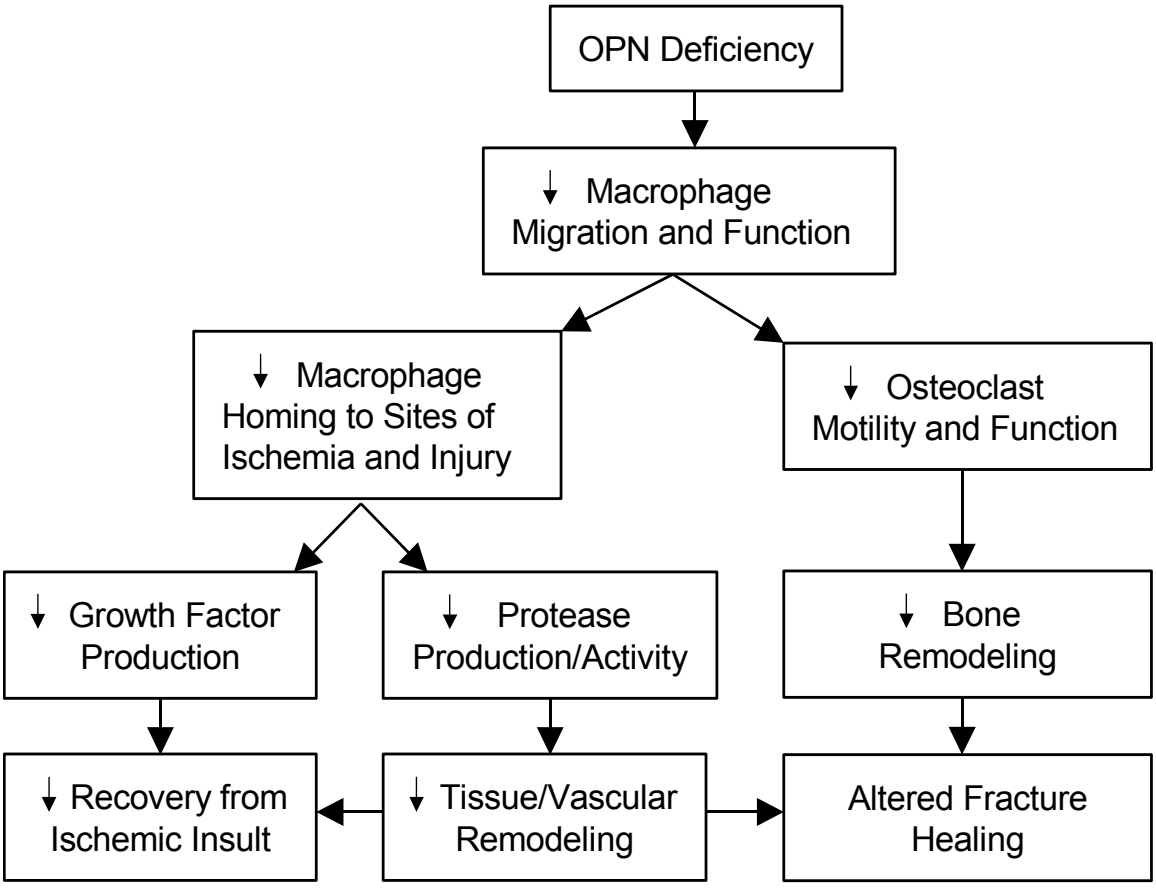

Figure 6.5. Flowchart displaying our hypothesized overall view on the effects of OPN deficiency in the animal models utilized in this dissertation. It should be emphasized that reduced macrophage function is not thought to directly lead to reduced osteoclast function. The right side of the flowchart is meant to infer that, since osteoclasts are derived from common haematopoietic progenitors and, therefore, closely related to macrophages, it is likely that OPN deficiency has parallel effects on the ability of these cells to carry out their specialized functions.

APPENDIX A

MICRO-CT VASCULAR PREPARATION

Reagents

1. 0.9% normal saline
2. Heparin
3. Contrast agent
4. 10% neutral buffered formalin

Solutions

1. 0.9% Normal saline (ie. 9 grams sodium chloride + 1000 ml deionized water)
2. Heparinized Saline (100 units heparin/ml normal saline)
3. *Note: Nitric Oxide donors can be used to ensure vasodilation

Materials

1. Small surgical scissors, hemostat forceps, and small dissecting forceps
2. 23 gauge butterfly needle
3. IV drip bags with tubing or perfusion pump

Procedure

1. Make Heparinized Saline and prepare IV bags with saline/formalin
2. Sacrifice animal by CO_2 asphyxiation or over-anesthetization
3. Prepare animal for perfusion
    a. Secure the animal on its back so that it is in a fully extended position.

b. Make a horizontal incision through the skin across the lower portion of the abdomen.
c. Raise the skin with small forceps (to avoid cutting into organs) and make a superficial, vertical incision up to the sternum.
d. Cut through the diaphragm to open the chest cavity, while avoiding cutting into the liver and lungs.
e. Cut diagonally through the thoracic cage approximately halfway between the sternum and backbone in a "Y" pattern to make the heart accessible.
f. Secure the lower part of the sternum with hemostat forceps and use the weight of the instrument to stabilize the ribcage in a cranial direction, exposing the heart.

4. Perfuse heparinized saline at physiologic pressure (~100 mm Hg) through an IV drip bag or using a perfusion pump
    a. Gently hold the heart with forceps and insert a butterfly needle (attached to tubing) into the left ventricle.
    b. A small drop of superglue can be a useful means for stabilizing the interface between the needle and the heart.
    c. Cut the inferior vena cava (IVC) to create a vent to drain out re-circulating blood and perfusate.
    d. Start the flow of the saline.
    e. Perfuse approximately 10 minutes or until the internal organs become blanched in appearance. The liver transitioning from a dark red to a light

grayish color is the best way to visually assess the completeness of the perfusion

5. Pressure Fixation:
    a. Proceed with this step only after blood has been completely cleared with heparinized saline.
    b. Attach the reservoir containing 10% formalin to the butterfly needle, which should never be displaced from the left ventricle.
    c. Perfusion fix the animal with approximately 30- 50 mL 10% formalin.
    d. When fixation is complete, the animal should become very stiff and pale yellow in appearance.
6. Briefly perfuse again with heparinized saline to clear the formalin from the vasculature
7. Perfuse with the contrast agent of choice (ie. iodinated contrast solutions, polymerizing Microfil injection agents, or barium sulfate / gelatin suspensions):
    a. It may be easiest to inject the contrast agent using a 10 ml syringe that attaches to the butterfly needle.
    b. Perfuse approximately 10 ml or until you see contrast agent re-circulate from the IVC at the top of the liver.
    c. Internal organs including the liver, kidneys, etc. should turn the color of the injected contrast agent if applicable

8. Dissect out the tissue of interest and immerse in 10% neutral buffered formalin until proceeding with micro-CT imaging. For cases where the vasculature of interest is in close proximity to bone, soak the specimen in a formic acid or other

decalcification agent to reduce the attenuation of these hard tissues and facilitate global thresholding-based segmentation of the contrast filled vasculature from the surrounding tissues.

APPENDIX B

HIND LIMB ISCHEMIA SURGERY

Materials

1. Small surgical scissors
2. Hemostat forceps
3. 2 small, curved dissecting forceps

Procedure

1. Sterilize instruments with glass bead sterilizer
2. Anesthetize mouse
3. Shave medial side of animals thigh from knee up
4. Remove remainder of hair in this region with depilatory cream
5. Cleanse skin with water to remove excess cream and hair and then clean skin with betadine
6. Make a single longitudinal skin incision along the medial thigh that tracks the path of the femoral artery.
7. Ligate the superficial femoral artery and vein proximal to the caudally branching deep femoral artery. Be sure to separate the femoral nerve form the vessels at the ligation point and do not loop the sutures around the nerve.
8. Perform the distal ligation just proximal to the branching of the tibial arteries. Again, do not ligate the nerve that is adjacent to the vessels being ligated.
9. Dissect the length of the femoral artery/vein free from the musculature and free from the adjacent nerve between the two ligation points.

10. Cut any vessels that branch off of the artery/vein that have been dissected free tissue and excise the entire artery/vein located between the ligation points.
11. Irrigate the surgical field and carefully close the skin incision using 5-0 silk sutures.
12. Place Elizabethan collar on mouse to hinder the mouse from biting at wound/sutures.
13. Allow the animal to awaken from anesthesia on a heating pad.
14. Allow animal to ambulate freely upon awakening.

APPENDIX C

FEMORAL FRACTURE SURGERY

Materials

1. Small surgical scissors
2. Hemostat forceps
3. Small dissecting forceps
4. No. 15 scalpel

Procedure

1. Sterilize instruments with glass bead sterilizer
2. Anesthetize mouse
3. Shave lateral side of animals thigh from knee up
4. Remove remainder of hair in this region with depilatory cream
5. Cleanse skin with water to remove excess cream and hair and then clean skin with betadine
6. Make longitudinal skin incision along lateral side of leg from knee towards hip
7. Using a No. 15 scalpel, make a longitudinal cut along the lateral condyle of the femur
8. Tease apart the biceps femoris and vastus lateralis muscles to expose the lateral side of the femur
9. Slide the patella to the medial side of the condyle
10. Flex knee to expose the condyle and insert a 25-gauge needle retrograde into the intramedullary canal. **Note**: I use the beveled needle to puncture the condyle and

then cut off the beveled “point” and then re-insert the needle to avoid puncturing the proximal end of the femur during insertion of the needle.

11. Then, using the No. 15 scalpel, create a mid-diaphyseal transverse fracture
12. Slide the needle slightly back out of the intramedullary canal of the femur and cut the needle to the appropriate length (so that the intramedullary support is flush with the surface of the condyle at the needle insertion point).
13. Slide the patella back into its native position, covering the condyle.
14. Using 5-0 silk sutures, place one suture to hold the biceps femoris and vastus lateralis muscles together.
15. Place one suture connecting the patellar ligament to the adjacent musculature on the lateral side (to keep the patella from sliding back out of place).
16. Close the skin incision using interrupted sutures and staples.
17. Allow the animal to awaken from anesthesia on a heating pad.
18. Allow animal to ambulate freely upon awakening.

REFERENCES

1. Murray CJ, Lopez AD 1997 Mortality by cause for eight regions of the world: Global Burden of Disease Study. Lancet **349**(9061)**:**1269-76.

2. Asou Y, Rittling SR, Yoshitake H, Tsuji K, Shinomiya K, Nifuji A, Denhardt DT, Noda M 2001 Osteopontin facilitates angiogenesis, accumulation of osteoclasts, and resorption in ectopic bone. Endocrinology **142**(3)**:**1325-32.

3. Takagi H, Suzuma K, Otani A, Oh H, Koyama S, Ohashi H, Watanabe D, Ojima T, Suganami E, Honda Y 2002 Role of vitronectin receptor-type integrins and osteopontin in ischemia-induced retinal neovascularization. Jpn J Ophthalmol **46**(3)**:**270-8.

4. Bonnarens F, Einhorn TA 1984 Production of a standard closed fracture in laboratory animal bone. Journal of Orthopaedic Research **2**(1)**:**97-101.

5. Scholz D, Ziegelhoeffer T, Helisch A, Wagner S, Friedrich C, Podzuweit T, Schaper W 2002 Contribution of arteriogenesis and angiogenesis to postocclusive hindlimb perfusion in mice. J Mol Cell Cardiol **34**(7)**:**775-87.

6. Arras M, Ito WD, Scholz D, Winkler B, Schaper J, Schaper W 1998 Monocyte activation in angiogenesis and collateral growth in the rabbit hindlimb. J Clin Invest **101**(1)**:**40-50.

7. Ito WD, Arras M, Scholz D, Winkler B, Htun P, Schaper W 1997 Angiogenesis but not collateral growth is associated with ischemia after femoral artery occlusion. Am J Physiol **273**(3 Pt 2)**:**H1255-65.

8. Risau W 1997 Mechanisms of angiogenesis. Nature **386**(6626)**:**671-4.

9. Asahara T, Masuda H, Takahashi T, Kalka C, Pastore C, Silver M, Kearne M, Magner M, Isner JM 1999 Bone marrow origin of endothelial progenitor cells responsible for postnatal vasculogenesis in physiological and pathological neovascularization. Circ Res **85**(3)**:**221-8.

10. Ziegelhoeffer T, Fernandez B, Kostin S, Heil M, Voswinckel R, Helisch A, Schaper W 2003 Bone Marrow-Derived Cells Do Not Incorporate Into the Adult Growing Vasculature. Circ Res.

11. Senger DR, Perruzzi CA, Feder J, Dvorak HF 1986 A highly conserved vascular permeability factor secreted by a variety of human and rodent tumor cell lines. Cancer Res **46**(11)**:**5629-32.

12. Senger DR, Galli SJ, Dvorak AM, Perruzzi CA, Harvey VS, Dvorak HF 1983 Tumor cells secrete a vascular permeability factor that promotes accumulation of ascites fluid. Science **219**(4587)**:**983-5.

13. Lobb RR, Key ME, Alderman EM, Fett JW 1985 Partial purification and characterization of a vascular permeability factor secreted by a human colon adenocarcinoma cell line. Int J Cancer **36**(4)**:**473-8.

14. Forsythe JA, Jiang BH, Iyer NV, Agani F, Leung SW, Koos RD, Semenza GL 1996 Activation of vascular endothelial growth factor gene transcription by hypoxia-inducible factor 1. Mol Cell Biol **16**(9)**:**4604-13.

15. Carmeliet P, Ferreira V, Breier G, Pollefeyt S, Kieckens L, Gertsenstein M, Fahrig M, Vandenhoeck A, Harpal K, Eberhardt C, Declercq C, Pawling J, Moons L, Collen D, Risau W, Nagy A 1996 Abnormal blood vessel development and lethality in embryos lacking a single VEGF allele. Nature **380**(6573)**:**435-9.

16. Fong GH, Rossant J, Gertsenstein M, Breitman ML 1995 Role of the Flt-1 receptor tyrosine kinase in regulating the assembly of vascular endothelium. Nature **376**(6535)**:**66-70.

17. Shalaby F, Rossant J, Yamaguchi TP, Gertsenstein M, Wu XF, Breitman ML, Schuh AC 1995 Failure of blood-island formation and vasculogenesis in Flk-1-deficient mice. Nature **376**(6535)**:**62-6.

18. Seghezzi G, Patel S, Ren CJ, Gualandris A, Pintucci G, Robbins ES, Shapiro RL, Galloway AC, Rifkin DB, Mignatti P 1998 Fibroblast growth factor-2 (FGF-2) induces vascular endothelial growth factor (VEGF) expression in the endothelial cells of forming capillaries: an autocrine mechanism contributing to angiogenesis. J Cell Biol **141**(7)**:**1659-73.

19. Katoh Y, Katoh M 2005 Comparative genomics on FGF7, FGF10, FGF22 orthologs, and identification of fgf25. Int J Mol Med **16**(4)**:**767-70.

20. Ago H, Kitagawa Y, Fujishima A, Matsuura Y, Katsube Y 1991 Crystal structure of basic fibroblast growth factor at 1.6 A resolution. J Biochem (Tokyo) **110**(3)**:**360-3.

21. Zhang JD, Cousens LS, Barr PJ, Sprang SR 1991 Three-dimensional structure of human basic fibroblast growth factor, a structural homolog of interleukin 1 beta. Proc Natl Acad Sci U S A **88**(8)**:**3446-50.

22. Miller DL, Ortega S, Bashayan O, Basch R, Basilico C 2000 Compensation by fibroblast growth factor 1 (FGF1) does not account for the mild phenotypic defects observed in FGF2 null mice. Mol Cell Biol **20**(6)**:**2260-8.

23. Ortega S, Ittmann M, Tsang SH, Ehrlich M, Basilico C 1998 Neuronal defects and delayed wound healing in mice lacking fibroblast growth factor 2. Proc Natl Acad Sci U S A **95**(10)**:**5672-7.

24. Ozaki H, Okamoto N, Ortega S, Chang M, Ozaki K, Sadda S, Vinores MA, Derevjanik N, Zack DJ, Basilico C, Campochiaro PA 1998 Basic fibroblast growth factor is neither necessary nor sufficient for the development of retinal neovascularization. Am J Pathol **153**(3)**:**757-65.

25. Powers CJ, McLeskey SW, Wellstein A 2000 Fibroblast growth factors, their receptors and signaling. Endocr Relat Cancer **7**(3)**:**165-97.

26. Mack CA, Patel SR, Schwarz EA, Zanzonico P, Hahn RT, Ilercil A, Devereux RB, Goldsmith SJ, Christian TF, Sanborn TA, Kovesdi I, Hackett N, Isom OW, Crystal RG, Rosengart TK 1998 Biologic bypass with the use of adenovirus-mediated gene transfer of the complementary deoxyribonucleic acid for vascular endothelial growth factor 121 improves myocardial perfusion and function in the ischemic porcine heart. J Thorac Cardiovasc Surg **115**(1)**:**168-76; discussion 176-7.

27. Takeshita S, Zheng LP, Brogi E, Kearney M, Pu LQ, Bunting S, Ferrara N, Symes JF, Isner JM 1994 Therapeutic angiogenesis. A single intraarterial bolus of vascular endothelial growth factor augments revascularization in a rabbit ischemic hind limb model. J Clin Invest **93**(2)**:**662-70.

28. Safi J, Jr., DiPaula AF, Jr., Riccioni T, Kajstura J, Ambrosio G, Becker LC, Anversa P, Capogrossi MC 1999 Adenovirus-mediated acidic fibroblast growth factor gene transfer induces angiogenesis in the nonischemic rabbit heart. Microvasc Res **58**(3)**:**238-49.

29. Banai S, Jaklitsch MT, Shou M, Lazarous DF, Scheinowitz M, Biro S, Epstein SE, Unger EF 1994 Angiogenic-induced enhancement of collateral blood flow to ischemic myocardium by vascular endothelial growth factor in dogs. Circulation **89**(5)**:**2183-9.

30. Unger EF, Banai S, Shou M, Lazarous DF, Jaklitsch MT, Scheinowitz M, Correa R, Klingbeil C, Epstein SE 1994 Basic fibroblast growth factor enhances myocardial collateral flow in a canine model. Am J Physiol **266**(4 Pt 2)**:**H1588-95.

31. Henry TD, Annex BH, McKendall GR, Azrin MA, Lopez JJ, Giordano FJ, Shah PK, Willerson JT, Benza RL, Berman DS, Gibson CM, Bajamonde A, Rundle AC, Fine J, McCluskey ER 2003 The VIVA trial: Vascular endothelial growth factor in Ischemia for Vascular Angiogenesis. Circulation **107**(10)**:**1359-65.

32. Rajagopalan S, Mohler ER, 3rd, Lederman RJ, Mendelsohn FO, Saucedo JF, Goldman CK, Blebea J, Macko J, Kessler PD, Rasmussen HS, Annex BH 2003 Regional angiogenesis with vascular endothelial growth factor in peripheral arterial disease: a phase II randomized, double-blind, controlled study of adenoviral delivery of vascular endothelial growth factor 121 in patients with disabling intermittent claudication. Circulation **108**(16)**:**1933-8.

33. Simons M, Annex BH, Laham RJ, Kleiman N, Henry T, Dauerman H, Udelson JE, Gervino EV, Pike M, Whitehouse MJ, Moon T, Chronos NA 2002 Pharmacological treatment of coronary artery disease with recombinant fibroblast growth factor-2: double-blind, randomized, controlled clinical trial. Circulation **105**(7)**:**788-93.

34. Lederman RJ, Mendelsohn FO, Anderson RD, Saucedo JF, Tenaglia AN, Hermiller JB, Hillegass WB, Rocha-Singh K, Moon TE, Whitehouse MJ, Annex BH 2002 Therapeutic angiogenesis with recombinant fibroblast growth factor-2 for intermittent claudication (the TRAFFIC study): a randomised trial. Lancet **359**(9323)**:**2053-8.

35. Serini G, Valdembri D, Bussolino F 2006 Integrins and angiogenesis: a sticky business. Exp Cell Res **312**(5)**:**651-8.

36. Davis GE, Senger DR 2005 Endothelial extracellular matrix: biosynthesis, remodeling, and functions during vascular morphogenesis and neovessel stabilization. Circ Res **97**(11)**:**1093-107.

37. Friedlander M, Brooks PC, Shaffer RW, Kincaid CM, Varner JA, Cheresh DA 1995 Definition of two angiogenic pathways by distinct alpha v integrins. Science **270**(5241)**:**1500-2.

38. Senger DR, Claffey KP, Benes JE, Perruzzi CA, Sergiou AP, Detmar M 1997 Angiogenesis promoted by vascular endothelial growth factor: regulation through alpha1beta1 and alpha2beta1 integrins. Proc Natl Acad Sci U S A **94**(25)**:**13612-7.

39. Wijelath ES, Murray J, Rahman S, Patel Y, Ishida A, Strand K, Aziz S, Cardona C, Hammond WP, Savidge GF, Rafii S, Sobel M 2002 Novel vascular endothelial growth factor binding domains of fibronectin enhance vascular endothelial growth factor biological activity. Circ Res **91**(1)**:**25-31.

40. Schaper J, Konig R, Franz D, Schaper W 1976 The endothelial surface of growing coronary collateral arteries. Intimal margination and diapedesis of monocytes. A combined SEM and TEM study. Virchows Arch A Pathol Anat Histol **370**(3)**:**193-205.

41. Polverini PJ, Cotran PS, Gimbrone MA, Jr., Unanue ER 1977 Activated macrophages induce vascular proliferation. Nature **269**(5631)**:**804-6.

42. Heil M, Ziegelhoeffer T, Pipp F, Kostin S, Martin S, Clauss M, Schaper W 2002 Blood monocyte concentration is critical for enhancement of collateral artery growth. Am J Physiol Heart Circ Physiol **283**(6)**:**H2411-9.

43. Bergmann CE, Hoefer IE, Meder B, Roth H, van Royen N, Breit SM, Jost MM, Aharinejad S, Hartmann S, Buschmann IR 2006 Arteriogenesis depends on circulating monocytes and macrophage accumulation and is severely depressed in op/op mice J Leukoc Biol, vol. 80, pp 59-65.

44. Goede V, Brogelli L, Ziche M, Augustin HG 1999 Induction of inflammatory angiogenesis by monocyte chemoattractant protein-1. Int J Cancer **82**(5)**:**765-70.

45. Marumo T, Schini-Kerth VB, Busse R 1999 Vascular endothelial growth factor activates nuclear factor-kappaB and induces monocyte chemoattractant protein-1 in bovine retinal endothelial cells. Diabetes **48**(5)**:**1131-7.

46. Wempe F, Lindner V, Augustin HG 1997 Basic fibroblast growth factor (bFGF) regulates the expression of the CC chemokine monocyte chemoattractant protein-1 (MCP-1) in autocrine-activated endothelial cells. Arterioscler Thromb Vasc Biol **17**(11)**:**2471-8.

47. Hoefer IE, van Royen N, Buschmann IR, Piek JJ, Schaper W 2001 Time course of arteriogenesis following femoral artery occlusion in the rabbit. Cardiovasc Res **49**(3)**:**609-17.

48. Voskuil M, van Royen N, Hoefer IE, Seidler R, Guth BD, Bode C, Schaper W, Piek JJ, Buschmann IR 2003 Modulation of collateral artery growth in a porcine hindlimb ligation model using MCP-1. Am J Physiol Heart Circ Physiol **284**(4)**:**H1422-8.

49. Ito WD, Arras M, Winkler B, Scholz D, Schaper J, Schaper W 1997 Monocyte chemotactic protein-1 increases collateral and peripheral conductance after femoral artery occlusion. Circ Res **80**(6)**:**829-37.

50. Muhs A, Lenter MC, Seidler RW, Zweigerdt R, Kirchengast M, Weser R, Ruediger M, Guth B 2004 Nonviral monocyte chemoattractant protein-1 gene transfer improves arteriogenesis after femoral artery occlusion. Gene Ther **11**(23)**:**1685-93.

51. Scholz D, Ito W, Fleming I, Deindl E, Sauer A, Wiesnet M, Busse R, Schaper J, Schaper W 2000 Ultrastructure and molecular histology of rabbit hind-limb collateral artery growth (arteriogenesis). Virchows Arch **436**(3)**:**257-70.

52. van Royen N, Hoefer I, Buschmann I, Kostin S, Voskuil M, Bode C, Schaper W, Piek JJ 2003 Effects of local MCP-1 protein therapy on the development of the collateral circulation and atherosclerosis in Watanabe hyperlipidemic rabbits. Cardiovasc Res **57**(1)**:**178-85.

53. van Royen N, Hoefer I, Bottinger M, Hua J, Grundmann S, Voskuil M, Bode C, Schaper W, Buschmann I, Piek JJ 2003 Local monocyte chemoattractant protein-1 therapy increases collateral artery formation in apolipoprotein E-deficient mice but induces systemic monocytic CD11b expression, neointimal formation, and plaque progression. Circ Res **92**(2)**:**218-25.

54. Heil M, Ziegelhoeffer T, Wagner S, Fernandez B, Helisch A, Martin S, Tribulova S, Kuziel WA, Bachmann G, Schaper W 2004 Collateral artery growth (arteriogenesis) after experimental arterial occlusion is impaired in mice lacking CC-chemokine receptor-2. Circ Res **94**(5)**:**671-7.

55. Voskuil M, Hoefer IE, van Royen N, Hua J, de Graaf S, Bode C, Buschmann IR, Piek JJ 2004 Abnormal monocyte recruitment and collateral artery formation in monocyte chemoattractant protein-1 deficient mice. Vasc Med **9**(4)**:**287-92.

56. Asahara T, Murohara T, Sullivan A, Silver M, van der Zee R, Li T, Witzenbichler B, Schatteman G, Isner JM 1997 Isolation of putative progenitor endothelial cells for angiogenesis. Science **275**(5302)**:**964-7.

57. Shi Q, Rafii S, Wu MH, Wijelath ES, Yu C, Ishida A, Fujita Y, Kothari S, Mohle R, Sauvage LR, Moore MA, Storb RF, Hammond WP 1998 Evidence for circulating bone marrow-derived endothelial cells. Blood **92**(2)**:**362-7.

58. Urbich C, Dimmeler S 2004 Endothelial progenitor cells: characterization and role in vascular biology. Circ Res **95**(4)**:**343-53.

59. Kalka C, Masuda H, Takahashi T, Kalka-Moll WM, Silver M, Kearney M, Li T, Isner JM, Asahara T 2000 Transplantation of ex vivo expanded endothelial progenitor cells for therapeutic neovascularization. Proc Natl Acad Sci U S A **97**(7)**:**3422-7.

60. Kamihata H, Matsubara H, Nishiue T, Fujiyama S, Tsutsumi Y, Ozono R, Masaki H, Mori Y, Iba O, Tateishi E, Kosaki A, Shintani S, Murohara T, Imaizumi T, Iwasaka T 2001 Implantation of bone marrow mononuclear cells into ischemic myocardium enhances collateral perfusion and regional function via side supply of angioblasts, angiogenic ligands, and cytokines. Circulation **104**(9)**:**1046-52.

61. Kawamoto A, Gwon HC, Iwaguro H, Yamaguchi JI, Uchida S, Masuda H, Silver M, Ma H, Kearney M, Isner JM, Asahara T 2001 Therapeutic potential of ex vivo expanded endothelial progenitor cells for myocardial ischemia. Circulation **103**(5)**:**634-7.

62. Kocher AA, Schuster MD, Szabolcs MJ, Takuma S, Burkhoff D, Wang J, Homma S, Edwards NM, Itescu S 2001 Neovascularization of ischemic myocardium by human bone-marrow-derived angioblasts prevents cardiomyocyte apoptosis, reduces remodeling and improves cardiac function. Nat Med **7**(4)**:**430-6.

63. Hess DC, Hill WD, Martin-Studdard A, Carroll J, Brailer J, Carothers J 2002 Bone marrow as a source of endothelial cells and NeuN-expressing cells After stroke. Stroke **33**(5)**:**1362-8.

64. Zhang ZG, Zhang L, Jiang Q, Chopp M 2002 Bone marrow-derived endothelial progenitor cells participate in cerebral neovascularization after focal cerebral ischemia in the adult mouse. Circ Res **90**(3)**:**284-8.

65. Lyden D, Hattori K, Dias S, Costa C, Blaikie P, Butros L, Chadburn A, Heissig B, Marks W, Witte L, Wu Y, Hicklin D, Zhu Z, Hackett NR, Crystal RG, Moore MA, Hajjar KA, Manova K, Benezra R, Rafii S 2001 Impaired recruitment of bone-marrow-derived endothelial and hematopoietic precursor cells blocks tumor angiogenesis and growth. Nat Med **7**(11)**:**1194-201.

66. Ziegelhoeffer T, Fernandez B, Kostin S, Heil M, Voswinckel R, Helisch A, Schaper W 2004 Bone marrow-derived cells do not incorporate into the adult growing vasculature. Circ Res **94**(2)**:**230-8.

67. Khmelewski E, Becker A, Meinertz T, Ito WD 2004 Tissue resident cells play a dominant role in arteriogenesis and concomitant macrophage accumulation. Circ Res **95**(6)**:**E56-64.

68. O'Neill TJt, Wamhoff BR, Owens GK, Skalak TC 2005 Mobilization of bone marrow-derived cells enhances the angiogenic response to hypoxia without transdifferentiation into endothelial cells. Circ Res **97**(10)**:**1027-35.

69. Machein MR, Renninger S, de Lima-Hahn E, Plate KH 2003 Minor contribution of bone marrow-derived endothelial progenitors to the vascularization of murine gliomas. Brain Pathol **13**(4)**:**582-97.

70. Larrivee B, Niessen K, Pollet I, Corbel SY, Long M, Rossi FM, Olive PL, Karsan A 2005 Minimal contribution of marrow-derived endothelial precursors to tumor vasculature. J Immunol **175**(5)**:**2890-9.

71. Gothert JR, Gustin SE, van Eekelen JA, Schmidt U, Hall MA, Jane SM, Green AR, Gottgens B, Izon DJ, Begley CG 2004 Genetically tagging endothelial cells in vivo: bone marrow-derived cells do not contribute to tumor endothelium. Blood **104**(6)**:**1769-77.

72. Hill JM, Zalos G, Halcox JP, Schenke WH, Waclawiw MA, Quyyumi AA, Finkel T 2003 Circulating endothelial progenitor cells, vascular function, and cardiovascular risk. N Engl J Med **348**(7)**:**593-600.

73. Vasa M, Fichtlscherer S, Aicher A, Adler K, Urbich C, Martin H, Zeiher AM, Dimmeler S 2001 Number and migratory activity of circulating endothelial progenitor cells inversely correlate with risk factors for coronary artery disease. Circ Res **89**(1)**:**E1-7.

74. Werner N, Kosiol S, Schiegl T, Ahlers P, Walenta K, Link A, Bohm M, Nickenig G 2005 Circulating endothelial progenitor cells and cardiovascular outcomes. N Engl J Med **353**(10)**:**999-1007.

75. Loomans CJ, de Koning EJ, Staal FJ, Rookmaaker MB, Verseyden C, de Boer HC, Verhaar MC, Braam B, Rabelink TJ, van Zonneveld AJ 2004 Endothelial progenitor cell dysfunction: a novel concept in the pathogenesis of vascular complications of type 1 diabetes. Diabetes **53**(1)**:**195-9.

76. Tepper OM, Galiano RD, Capla JM, Kalka C, Gagne PJ, Jacobowitz GR, Levine JP, Gurtner GC 2002 Human endothelial progenitor cells from type II diabetics exhibit impaired proliferation, adhesion, and incorporation into vascular structures. Circulation **106**(22)**:**2781-6.

77. Kondo T, Hayashi M, Takeshita K, Numaguchi Y, Kobayashi K, Iino S, Inden Y, Murohara T 2004 Smoking cessation rapidly increases circulating progenitor cells in peripheral blood in chronic smokers. Arterioscler Thromb Vasc Biol **24**(8)**:**1442-7.

78. Chen JZ, Zhang FR, Tao QM, Wang XX, Zhu JH 2004 Number and activity of endothelial progenitor cells from peripheral blood in patients with hypercholesterolaemia. Clin Sci (Lond) **107**(3)**:**273-80.

79. Llevadot J, Murasawa S, Kureishi Y, Uchida S, Masuda H, Kawamoto A, Walsh K, Isner JM, Asahara T 2001 HMG-CoA reductase inhibitor mobilizes bone marrow--derived endothelial progenitor cells. J Clin Invest **108**(3)**:**399-405.

80. Laufs U, Werner N, Link A, Endres M, Wassmann S, Jurgens K, Miche E, Bohm M, Nickenig G 2004 Physical training increases endothelial progenitor cells, inhibits neointima formation, and enhances angiogenesis. Circulation **109**(2)**:**220-6.

81. Schachinger V, Assmus B, Britten MB, Honold J, Lehmann R, Teupe C, Abolmaali ND, Vogl TJ, Hofmann WK, Martin H, Dimmeler S, Zeiher AM 2004 Transplantation of progenitor cells and regeneration enhancement in acute myocardial infarction: final one-year results of the TOPCARE-AMI Trial. J Am Coll Cardiol **44**(8)**:**1690-9.

82. Wollert KC, Meyer GP, Lotz J, Ringes-Lichtenberg S, Lippolt P, Breidenbach C, Fichtner S, Korte T, Hornig B, Messinger D, Arseniev L, Hertenstein B, Ganser A, Drexler H 2004 Intracoronary autologous bone-marrow cell transfer after myocardial infarction: the BOOST randomised controlled clinical trial. Lancet **364**(9429)**:**141-8.

83. Folkman J 1971 Tumor angiogenesis: therapeutic implications. N Engl J Med **285**(21)**:**1182-6.

84. Kim KJ, Li B, Winer J, Armanini M, Gillett N, Phillips HS, Ferrara N 1993 Inhibition of vascular endothelial growth factor-induced angiogenesis suppresses tumour growth in vivo. Nature **362**(6423)**:**841-4.

85. Ferrara N, Hillan KJ, Gerber HP, Novotny W 2004 Discovery and development of bevacizumab, an anti-VEGF antibody for treating cancer. Nat Rev Drug Discov **3**(5)**:**391-400.

86. Jain RK, Duda DG, Clark JW, Loeffler JS 2006 Lessons from phase III clinical trials on anti-VEGF therapy for cancer. Nat Clin Pract Oncol **3**(1)**:**24-40.

87. Ferrara N 2004 Vascular endothelial growth factor: basic science and clinical progress. Endocr Rev **25**(4)**:**581-611.

88. Ng EW, Shima DT, Calias P, Cunningham ET, Jr., Guyer DR, Adamis AP 2006 Pegaptanib, a targeted anti-VEGF aptamer for ocular vascular disease. Nat Rev Drug Discov **5**(2)**:**123-32.

89. Tolentino MJ, Brucker AJ, Fosnot J, Ying GS, Wu IH, Malik G, Wan S, Reich SJ 2004 Intravitreal injection of vascular endothelial growth factor small interfering RNA inhibits growth and leakage in a nonhuman primate, laser-induced model of choroidal neovascularization. Retina **24**(4)**:**660.

90. Shen J, Samul R, Silva RL, Akiyama H, Liu H, Saishin Y, Hackett SF, Zinnen S, Kossen K, Fosnaugh K, Vargeese C, Gomez A, Bouhana K, Aitchison R, Pavco

P, Campochiaro PA 2006 Suppression of ocular neovascularization with siRNA targeting VEGF receptor 1. Gene Ther **13**(3)**:**225-34.

91. Kurup A, Lin CW, Murry DJ, Dobrolecki L, Estes D, Yiannoutsos CT, Mariano L, Sidor C, Hickey R, Hanna N 2006 Recombinant human angiostatin (rhAngiostatin) in combination with paclitaxel and carboplatin in patients with advanced non-small-cell lung cancer: a phase II study from Indiana University. Ann Oncol **17**(1)**:**97-103.

92. Arvelo F, Cotte C 2006 [Metalloproteinases in tumor progression. Review]. Invest Clin **47**(2)**:**185-205.

93. Cai W, Chen X 2006 Anti-angiogenic cancer therapy based on integrin alphavbeta3 antagonism. Anticancer Agents Med Chem **6**(5)**:**407-28.

94. Berger AC, Wang XQ, Zalatoris A, Cenna J, Watson JC 2004 A murine model of ex vivo angiogenesis using aortic disks grown in fibrin clot. Microvasc Res **68**(3)**:**179-87.

95. Nicosia RF, Ottinetti A 1990 Growth of microvessels in serum-free matrix culture of rat aorta. A quantitative assay of angiogenesis in vitro. Lab Invest **63**(1)**:**115-22.

96. Masson VV, Devy L, Grignet-Debrus C, Bernt S, Bajou K, Blacher S, Roland G, Chang Y, Fong T, Carmeliet P, Foidart JM, Noel A 2002 Mouse Aortic Ring Assay: A New Approach of the Molecular Genetics of Angiogenesis. Biol Proced Online **4:**24-31.

97. Auerbach R, Kubai L, Knighton D, Folkman J 1974 A simple procedure for the long-term cultivation of chicken embryos. Dev Biol **41**(2)**:**391-4.

98. Nguyen M, Shing Y, Folkman J 1994 Quantitation of angiogenesis and antiangiogenesis in the chick embryo chorioallantoic membrane. Microvasc Res **47**(1)**:**31-40.

99. Passaniti A, Taylor RM, Pili R, Guo Y, Long PV, Haney JA, Pauly RR, Grant DS, Martin GR 1992 A simple, quantitative method for assessing angiogenesis and antiangiogenic agents using reconstituted basement membrane, heparin, and fibroblast growth factor. Lab Invest **67**(4)**:**519-28.

100. Andrade SP, Fan TP, Lewis GP 1987 Quantitative in-vivo studies on angiogenesis in a rat sponge model. Br J Exp Pathol **68**(6)**:**755-66.

101. Kowalski J, Kwan HH, Prionas SD, Allison AC, Fajardo LF 1992 Characterization and applications of the disc angiogenesis system. Exp Mol Pathol **56**(1)**:**1-19.

102. Fajardo LF, Kowalski J, Kwan HH, Prionas SD, Allison AC 1988 The disc angiogenesis system. Lab Invest **58**(6)**:**718-24.

103. Kenyon BM, Voest EE, Chen CC, Flynn E, Folkman J, D'Amato RJ 1996 A model of angiogenesis in the mouse cornea. Invest Ophthalmol Vis Sci **37**(8)**:**1625-32.

104. Gimbrone MA, Jr., Cotran RS, Leapman SB, Folkman J 1974 Tumor growth and neovascularization: an experimental model using the rabbit cornea. J Natl Cancer Inst **52**(2)**:**413-27.

105. Muthukkaruppan V, Auerbach R 1979 Angiogenesis in the mouse cornea. Science **205**(4413)**:**1416-8.

106. Gimbrone MA, Jr., Leapman SB, Cotran RS, Folkman J 1972 Tumor dormancy in vivo by prevention of neovascularization. J Exp Med **136**(2)**:**261-76.

107. Couffinhal T, Silver M, Zheng LP, Kearney M, Witzenbichler B, Isner JM 1998 Mouse model of angiogenesis. Am J Pathol **152**(6)**:**1667-79.

108. Hendricks DL, Pevec WC, Shestak KC, Rosenthal MC, Webster MW, Steed DL 1990 A model of persistent partial hindlimb ischemia in the rabbit. J Surg Res **49**(5)**:**453-7.

109. Pu LQ, Jackson S, Lachapelle KJ, Arekat Z, Graham AM, Lisbona R, Brassard R, Carpenter S, Symes JF 1994 A persistent hindlimb ischemia model in the rabbit. J Invest Surg **7**(1)**:**49-60.

110. Conrad MC 1977 Effects of therapy on maximal walking time following femoral ligation in the rat. Circ Res **41**(6)**:**775-8.

111. Silvestre JS, Tamarat R, Ebrahimian TG, Le-Roux A, Clergue M, Emmanuel F, Duriez M, Schwartz B, Branellec D, Levy BI 2003 Vascular endothelial growth factor-B promotes in vivo angiogenesis. Circ Res **93**(2)**:**114-23.

112. Abe M, Sata M, Nishimatsu H, Nagata D, Suzuki E, Terauchi Y, Kadowaki T, Minamino N, Kangawa K, Matsuo H, Hirata Y, Nagai R 2003 Adrenomedullin augments collateral development in response to acute ischemia. Biochem Biophys Res Commun **306**(1)**:**10-5.

113. Amano K, Matsubara H, Iba O, Okigaki M, Fujiyama S, Imada T, Kojima H, Nozawa Y, Kawashima S, Yokoyama M, Iwasaka T 2003 Enhancement of ischemia-induced angiogenesis by eNOS overexpression. Hypertension **41**(1)**:**156-62.

114. Silvestre JS, Tamarat R, Senbonmatsu T, Icchiki T, Ebrahimian T, Iglarz M, Besnard S, Duriez M, Inagami T, Levy BI 2002 Antiangiogenic effect of angiotensin II type 2 receptor in ischemia-induced angiogenesis in mice hindlimb. Circ Res **90**(10)**:**1072-9.

115. Mallat Z, Silvestre JS, Le Ricousse-Roussanne S, Lecomte-Raclet L, Corbaz A, Clergue M, Duriez M, Barateau V, Akira S, Tedgui A, Tobelem G, Chvatchko Y, Levy BI 2002 Interleukin-18/interleukin-18 binding protein signaling modulates ischemia-induced neovascularization in mice hindlimb. Circ Res **91**(5)**:**441-8.

116. Brevetti LS, Paek R, Brady SE, Hoffman JI, Sarkar R, Messina LM 2001 Exercise-induced hyperemia unmasks regional blood flow deficit in experimental hindlimb ischemia. J Surg Res **98**(1)**:**21-6.

117. Kowallik P, Schulz R, Guth BD, Schade A, Paffhausen W, Gross R, Heusch G 1991 Measurement of regional myocardial blood flow with multiple colored microspheres. Circulation **83**(3)**:**974-82.

118. Prinzen FW, Glenny RW 1994 Developments in non-radioactive microsphere techniques for blood flow measurement. Cardiovasc Res **28**(10)**:**1467-75.

119. Van Oosterhout MF, Willigers HM, Reneman RS, Prinzen FW 1995 Fluorescent microspheres to measure organ perfusion: validation of a simplified sample processing technique. Am J Physiol **269**(2 Pt 2)**:**H725-33.

120. Deveci D, Egginton S 1999 Development of the fluorescent microsphere technique for quantifying regional blood flow in small mammals. Exp Physiol **84**(4)**:**615-30.

121. Bentley MD, Ortiz MC, Ritman EL, Romero JC 2002 The use of microcomputed tomography to study microvasculature in small rodents. Am J Physiol Regul Integr Comp Physiol **282**(5)**:**R1267-79.

122. Garcia-Sanz A, Rodriguez-Barbero A, Bentley MD, Ritman EL, Romero JC 1998 Three-dimensional microcomputed tomography of renal vasculature in rats. Hypertension **31**(1 Pt 2)**:**440-4.

123. Holdsworth DW, Thornton MM 2002 Micro-CT in small animal and specimen imaging. Trends Biotechnol **20**(8)**:**S34-9.

124. Jorgensen SM, Demirkaya O, Ritman EL 1998 Three-dimensional imaging of vasculature and parenchyma in intact rodent organs with X-ray micro-CT. Am J Physiol **275**(3 Pt 2)**:**H1103-14.

125. Ortiz MC, Garcia-Sanz A, Bentley MD, Fortepiani LA, Garcia-Estan J, Ritman EL, Romero JC, Juncos LA 2000 Microcomputed tomography of kidneys following chronic bile duct ligation. Kidney Int **58**(4)**:**1632-40.

126. Rodriguez-Porcel M, Lerman A, Ritman EL, Wilson SH, Best PJ, Lerman LO 2000 Altered myocardial microvascular 3D architecture in experimental hypercholesterolemia. Circulation **102**(17)**:**2028-30.

127. Simopoulos DN, Gibbons SJ, Malysz J, Szurszewski JH, Farrugia G, Ritman EL, Moreland RB, Nehra A 2001 Corporeal structural and vascular micro architecture with X-ray micro computerized tomography in normal and diabetic rabbits: histopathological correlation. J Urol **165**(5)**:**1776-82.

128. Wilson SH, Herrmann J, Lerman LO, Holmes DR, Jr., Napoli C, Ritman EL, Lerman A 2002 Simvastatin preserves the structure of coronary adventitial vasa vasorum in experimental hypercholesterolemia independent of lipid lowering. Circulation **105**(4)**:**415-8.

129. Maehara N 2003 Experimental microcomputed tomography study of the 3D microangioarchitecture of tumors. Eur Radiol **13**(7)**:**1559-65.

130. Duvall CL, Robert Taylor W, Weiss D, Guldberg RE 2004 Quantitative microcomputed tomography analysis of collateral vessel development after ischemic injury. Am J Physiol Heart Circ Physiol **287**(1)**:**H302-10.

131. Hounsfield GN 1973 Computerized transverse axial scanning (tomography). 1. Description of system. Br J Radiol **46**(552)**:**1016-22.

132. Hounsfield GN 1980 Nobel lecture, 8 December 1979. Computed medical imaging. J Radiol **61**(6-7)**:**459-68.

133. Feldkamp LA, Goldstein SA, Parfitt AM, Jesion G, Kleerekoper M 1989 The direct examination of three-dimensional bone architecture in vitro by computed tomography. J Bone Miner Res **4**(1)**:**3-11.

134. Feldkamp LA, C. DL 1984 Practical cone-beam algorithm. J Opt Soc Am **1:**612-619.

135. Hildebrand T, Ruegsegger P 1997 A new method for the model-independent assessment of thickness in three-dimensional images. J Microsc **185:**67-75.

136. Hildebrand T, Laib A, Muller R, Dequeker J, Ruegsegger P 1999 Direct three-dimensional morphometric analysis of human cancellous bone: microstructural data from spine, femur, iliac crest, and calcaneus. J Bone Miner Res **14**(7)**:**1167-74.

137. Odgaard A, Gundersen HJ 1993 Quantification of connectivity in cancellous bone, with special emphasis on 3-D reconstructions. Bone **14**(2)**:**173-82.

138. Guldberg RE, Ballock RT, Boyan BD, Duvall CL, Lin AS, Nagaraja S, Oest M, Phillips J, Porter BD, Robertson G, Taylor WR 2003 Analyzing bone, blood vessels, and biomaterials with microcomputed tomography. IEEE Eng Med Biol Mag **22**(5)**:**77-83.

139. Guldberg RE, Lin AS, Coleman R, Robertson G, Duvall C 2004 Microcomputed tomography imaging of skeletal development and growth. Birth Defects Res C Embryo Today **72**(3)**:**250-9.

140. American Society for Metals., ASM Handbook Committee. 1989 Nondestructive evaluation and quality control. ASM International, Metals Park, Ohio, pp xi, 795.

141. Ferguson C, Alpern E, Miclau T, Helms JA 1999 Does adult fracture repair recapitulate embryonic skeletal formation? Mech Dev **87**(1-2)**:**57-66.

142. McKibbin B 1978 The biology of fracture healing in long bones. J Bone Joint Surg Br **60-B**(2)**:**150-62.

143. Le AX, Miclau T, Hu D, Helms JA 2001 Molecular aspects of healing in stabilized and non-stabilized fractures. J Orthop Res **19**(1)**:**78-84.

144. Einhorn TA 1998 The cell and molecular biology of fracture healing. Clin Orthop (355 Suppl)**:**S7-21.

145. Einhorn TA, Majeska RJ, Rush EB, Levine PM, Horowitz MC 1995 The expression of cytokine activity by fracture callus. J Bone Miner Res **10**(8)**:**1272-81.

146. Kon T, Cho TJ, Aizawa T, Yamazaki M, Nooh N, Graves D, Gerstenfeld LC, Einhorn TA 2001 Expression of osteoprotegerin, receptor activator of NF-kappaB ligand (osteoprotegerin ligand) and related proinflammatory cytokines during fracture healing. J Bone Miner Res **16**(6)**:**1004-14.

147. De Biase P, Capanna R 2005 Clinical applications of BMPs. Injury **36 Suppl 3:**S43-6.

148. Ding RK, Wang WC, Ni JD 2001 [Experimental study of bovine bone morphogenetic protein combined with sintered bone in the treatment of bone defects]. Hunan Yi Ke Da Xue Xue Bao **26**(6)**:**537-9.

149. Deckers MM, van Bezooijen RL, van der Horst G, Hoogendam J, van Der Bent C, Papapoulos SE, Lowik CW 2002 Bone morphogenetic proteins stimulate angiogenesis through osteoblast-derived vascular endothelial growth factor A. Endocrinology **143**(4)**:**1545-53.

150. Hoffmann A, Weich HA, Gross G, Hillmann G 2001 Perspectives in the biological function, the technical and therapeutic application of bone morphogenetic proteins. Appl Microbiol Biotechnol **57**(3)**:**294-308.

151. Street J, Bao M, deGuzman L, Bunting S, Peale FV, Jr., Ferrara N, Steinmetz H, Hoeffel J, Cleland JL, Daugherty A, van Bruggen N, Redmond HP, Carano RA,

Filvaroff EH 2002 Vascular endothelial growth factor stimulates bone repair by promoting angiogenesis and bone turnover. Proc Natl Acad Sci U S A **99**(15)**:**9656-61.

152. Hausman MR, Schaffler MB, Majeska RJ 2001 Prevention of fracture healing in rats by an inhibitor of angiogenesis. Bone **29**(6)**:**560-4.

153. Colnot C, Thompson Z, Miclau T, Werb Z, Helms JA 2003 Altered fracture repair in the absence of MMP9. Development **130**(17)**:**4123-33.

154. Alford AI, Hankenson KD 2006 Matricellular proteins: extracellular modulators of bone development, remodeling, and regeneration. Bone **38**(6)**:**749-57.

155. Denhardt DT, Noda M, O'Regan AW, Pavlin D, Berman JS 2001 Osteopontin as a means to cope with environmental insults: regulation of inflammation, tissue remodeling, and cell survival. J Clin Invest **107**(9)**:**1055-61.

156. Bornstein P 2000 Matricellular proteins: an overview. Matrix Biol **19**(7)**:**555-6.

157. Liaw L, Skinner MP, Raines EW, Ross R, Cheresh DA, Schwartz SM, Giachelli CM 1995 The adhesive and migratory effects of osteopontin are mediated via distinct cell surface integrins. Role of alpha v beta 3 in smooth muscle cell migration to osteopontin in vitro. J Clin Invest **95**(2)**:**713-24.

158. Bayless KJ, Meininger GA, Scholtz JM, Davis GE 1998 Osteopontin is a ligand for the alpha4beta1 integrin. J Cell Sci **111 (Pt 9):**1165-74.

159. Barry ST, Ludbrook SB, Murrison E, Horgan CM 2000 A regulated interaction between alpha5beta1 integrin and osteopontin. Biochem Biophys Res Commun **267**(3)**:**764-9.

160. Denda S, Reichardt LF, Muller U 1998 Identification of osteopontin as a novel ligand for the integrin alpha8 beta1 and potential roles for this integrin-ligand interaction in kidney morphogenesis. Mol Biol Cell **9**(6)**:**1425-35.

161. Smith LL, Cheung HK, Ling LE, Chen J, Sheppard D, Pytela R, Giachelli CM 1996 Osteopontin N-terminal domain contains a cryptic adhesive sequence recognized by alpha9beta1 integrin. J Biol Chem **271**(45)**:**28485-91.

162. Senger DR, Perruzzi CA, Papadopoulos-Sergiou A, Van de Water L 1994 Adhesive properties of osteopontin: regulation by a naturally occurring thrombin-cleavage in close proximity to the GRGDS cell-binding domain. Mol Biol Cell **5**(5)**:**565-74.

163. Helluin O, Chan C, Vilaire G, Mousa S, DeGrado WF, Bennett JS 2000 The activation state of alphavbeta 3 regulates platelet and lymphocyte adhesion to intact and thrombin-cleaved osteopontin. J Biol Chem **275**(24)**:**18337-43.

164. Goodison S, Urquidi V, Tarin D 1999 CD44 cell adhesion molecules. Mol Pathol **52**(4)**:**189-96.

165. Weber GF, Ashkar S, Glimcher MJ, Cantor H 1996 Receptor-ligand interaction between CD44 and osteopontin (Eta-1). Science **271**(5248)**:**509-12.

166. Katagiri YU, Sleeman J, Fujii H, Herrlich P, Hotta H, Tanaka K, Chikuma S, Yagita H, Okumura K, Murakami M, Saiki I, Chambers AF, Uede T 1999 CD44 variants but not CD44s cooperate with beta1-containing integrins to permit cells to bind to osteopontin independently of arginine-glycine-aspartic acid, thereby stimulating cell motility and chemotaxis. Cancer Res **59**(1)**:**219-26.

167. Zohar R, Suzuki N, Suzuki K, Arora P, Glogauer M, McCulloch CA, Sodek J 2000 Intracellular osteopontin is an integral component of the CD44-ERM complex involved in cell migration. J Cell Physiol **184**(1)**:**118-30.

168. Senger DR, Wirth DF, Hynes RO 1979 Transformed mammalian cells secrete specific proteins and phosphoproteins. Cell **16**(4)**:**885-93.

169. Rittling SR, Chambers AF 2004 Role of osteopontin in tumour progression. Br J Cancer **90**(10)**:**1877-81.

170. Liaw L, Birk DE, Ballas CB, Whitsitt JS, Davidson JM, Hogan BL 1998 Altered wound healing in mice lacking a functional osteopontin gene (spp1). J Clin Invest **101**(7)**:**1468-78.

171. Stier S, Ko Y, Forkert R, Lutz C, Neuhaus T, Grunewald E, Cheng T, Dombkowski D, Calvi LM, Rittling SR, Scadden DT 2005 Osteopontin is a hematopoietic stem cell niche component that negatively regulates stem cell pool size. J Exp Med **201**(11)**:**1781-91.

172. Nilsson SK, Johnston HM, Whitty GA, Williams B, Webb RJ, Denhardt DT, Bertoncello I, Bendall LJ, Simmons PJ, Haylock DN 2005 Osteopontin, a key component of the hematopoietic stem cell niche and regulator of primitive hematopoietic progenitor cells. Blood **106**(4)**:**1232-9.

173. Myers DL, Harmon KJ, Lindner V, Liaw L 2003 Alterations of arterial physiology in osteopontin-null mice. Arterioscler Thromb Vasc Biol **23**(6)**:**1021-8.

174. O'Brien ER, Garvin MR, Stewart DK, Hinohara T, Simpson JB, Schwartz SM, Giachelli CM 1994 Osteopontin is synthesized by macrophage, smooth muscle, and endothelial cells in primary and restenotic human coronary atherosclerotic plaques. Arterioscler Thromb **14**(10)**:**1648-56.

175. Scatena M, Almeida M, Chaisson ML, Fausto N, Nicosia RF, Giachelli CM 1998 NF-kappaB mediates alphavbeta3 integrin-induced endothelial cell survival. J Cell Biol **141**(4)**:**1083-93.

176. Senger DR, Ledbetter SR, Claffey KP, Papadopoulos-Sergiou A, Peruzzi CA, Detmar M 1996 Stimulation of endothelial cell migration by vascular permeability factor/vascular endothelial growth factor through cooperative mechanisms involving the alphavbeta3 integrin, osteopontin, and thrombin. Am J Pathol **149**(1)**:**293-305.

177. Leali D, Dell'Era P, Stabile H, Sennino B, Chambers AF, Naldini A, Sozzani S, Nico B, Ribatti D, Presta M 2003 Osteopontin (Eta-1) and fibroblast growth factor-2 cross-talk in angiogenesis. J Immunol **171**(2)**:**1085-93.

178. Giachelli CM, Lombardi D, Johnson RJ, Murry CE, Almeida M 1998 Evidence for a role of osteopontin in macrophage infiltration in response to pathological stimuli in vivo. Am J Pathol **152**(2)**:**353-8.

179. Liaw L, Almeida M, Hart CE, Schwartz SM, Giachelli CM 1994 Osteopontin promotes vascular cell adhesion and spreading and is chemotactic for smooth muscle cells in vitro. Circ Res **74**(2)**:**214-24.

180. Yue TL, McKenna PJ, Ohlstein EH, Farach-Carson MC, Butler WT, Johanson K, McDevitt P, Feuerstein GZ, Stadel JM 1994 Osteopontin-stimulated vascular smooth muscle cell migration is mediated by beta 3 integrin. Exp Cell Res **214**(2)**:**459-64.

181. Shijubo N, Uede T, Kon S, Maeda M, Segawa T, Imada A, Hirasawa M, Abe S 1999 Vascular endothelial growth factor and osteopontin in stage I lung adenocarcinoma. Am J Respir Crit Care Med **160**(4)**:**1269-73.

182. Jin Y, Kuroda N, Kakiuchi S, Yamasaki Y, Miyazaki E, Hayashi Y, Toi M, Naruse K, Hiroi M, Enzan H 2000 Bronchial granular cell tumor with osteopontin and osteonectin expression: a case report. Pathol Int **50**(5)**:**421-6.

183. Euer N, Schwirzke M, Evtimova V, Burtscher H, Jarsch M, Tarin D, Weidle UH 2002 Identification of genes associated with metastasis of mammary carcinoma in metastatic versus non-metastatic cell lines. Anticancer Res **22**(2A)**:**733-40.

184. Khanna C, Prehn J, Yeung C, Caylor J, Tsokos M, Helman L 2000 An orthotopic model of murine osteosarcoma with clonally related variants differing in pulmonary metastatic potential. Clin Exp Metastasis **18**(3)**:**261-71.

185. Takahashi F, Akutagawa S, Fukumoto H, Tsukiyama S, Ohe Y, Takahashi K, Fukuchi Y, Saijo N, Nishio K 2002 Osteopontin induces angiogenesis of murine neuroblastoma cells in mice. Int J Cancer **98**(5)**:**707-12.

186. Nakase T, Takaoka K, Hirakawa K, Hirota S, Takemura T, Onoue H, Takebayashi K, Kitamura Y, Nomura S 1994 Alterations in the expression of osteonectin, osteopontin and osteocalcin mRNAs during the development of skeletal tissues in vivo. Bone Miner **26**(2)**:**109-22.

187. Rittling SR, Matsumoto HN, McKee MD, Nanci A, An XR, Novick KE, Kowalski AJ, Noda M, Denhardt DT 1998 Mice lacking osteopontin show normal development and bone structure but display altered osteoclast formation in vitro. J Bone Miner Res **13**(7)**:**1101-11.

188. Hunter GK, Hauschka PV, Poole AR, Rosenberg LC, Goldberg HA 1996 Nucleation and inhibition of hydroxyapatite formation by mineralized tissue proteins. Biochem J **317 (Pt 1):**59-64.

189. Boskey AL, Maresca M, Ullrich W, Doty SB, Butler WT, Prince CW 1993 Osteopontin-hydroxyapatite interactions in vitro: inhibition of hydroxyapatite formation and growth in a gelatin-gel. Bone Miner **22**(2)**:**147-59.

190. Boskey AL, Spevak L, Paschalis E, Doty SB, McKee MD 2002 Osteopontin deficiency increases mineral content and mineral crystallinity in mouse bone. Calcif Tissue Int **71**(2)**:**145-54.

191. Chellaiah MA, Kizer N, Biswas R, Alvarez U, Strauss-Schoenberger J, Rifas L, Rittling SR, Denhardt DT, Hruska KA 2003 Osteopontin Deficiency Produces Osteoclast Dysfunction Due to Reduced CD44 Surface Expression. Mol Biol Cell **14**(1)**:**173-89.

192. Suzuki K, Zhu B, Rittling SR, Denhardt DT, Goldberg HA, McCulloch CA, Sodek J 2002 Colocalization of intracellular osteopontin with CD44 is associated with migration, cell fusion, and resorption in osteoclasts. J Bone Miner Res **17**(8)**:**1486-97.

193. Ishijima M, Rittling SR, Yamashita T, Tsuji K, Kurosawa H, Nifuji A, Denhardt DT, Noda M 2001 Enhancement of osteoclastic bone resorption and suppression of osteoblastic bone formation in response to reduced mechanical stress do not occur in the absence of osteopontin. J Exp Med **193**(3)**:**399-404.

194. Yoshitake H, Rittling SR, Denhardt DT, Noda M 1999 Osteopontin-deficient mice are resistant to ovariectomy-induced bone resorption. Proc Natl Acad Sci U S A **96**(14)**:**8156-60.

195. Ihara H, Denhardt DT, Furuya K, Yamashita T, Muguruma Y, Tsuji K, Hruska KA, Higashio K, Enomoto S, Nifuji A, Rittling SR, Noda M 2001 Parathyroid hormone-induced bone resorption does not occur in the absence of osteopontin. J Biol Chem **276**(16)**:**13065-71.

196. Koyama Y, Rittling SR, Tsuji K, Hino K, Salincarnboriboon R, Yano T, Taketani Y, Nifuji A, Denhardt DT, Noda M 2006 Osteopontin deficiency suppresses high phosphate load-induced bone loss via specific modulation of osteoclasts. Endocrinology **147**(6)**:**3040-9.

197. Yamazaki M, Nakajima F, Ogasawara A, Moriya H, Majeska RJ, Einhorn TA 1999 Spatial and temporal distribution of CD44 and osteopontin in fracture callus. J Bone Joint Surg Br **81**(3)**:**508-15.

198. Hirakawa K, Hirota S, Ikeda T, Yamaguchi A, Takemura T, Nagoshi J, Yoshiki S, Suda T, Kitamura Y, Nomura S 1994 Localization of the mRNA for bone matrix proteins during fracture healing as determined by in situ hybridization. J Bone Miner Res **9**(10)**:**1551-7.

199. Nakase T, Sugimoto M, Sato M, Kaneko M, Tomita T, Sugamoto K, Nomura S, Kitamura Y, Yoshikawa H, Yasui N, Yonenobu K, Ochi T 1998 Switch of osteonectin and osteopontin mRNA expression in the process of cartilage-to-bone transition during fracture repair. Acta Histochem **100**(3)**:**287-95.

200. Steitz SA, Speer MY, McKee MD, Liaw L, Almeida M, Yang H, Giachelli CM 2002 Osteopontin inhibits mineral deposition and promotes regression of ectopic calcification. Am J Pathol **161**(6)**:**2035-46.

201. Hirota S, Asada H, Kohri K, Tsukamoto Y, Ito A, Yoshikawa K, Xu Z, Nomura S, Kitamura Y 1995 Possible role of osteopontin in deposition of calcium phosphate in human pilomatricomas. J Invest Dermatol **105**(1)**:**138-42.

202. Huang W, Carlsen B, Rudkin G, Berry M, Ishida K, Yamaguchi DT, Miller TA 2004 Osteopontin is a negative regulator of proliferation and differentiation in MC3T3-E1 pre-osteoblastic cells. Bone **34**(5)**:**799-808.

203. Gundersen HJ, Jensen TB, Osterby R 1978 Distribution of membrane thickness determined by lineal analysis. J Microsc **113**(1)**:**27-43.

204. Gole GA, Browning J, Elts SM 1990 The mouse model of oxygen-induced retinopathy: a suitable animal model for angiogenesis research. Doc Ophthalmol **74**(3)**:**163-9.

205. Rajagopalan S, Mohler E, 3rd, Lederman RJ, Saucedo J, Mendelsohn FO, Olin J, Blebea J, Goldman C, Trachtenberg JD, Pressler M, Rasmussen H, Annex BH, Hirsch AT 2003 Regional Angiogenesis with Vascular Endothelial Growth Factor (VEGF) in peripheral arterial disease: Design of the RAVE trial. Am Heart J **145**(6)**:**1114-8.

206. Baumgartner I, Pieczek A, Manor O, Blair R, Kearney M, Walsh K, Isner JM 1998 Constitutive expression of phVEGF165 after intramuscular gene transfer promotes collateral vessel development in patients with critical limb ischemia. Circulation **97**(12)**:**1114-23.

207. Lazarous DF, Unger EF, Epstein SE, Stine A, Arevalo JL, Chew EY, Quyyumi AA 2000 Basic fibroblast growth factor in patients with intermittent claudication: results of a phase I trial. J Am Coll Cardiol **36**(4)**:**1239-44.

208. Mohler ER, 3rd, Rajagopalan S, Olin JW, Trachtenberg JD, Rasmussen H, Pak R, Crystal RG 2003 Adenoviral-mediated gene transfer of vascular endothelial growth factor in critical limb ischemia: safety results from a phase I trial. Vasc Med **8**(1)**:**9-13.

209. Rajagopalan S, Trachtenberg J, Mohler E, Olin J, McBride S, Pak R, Rasmussen H, Crystal R 2002 Phase I study of direct administration of a replication deficient adenovirus vector containing the vascular endothelial growth factor cDNA (CI-1023) to patients with claudication. Am J Cardiol **90**(5)**:**512-6.

210. Makinen K, Manninen H, Hedman M, Matsi P, Mussalo H, Alhava E, Yla-Herttuala S 2002 Increased vascularity detected by digital subtraction angiography after VEGF gene transfer to human lower limb artery: a randomized, placebo-controlled, double-blinded phase II study. Mol Ther **6**(1)**:**127-33.

211. Isner JM, Walsh K, Symes J, Pieczek A, Takeshita S, Lowry J, Rosenfield K, Weir L, Brogi E, Jurayj D 1996 Arterial gene transfer for therapeutic angiogenesis in patients with peripheral artery disease. Hum Gene Ther **7**(8)**:**959-88.

212. Isner JM, Pieczek A, Schainfeld R, Blair R, Haley L, Asahara T, Rosenfield K, Razvi S, Walsh K, Symes JF 1996 Clinical evidence of angiogenesis after arterial gene transfer of phVEGF165 in patient with ischaemic limb. Lancet **348**(9024)**:**370-4.

213. Hershey JC, Baskin EP, Glass JD, Hartman HA, Gilberto DB, Rogers IT, Cook JJ 2001 Revascularization in the rabbit hindlimb: dissociation between capillary sprouting and arteriogenesis. Cardiovasc Res **49**(3)**:**618-25.

214. Hershey JC, Baskin EP, Corcoran HA, Bett A, Dougherty NM, Gilberto DB, Mao X, Thomas KA, Cook JJ 2003 Vascular endothelial growth factor stimulates angiogenesis without improving collateral blood flow following hindlimb ischemia in rabbits. Heart Vessels **18**(3)**:**142-9.

215. Thurston G, Murphy TJ, Baluk P, Lindsey JR, McDonald DM 1998 Angiogenesis in mice with chronic airway inflammation: strain-dependent differences. Am J Pathol **153**(4)**:**1099-112.

216. Rohan RM, Fernandez A, Udagawa T, Yuan J, D'Amato RJ 2000 Genetic heterogeneity of angiogenesis in mice. Faseb J **14**(7)**:**871-6.

217. Moore DC, Leblanc CW, Muller R, Crisco JJ, 3rd, Ehrlich MG 2003 Physiologic weight-bearing increases new vessel formation during distraction osteogenesis: a micro-tomographic imaging study. J Orthop Res **21**(3)**:**489-96.

218. Sugimoto K, Sakurai N, Kaneko M, Shirasawa H, Shibata K, Miyata M, Noguchi T, Uematsu K, Shimoda K, Sakata J 1991 Application of renal microangiography to normal and diseased kidneys of cattle and mice. Am J Vet Res **52**(1)**:**157-63.

219. Baumgartner I, Schainfeld R, Graziani L 2005 Management of peripheral vascular disease. Annu Rev Med **56:**249-72.

220. Matsumoto K, Ishihara K, Tanaka K, Inoue K, Fushiki T 1996 An adjustable-current swimming pool for the evaluation of endurance capacity of mice. J Appl Physiol **81**(4)**:**1843-9.

221. Zhu B, Suzuki K, Goldberg HA, Rittling SR, Denhardt DT, McCulloch CA, Sodek J 2004 Osteopontin modulates CD44-dependent chemotaxis of peritoneal macrophages through G-protein-coupled receptors: evidence of a role for an intracellular form of osteopontin. J Cell Physiol **198**(1)**:**155-67.

222. Moldovan NI, Goldschmidt-Clermont PJ, Parker-Thornburg J, Shapiro SD, Kolattukudy PE 2000 Contribution of monocytes/macrophages to compensatory neovascularization: the drilling of metalloelastase-positive tunnels in ischemic myocardium. Circ Res **87**(5)**:**378-84.

223. Junqueira LC, Bignolas G, Brentani RR 1979 Picrosirius staining plus polarization microscopy, a specific method for collagen detection in tissue sections. Histochem J **11**(4)**:**447-55.

224. Dayan D, Hiss Y, Hirshberg A, Bubis JJ, Wolman M 1989 Are the polarization colors of picrosirius red-stained collagen determined only by the diameter of the fibers? Histochemistry **93**(1)**:**27-9.

225. Woessner JF, Jr. 1961 The determination of hydroxyproline in tissue and protein samples containing small proportions of this imino acid. Arch Biochem Biophys **93:**440-7.

226. Yasuda H, Shima N, Nakagawa N, Yamaguchi K, Kinosaki M, Mochizuki S, Tomoyasu A, Yano K, Goto M, Murakami A, Tsuda E, Morinaga T, Higashio K, Udagawa N, Takahashi N, Suda T 1998 Osteoclast differentiation factor is a

ligand for osteoprotegerin/osteoclastogenesis-inhibitory factor and is identical to TRANCE/RANKL. Proc Natl Acad Sci U S A **95**(7)**:**3597-602.

227. Jepsen KJ, Pennington DE, Lee YL, Warman M, Nadeau J 2001 Bone brittleness varies with genetic background in A/J and C57BL/6J inbred mice. J Bone Miner Res **16**(10)**:**1854-62.

228. Helisch A, Wagner S, Khan N, Drinane M, Wolfram S, Heil M, Ziegelhoeffer T, Brandt U, Pearlman JD, Swartz HM, Schaper W 2006 Impact of mouse strain differences in innate hindlimb collateral vasculature. Arterioscler Thromb Vasc Biol **26**(3)**:**520-6.

229. Dansky HM, Charlton SA, Sikes JL, Heath SC, Simantov R, Levin LF, Shu P, Moore KJ, Breslow JL, Smith JD 1999 Genetic background determines the extent of atherosclerosis in ApoE-deficient mice. Arterioscler Thromb Vasc Biol **19**(8)**:**1960-8.

230. Li CY, Schaffler MB, Wolde-Semait HT, Hernandez CJ, Jepsen KJ 2005 Genetic background influences cortical bone response to ovariectomy. J Bone Miner Res **20**(12)**:**2150-8.

231. Amblard D, Lafage-Proust MH, Laib A, Thomas T, Ruegsegger P, Alexandre C, Vico L 2003 Tail suspension induces bone loss in skeletally mature mice in the C57BL/6J strain but not in the C3H/HeJ strain. J Bone Miner Res **18**(3)**:**561-9.

232. Kaartinen MT, Pirhonen A, Linnala-Kankkunen A, Maenpaa PH 1999 Cross-linking of osteopontin by tissue transglutaminase increases its collagen binding properties. J Biol Chem **274**(3)**:**1729-35.

233. Fantner GE, Hassenkam T, Kindt JH, Weaver JC, Birkedal H, Pechenik L, Cutroni JA, Cidade GA, Stucky GD, Morse DE, Hansma PK 2005 Sacrificial bonds and hidden length dissipate energy as mineralized fibrils separate during bone fracture. Nat Mater **4**(8)**:**612-6.

234. Hansma PK, Fantner GE, Kindt JH, Thurner PJ, Schitter G, Turner PJ, Udwin SF, Finch MM 2005 Sacrificial bonds in the interfibrillar matrix of bone. J Musculoskelet Neuronal Interact **5**(4)**:**313-5.

235. Lorigo LM, Faugeras OD, Grimson WE, Keriven R, Kikinis R, Nabavi A, Westin CF 2001 CURVES: curve evolution for vessel segmentation. Med Image Anal **5**(3)**:**195-206.

236. Lorigo L 1999 CURVES: Vessel Segmentation System. Retrieved December 10, 2006 from http://groups.csail.mit.edu/vision/medical-vision/liana-3dcurves/compare.html.

237. Mukundan S, Jr., Ghaghada KB, Badea CT, Kao CY, Hedlund LW, Provenzale JM, Johnson GA, Chen E, Bellamkonda RV, Annapragada A 2006 A liposomal nanoscale contrast agent for preclinical CT in mice. AJR Am J Roentgenol **186**(2)**:**300-7.

238. Thompson JB, Kindt JH, Drake B, Hansma HG, Morse DE, Hansma PK 2001 Bone indentation recovery time correlates with bond reforming time. Nature **414**(6865)**:**773-6.

239. Fantner GE, Birkedal H, Kindt JH, Hassenkam T, Weaver JC, Cutroni JA, Bosma BL, Bawazer L, Finch MM, Cidade GA, Morse DE, Stucky GD, Hansma PK 2004 Influence of the degradation of the organic matrix on the microscopic fracture behavior of trabecular bone. Bone **35**(5)**:**1013-22.

240. Fantner GE, Oroudjev E, Schitter G, Golde LS, Thurner P, Finch MM, Turner P, Gutsmann T, Morse DE, Hansma H, Hansma PK 2006 Sacrificial bonds and hidden length: unraveling molecular mesostructures in tough materials. Biophys J **90**(4)**:**1411-8.

VITA

CRAIG L. DUVALL

Craig was born to his parents, James and Wanda, in the bustling metropolis of Greenville, KY (population 4,000) on August 25, 1979. He was preceded in the family by 3 years by his older sister, Jennifer. He attended Lake Malone and Longest Elementary Schools, followed by Muhlenberg South Middle and High Schools. Craig enjoyed playing baseball and basketball throughout his childhood and lettered in these sports in high school. In 1997, Craig moved to Lexington, KY to attend the University of Kentucky, where he cheered the Wildcats to a national championship in basketball his freshman year and to berths in the Outback and Music City Bowls in subsequent years. He also got an education on the side, and in May of 2001, Craig graduated with a B.S. in Biosystems and Agricultural Engineering with a focus in biomedical engineering. From there, Craig moved to Atlanta, GA to study biomedical engineering and pursue his doctorate at the Georgia Tech / Emory joint Department of Biomedical Engineering. After over 5½ years in Atlanta, Craig still participates in intramural basketball, football, and softball leagues, and in the meantime, has added mountain and road biking to his list of favorite leisure activities.